REPORT NO. 49

DECEMBER, 1951

THE COLLEGE OF AERONAUTICS

CRANFIELD

AN INVESTIGATION OF BOUNDARY LAYER EFFECTS ON TWO DIMENSIONAL SUPERSONIC AEROFOILS

-by-

H.K. ZIENKIEWICZ, D.C.Ae.(Dist.).

SUMMARY

The phenomena of viscous flow over two-dimensional supersonic aerofoils are investigated with a view to developing a method for estimating their effects on the aerodynamic characteristics of the aerofoils.

In regions where the flow is unaffected by shock waves and where the assumptions of the boundary layer theory hold, the concept of the displacement thickness and the equivalent wing profile is applied to determine the changes in the local pressure distribution and the resulting increments of force and moment coefficients. It is found that these increments vary with the Reynolds number approximately as $R^{-\frac{1}{2}}$ for the laminar boundary layer and as R^{-n}, $n \approx 0.2$, for the turbulent.

A drag-entropy relation and a lift relation are derived from the momentum theorem and are used to demonstrate the overall effects of the boundary layer - shock wave interaction. Local flow conditions affected by this interaction are examined in detail. On the basis of available experimental data an empirical correction is suggested for the effects of flow separation at the trailing edge, and it is found that with the laminar boundary layer these effects are of major importance. It is expected that their influence will diminish at high Reynolds numbers and will be negligible with turbulent boundary layers.

The suggested method of estimating the boundary layer effects is applied to the particular case of a 10 per cent

/circular ...

MEP

circular arc profile at $M = 2.13$ and $R = 0.64 \times 10^6$. Comparison with experiment is not conclusive, owing to the lack of reliable data.

A new integral relation for laminar boundary layers in simple-wave flow and zero heat transfer is developed and is found to give good agreement with the approximate method of Howarth.

A brief discussion is also given of the relative merits of circular arc and double-wedge profiles.

/LIST OF CONTENTS ...

LIST OF CONTENTS

/NOTATION ...

NOTATION

A, B, C	functions of aerofoil dimensions and free stream conditions (Appendix I)
C_X, C_Y	aerodynamic coefficients of force components in directions x,y
C_{D_w}	basic wave drag coefficient
C_{D_f}	skin friction drag coefficient
$c_f \equiv \frac{2\tau_w}{\rho_o U_o^2}$	local skin friction coefficient
C_M	pitching moment coefficient about the leading edge
$f(\theta)$, $g(\theta)$, $m(\theta)$, $j(\theta)$, $J_g(\theta)$, $K(\theta)$, $L(\theta)$, $M(\theta)$ -	functions of simple-wave flow direction θ, used in boundary layer equations (Appendix I)
$H = \frac{\delta_1}{\vartheta}$	ratio of boundary layer displacement thickness to momentum thickness
J	mechanical equivalent of heat
k	coefficient of conductivity of heat
K	streamline curvature
p	static pressure
p_s	stagnation (reservoir) pressure
$q_o = \frac{1}{2}\rho_o U_o^2$	free stream dynamic head
q	resultant velocity
$R_o = \frac{U_o c}{\nu_o}$	Reynolds number based on chord
R_ϑ, R_{δ_1}	local Reynolds numbers based on momentum and displacement thicknesses, respectively
S	entropy
s, n	curvilinear orthogonal coordinates parallel and normal to the aerofoil surface
t	maximum thickness of aerofoil sections
T	static temperature
u, v	velocity components in directions x,y or s,n (as defined)
U_o	free stream velocity
x, y	rectangular Cartesian coordinates parallel and normal to aerofoil chord (except when otherwise stated)
x_{cp}	distance of centre of pressure from leading edge

/Y = ...

$Y = \int \frac{\mu_1}{\mu} dn$	transformed boundary layer coordinate (Appendix I)
α	angle of incidence
$\beta = \tan^{-1} \frac{dy}{dx}$	slope of the aerofoil surface
$\gamma = C_p/C_v$	ratio of specific heats (taken as 1.4)
δ	boundary layer thickness, also deflection of flow across an oblique shock
δ^*	boundary layer thickness in terms of Y
δ_1	boundary layer displacement thickness
ϑ	boundary layer momentum thickness
θ	angle of simple-wave flow expansion from sonic velocity
ϕ	angular distance along surface of circular arc profile
K	curvature
λ	modified Pohlhausen parameter
μ, ν	coefficients of viscosity and kinematic viscosity, respectively
ρ	density
$\sigma = \frac{\mu C_p}{k}$	Prandtl number (taken as 0.72)
τ_w	shear stress at the wall
Δ	increment or change of a quantity

Suffix o refers to free stream conditions

1 main stream conditions at the edge of boundary layer

s stagnation conditions

∞ conditions at infinity

Bar ($\bar{}$) over a quantity denotes that the quantity is non-dimensional.

Standard symbols (C_L, M, etc.) are not included in the above list. All other symbols are defined when first introduced.

/INTRODUCTION ...

1. INTRODUCTION

Whilst boundary layer phenomena on two-dimensional aerofoils in incompressible flow have been extensively studied, both theoretically and experimentally, little work has so far been done on the corresponding problem in the supersonic flow. This may partly be ascribed to the fact that in incompressible flow, a recourse to the boundary layer theory is the only means of estimating theoretically the drag, whereas at supersonic speeds the pressure or wave drag, which forms the major contribution to the total drag, is given by the inviscid flow theory and, as a rule, the boundary layer can be expected to have only secondary effects.

The investigation reported here had been suggested by the work of Preston (refs. 1,2 and 3), which was primarily concerned with changes in circulation produced by the boundary layer on two-dimensional aerofoils in incompressible flow. Briefly, Preston's method is based on G.I. Taylor's theorem that equal amounts of positive and negative vorticity are discharged into the wake of an aerofoil. This permits the determination of the velocities at the trailing edge; the aerofoil is then replaced by a new shape displaced from the original aerofoil by the amount equal to the displacement thickness of the boundary layer, and the changes in the circulation found by determining the thickness and the camber effect of the displacement thickness. The changes in local pressure distribution can then be found in the usual manner, by using the new value of the circulation.

It would appear, at first sight, that the corresponding problem in the supersonic flow should be very much simpler, since the changes in the pressure distribution can be determined directly from the local changes of the direction of flow at the surface, produced by the boundary layer displacement thickness. A closer examination of the problem reveals, however, that this advantage is offset by the fact that on supersonic aerofoils there exist regions of flow where the classical boundary layer theory cannot be applied. These are the regions in the vicinity of the leading and trailing edges and of the sharp shoulders of wedge sections, where shock waves and strong expansion waves interact with the boundary layer causing upstream and downstream diffusion of pressure through the subsonic part of the boundary layer and, in many cases, inducing flow separation.

The mechanism of this interaction is not yet fully understood and presents a problem of such formidable complexity that, although in recent years it has attracted the attention of many research workers, only very limited progress has so far been

/reported ...

reported (this is discussed in more detail in section 3.3. below). In the majority of cases, even the positive results achieved are of little practical use, as only the simplest idealised flow conditions have so far proved amenable to mathematical treatment. Consequently, until a comprehensive theory for the boundary layer - shock wave interaction is developed, it appears that the only approach at one's disposal of theoretically assessing the boundary layer effects is a discriminate use of the existing boundary layer theory where it is applicable, combined with empirical or semi-empirical corrections for effects for which there is no theory available.

The present study was carried out to investigate the possibilities of such an assessment on the basis of the existing theories and the available experimental evidence. Typical flow patterns observed in wind tunnel tests on two-dimensional supersonic aerofoils are briefly discussed and the overall effects of flow separation are demonstrated by means of a drag-entropy and a lift relation, derived from the momentum theorem. The effects of the displacement of flow by the boundary layer are then found, neglecting the shock wave - boundary layer interaction. This is followed by a detailed examination of the regions of flow where this interaction may be of major importance. Qualitative explanations of the observed phenomena are suggested and, where possible, quantitative assessments of their importance are attempted. A new integral relation for laminar boundary layers on supersonic aerofoils in simple-wave flow is derived and is used to calculate the effects of the boundary layer on the force and moment coefficients in the particular case of a 10 per cent arc profile at the Mach number of 2.13 and the Reynolds number of 0.64×10^6. Effects of separation are accounted for empirically and comparison is made with some experimental results. Finally, the relative merits of various aerofoil sections as affected by the viscous effects are discussed briefly.

2. GENERAL THEORETICAL CONSIDERATIONS

2.1. Preliminary Remarks

The development of techniques of optical exploration of two-dimensional supersonic flows has provided a most attractive and useful tool of experimental research, and made it possible to obtain directly a clear picture of the actual flow conditions. With its aid, it soon became apparent that

/flow ...

flow patterns found in practice differ appreciably from those predicted by the inviscid theory. This was first conclusively demonstrated by Ferri in a series of tests carried out at Guidonia in 1939 (ref. 4), on a number of two-dimensional supersonic aeorfoils at Mach numbers of 1.85 and 2.13. More recently, similar results have been obtained at the N.P.L. by Valensi and Pruden (ref. 5), Holder and others (refs. 6 to 9), and at the R.A.E. by Beastall and Pallant (ref. 10). Although the results of these experiments differ in minor details, they present a fairly coherent and consistent picture of viscous flow over two-dimensional supersonic aerofoils. A detailed examination of local flow conditions is given in section 3, and at this stage only the general features will be discussed.

Referring to fig.1, the diagram (a) shows the flow pattern over a typical supersonic aerofoil as given by the inviscid shock-expansion theory. The incidence of the aerofoil is such that on the upper surface the airstream undergoes a Prandtl-Meyer expansion at the leading edge, expands gradually along the surface and is returned to approximately the free stream direction by the shock wave at the trailing edge; on the lower surface this order is reversed - there is an attached shock wave at the leading edge, followed by the expansion along the surface and at the trailing edge. In fig. 1(b) is shown a typical example of the actual flow over the same aerofoil with a laminar boundary layer and the Reynolds number of the order of $5 \times 10^5 - 10^6$. The Prandtl-Meyer expansion at the leading edge is now preceded by a weak shock, and that at the trailing edge followed by a shock where the boundary layers from the top and bottom surfaces join to form the wake. The most striking feature is the separation of flow occuring towards the rear of the upper surface. At a high Reynolds number, when the boundary layer is turbulent one would expect (for reasons explained later) either a complete absence of separation or, at least, a very much smaller separated region, limited to the immediate vicinity of the trailing edge (fig. 1c).

It is clear that these modified flow conditions result in a surface pressure distribution which is different from that determined by the inviscid theory, thus affecting the similarly derived aerodynamic characteristics of the aerofoil. Although one can account qualitatively for the flow patterns just described, one must await the development of the theory of viscous compressible flow, before a full theoretical treatment of the boundary layer effects can be attempted. As was already pointed

/out ...

out in the Introduction, at the present stage one can only apply the classical boundary layer theory to regions of flow where the basic assumptions of the theory are valid, and try to establish empirical corrections for the effects of separation. It is, however, possible to demonstrate the nature of the latter effects, without having to go into their mechanism. This is shown in the next paragraph by applying the momentum theorem to the flow over an aerofoil, whilst the changes in the local flow conditions are found by utilising the concept of the displacement thickness and of the effective shape of the aerofoil.

2.2. Overall Effects of Separation - Momentum Theorem

The derivation of the results which follow is given in detail in the Appendix II, and only an outline of the argument will be repeated here.

By applying the momentum theorem to flow past a two-dimensional supersonic aerofoil, the components of the aerodynamic force acting on the aerofoil are found to be (eqns. AII, 1.2 and 1.3):

$$-D = \int_C \rho u(u\,dy - v\,dx) + \int_C (p_{yx}dx - p_{xx}dy) \quad \ldots 2.2.2$$

$$-L = \int_C \rho v(u\,dy - v\,dx) + \int_C (p_{yy}dx - p_{xx}dy) \quad \ldots 2.2.1$$

where p_{xx}, p_{yy}, p_{yx} are stress components defined by eqn. AII. 1.4, and C is a simply connected boundary enclosing the aerofoil (fig. 2a).

If C is taken as a rectangular control surface C_1 (shown in fig. 2b), and if it is assumed that on AB, which is far downstream, the velocity of flow has the free stream direction and that the static pressure is equal to the free stream static pressure, the drag component of the aerodynamic force becomes

$$D = \int_{\infty(W)-\infty} \rho u\,(u_o - u)dy + \int_W \rho u(u_o - u)dy \quad \ldots\ldots\ldots 2.2.3$$

where $\infty(W)-\infty$ indicates integration from $-\infty$ to ∞, excluding the wake. For low speed flow $u = u_o$ outside the wake, far downstream, and

$$D_p = \int_W \rho u(u_o - u)dy \quad \ldots\ldots\ldots 2.2.3a$$

/which ...

which is the familiar expression for the profile drag at low speeds. Hence, the first integral in eqn. 2.2.3 must represent the wave drag in supersonic flow and we can write:

$$D = D_w + D_p$$

where

$$D_w = \int_{\infty(W)-\infty} \rho u(u_o - u)\,dy$$

so that $C_{D_w} = \dfrac{D}{\frac{1}{2}\rho_o u_o^2 c} = 2\int_{\infty(W)-\infty} \dfrac{\rho u}{\rho_o u_o}\left(1 - \dfrac{u}{u_o}\right) d(y/c)$ ..2.2.4

If we now assume that viscosity in the main stream is negligible and use the energy equation for zero heat transfer and the Prandtl number of unity, we can express C_{D_w} in terms of the increase of entropy across the aerofoil shock system, and we find that:

$$C_{D_w} = 2\int_{\infty(W)-\infty} \left[k - (k+1)e^{-\Delta S/C_p} + \sqrt{(k+1)e^{-2\Delta S/C_p} - ke^{-\Delta S/C_p}}\right] d(y/c)$$

.....2.2.5

where $\Delta S \equiv S - S_o = C_p \dfrac{\gamma-1}{\gamma} \log\left(\dfrac{p_{so}}{p_{so}}\right)$ = increase of entropy along a streamline,

$$k = \frac{2}{\gamma-1}\,\frac{1}{M_o^2}$$

To gain a better insight into the nature of the variation of C_{D_w} with ΔS, we note that to the first order in ΔS eqn. 2.2.5 reduces to

$$C_{D_w} = \frac{k}{C_p}\int_{\infty(W)-\infty} \Delta S\, d(y/c) \qquad .....2.2.6$$

This relation is equivalent to the one given by Liepmann in ref. 11, but had been obtained independently, before a copy of Liepmann's paper became available.

Referring again to fig.1, it will be seen that as the separation near the trailing edge makes the contour ABDCA the effective 'wave-making' contour of the aerofoil, the strength of the trailing edge shock wave is less than that given by the inviscid theory. Now, since ΔS is approximately

/proportional ...

proportional to the third power of the static pressure rise across the shock, one can expect the separation to result in a decrease of the wave drag, owing to the decreased strength of the trailing edge shock. On the other hand, the presence of a weak shock wave just upstream of the Prandtl-Meyer expansion at the leading edge will have the opposite effect. In general, the latter effect is far less significant than the former, as the interaction of expansion waves with the shock wave reduces it, within a short distance from the aerofoil, to little more than a Mach wave (this is discussed in more detail in para. 3.1. below).

If the momentum theorem is now applied to the control surface C_2 (shown in Fig. 2c) and viscosity outside the wake is neglected, the lift on the aerofoil is given by (eqn. AII, 3.2):

$$L = -\int_{AC,DF} \rho u\, v\, dy - \int_{W} \mu\, \zeta\, dy$$

The second term represents the effect of the wake and, as shown in the Appendix II, its contribution to the lift coefficient is $O(R^{-1})$, where R is the Reynolds number based on the aerofoil chord. This is clearly a very small quantity and can be neglected. Hence

$$L = -\int_{AC,DF} \rho u\, v\, dy \qquad \ldots\ldots\ldots 2.2.7$$

To demonstrate the effect of separation it is more convenient to consider the linearised form of 2.2.7, which is obtained by expressing ρ, u, and v as

$$\rho = \rho_o + \rho' \; ; \quad u = u_o + u' \; ; \quad v = v'$$

where ρ', u', v' are perturbation quantities whose products and powers higher than 1 can be neglected. Eqn. 2.2.7 then yields

$$L \doteq -\rho_o u_o \int_{AC,DF} v'\, dy \qquad \ldots\ldots\ldots 2.2.8$$

that is, lift is approximately proportional to the integral of the 'downwash' velocity v', taken along a line downstream of the aerofoil and perpendicular to the free stream direction. Referring again to fig. 1, it will be seen that in addition to decreasing the strength of the trailing edge shock waves, the

/separated ...

separated flow also decreases the 'downwash' velocity above the upper surface, so that the lift coefficient will also be less than that predicted from the inviscid theory.

Summarising, it can be stated without going into the mechanism of the separation at the trailing edge of a supersonic aerofoil, or into the details of the surface pressure distribution, that one can, in general, expect the separation to reduce both the lift and the wave drag. In addition, of course, there is also a further reduction in the total drag, namely that resulting from a decreased skin friction in the separated region where it is either zero or negligibly small.

2.3. Effects of Boundary Layer Displacement Thickness

2.3.1. Concept of the 'equivalent profile'

The fundamental concept of the boundary layer displacement thickness and the 'displacement flux' is not new, but it is only recently that it was successfully applied by Preston (refs. 1 - 3) to assess boundary layer effects on two-dimensional aerofoils in incompressible flow. In ref. 2 Preston shows in detail how the problem of computing the potential flow external to the boundary layer on an aerofoil reduces to the calculation of the potential flow about an 'equivalent profile' formed by adding the boundary layer displacement thickness, δ_1, to the aerofoil; this proof is extended to compressible flow in ref. 13.

In the simple-wave supersonic flow this leads to a particularly simple relation for the change of the local pressure due to the boundary layer which, in turn, permits a direct evaluation of changes in the force coefficients to be made. In the argument that follows the interaction of expansion and shock waves with the boundary layer is ignored, as these effects are dealt with separately.

2.3.2. Aerofoils of arbitrary shape

Consider an aerofoil (fig.3) of arbitrary shape in a uniform supersonic airstream at Mach number M_o; the leading and trailing edges are assumed to be sharp and the slopes of the upper and lower surfaces continuous; the incidence, α, is such that the leading edge shock waves are attached and the flow is everywhere supersonic. The flow over the aerofoil outside the boundary layer is assumed to be irrotational and vorticity behind curved shocks is neglected (c.f. para. 2.6). x, y are

/Cartesian ...

Cartesian coordinates, origin at the leading edge and the x-axis along the aerofoil chord; s, n are curvilinear orthogonal coordinates parallel and normal to the aerofoil surface, respectively. F is the resultant aerodynamic force on the aerofoil, with components X and Y parallel to the x- and y-axes respectively.

Lift and drag coefficients are then given by

$$C_L = C_Y \cos\alpha - C_X \sin\alpha \qquad \ldots\ldots\ldots 2.3.1$$

$$C_{D_w} = C_Y \sin\alpha + C_X \cos\alpha \qquad \ldots\ldots\ldots 2.3.2$$

where $$C_X = \frac{X}{\frac{1}{2}\rho_o U_o^2 c} = \frac{2X}{\gamma p_o M_o^2 c} = \frac{X}{q_o c}\,; \quad C_Y = \frac{Y}{q_o c}$$

The pitching moment coefficient about the leading edge is

$$C_M = \frac{x_{c.p.}}{c} C_Y = \bar{x}_{c.p.} C_Y \qquad \ldots\ldots\ldots 2.3.3$$

where $x_{c.p.}$ = distance of the centre of pressure from the leading edge. Further, denoting by L and U the conditions on the lower and upper surfaces respectively, we have

$$C_Y = \frac{1}{q_o}\left[\int_o^1 p_L \, d\left(\frac{x}{c}\right) - \int_o^1 p_U \, d\left(\frac{x}{c}\right)\right] \qquad \ldots\ldots\ldots 2.3.4$$

$$C_X = \frac{1}{q_o}\left[\int_o^{t_L/c} p_L \, d\left(\frac{Y}{c}\right) + \int_o^{t_U/c} p_U \, d\left(\frac{Y}{c}\right)\right] \qquad \ldots\ldots\ldots 2.3.5$$

$$C_M = \frac{1}{q_o}\left[\int_o^1 p_L\left(\frac{x}{c}\right) d\left(\frac{x}{c}\right) - \int_o^1 p_U\left(\frac{x}{c}\right) d\left(\frac{x}{c}\right)\right.$$

$$\left. + \int_o^{t_L/c} p_L\left(\frac{Y}{c}\right) d\left(\frac{Y}{c}\right) - \int_o^{t_U/c} p_U\left(\frac{Y}{c}\right) d\left(\frac{Y}{c}\right)\right] \qquad \ldots 2.3.6$$

Now, let Δp be the local static pressure increment due to the displacement of flow by the boundary layer. Referring to fig. 4, ψ is the angle between the tangent to the aerofoil surface at a point P and that at the leading edge. At the corresponding point P' at the edge of the equivalent surface formed by adding the boundary layer displacement thickness, the corresponding angle will be $\psi' = \psi - \Delta\psi$,

/where ...

where

$$\Delta\psi = \tan^{-1}\frac{d\delta_1}{ds} \doteq \frac{d\delta_1}{ds}$$

Thus, the change in the local direction of flow due to the presence of the boundary layer is also

$$\Delta\psi = \frac{d\delta_1}{ds} \ .$$

Now, since outside the boundary layer simple-wave flow is assumed

$$-\frac{dp}{p} = \frac{\gamma M^2}{\sqrt{M^2 - 1}}\, d\theta$$

where θ is the flow direction measured from some fixed datum, so that $\theta = \psi + \text{const}$; $d\theta = d\psi$

Thus, we have, approximately

$$\Delta p = \frac{dp}{d\theta}\Delta\theta = \frac{dp}{d\theta}\Delta\psi$$

so that

$$\Delta p = -\frac{d\delta_1}{ds}\frac{dp}{d\theta} = \frac{\gamma p M^2}{\sqrt{M^2 - 1}}\frac{d\delta_1}{ds} \qquad \text{.....2.3.7}$$

Hence, the corresponding increments in the force coefficients are

$$\Delta C_Y = \frac{1}{q_o}\left[\int_o^1 \Delta p_L\, d\left(\frac{x}{c}\right) - \int_o^1 \Delta p_U\, d\left(\frac{x}{c}\right)\right] \qquad \text{.....2.3.8}$$

$$\Delta C_X = \frac{1}{q_o}\left[\int_o^{t_L/c} \Delta p_L\, d\left(\frac{y}{c}\right) + \int_o^{t_U/c} \Delta p_U\, d\left(\frac{y}{c}\right)\right] \qquad \text{....2.3.9}$$

$$\Delta C_M = \frac{1}{q_o}\left[\int_o^1 \Delta p_L \left(\frac{x}{c}\right) d\left(\frac{x}{c}\right) - \int_o^1 \Delta p_U \left(\frac{x}{c}\right) d\left(\frac{x}{c}\right)\right.$$

$$\left. + \int_o^{t_L/c} \Delta p_L \left(\frac{y}{c}\right) d\left(\frac{y}{c}\right) - \int_o^{t_U/c} \Delta p_U \left(\frac{y}{c}\right) d\left(\frac{y}{c}\right)\right]$$

.....2.3.10

where $\Delta p_{L,U}$ is determined from eqn. 2.3.7.

The change in the position of the centre of pressure is given by

$$\frac{\Delta \bar{x}_{c.p.}}{\bar{x}_{c.p.}} \doteq \frac{\Delta C_M}{C_M} - \frac{\Delta C_Y}{C_Y} \qquad \text{.....2.3.11}$$

/Finally ...

Finally,

$$\left.\begin{aligned} \Delta C_L &= \Delta C_Y \cos\alpha - \Delta C_X \sin\alpha \\ \Delta C_{D_w} &= \Delta C_Y \sin\alpha + \Delta C_X \cos\alpha \end{aligned}\right\} \quad \ldots\ldots\ldots 2.3.12$$

If the distribution of the displacement thickness over the surface is known, $\frac{d\delta_1}{ds}$ can be calculated and with eqns. 2.3.7 - 2.3.12 the increments of the force and moment coefficients can be determined. As the first approximation the surface pressure distribution, $\frac{dp}{d\theta}$, is taken as that given by the inviscid shock-expansion theory and, strictly speaking, one should then use the modified pressure distribution to recalculate the development of the boundary layer, which would, in turn, lead to a second approximation to Δp. In practice, however, it is found that the process is rapidly convergent and the first approximation is usually sufficiently accurate, unless the rate of growth of the boundary layer is large.

The methods to be used for computing the development of the boundary layer are discussed in section 4. Even neglecting the heat transfer, δ_1 will be a complicated function of the flow conditions outside the boundary layer, the boundary layer thickness and the Reynolds number:

$$\delta_1 = f\left(M_1 \frac{dp}{ds}, \frac{d^2p}{ds^2}, \delta_1 R_o\right); \quad R_o = \frac{U_o c}{\nu_o} \quad \ldots\ldots 2.3.13$$

and with the existing boundary layer theories it is not possible to express $\frac{d\delta_1}{ds}$ analytically, except for the simplest case of a flat plate. In general, however, for given free stream conditions, angle of incidence and aerofoil shape and with the boundary layer laminar, $\delta_1 \propto \frac{1}{\sqrt{R_o}}$, very nearly so that, other factors being equal,

$$\Delta C_L, \ \Delta C_{D_w}, \ \Delta C_M, \ \Delta \bar{x}_{c.p.} \propto R_o^{-\frac{1}{2}}$$

When the boundary layer is turbulent $\delta_1 \propto \frac{1}{R_o^n}$ where n depends on the index of power assumed for the power law velocity distribution, and is of the order of 0.2. Thus, the effect of the Reynolds number will be more pronounced with the laminar boundary layer than with the turbulent one.

We can gain some further insight into the magnitude of these effects by considering the case of a thin circular arc profile, where certain approximations can be made.

/2.3.3. ...

2.3.3. Thin circular arc profiles

In addition to the system of coordinates used for sections of arbitrary shape, $\emptyset$, the 'angular distance' along the surface is introduced, such that

$$s = r\emptyset \ , \quad \theta = \theta_{L.E.} + \emptyset$$

where r = the radius of the circular arc.

The pressure increment $\triangle p$ (eqn. 2.3.7) is then

$$\triangle p = \frac{d\delta_1}{ds} \cdot \frac{dp}{d\emptyset} = - r \frac{dp}{ds} \cdot \frac{d\delta_1}{ds}$$

Since the profile is assumed to be thin, $s \doteq x$ and

$$\triangle p \doteq - r \frac{d\delta_1}{dx} \frac{dp}{dx} \qquad \ldots\ldots\ldots 2.3.13$$

For simplicity, only the lower surface will be considered.
From 2.3.8

$$\triangle C_Y = - \frac{1}{q_o} \int_o^c \frac{r}{c} \frac{d\delta_1}{dx} \frac{dp}{dx} \, dx$$

By the mean value theorem

$$\triangle C_Y = - \frac{1}{q_o} \frac{r}{c} \left(\overline{\frac{dp}{dx}}\right) \int_o^c \frac{d\delta_1}{dx} \, dx$$

hence

$$\triangle C_Y = - \frac{1}{q_o} \frac{r}{c} \left(\overline{\frac{dp}{dx}}\right) (\delta_1)_{T.E.} \qquad \ldots\ldots\ldots 2.3.14$$

where $\left(\overline{\frac{dp}{dx}}\right)$ is the value of $\frac{dp}{dx}$ at some point between the leading edge ($x = 0$) and the trailing edge ($x = c$). Now, on a circular arc profile the pressure gradient is highest at the leading edge and hence

$$\triangle C_Y \leqslant \frac{1}{q_o} \frac{r}{c} \left| \left(\frac{dp}{dx}\right)_{L.E.} \right| (\delta_1)_{T.E.} \qquad \ldots\ldots\ldots 2.3.15$$

Now, $\frac{1}{q_o} \left(\frac{dp}{dx}\right) c$ is clearly of the same order of magnitude as C_Y, hence

$$\frac{\triangle C_Y}{C_Y} \leqslant O\left[\frac{r}{c}\left(\frac{\delta_1}{c}\right)_{T.E.}\right]$$

/Similarly ...

Similarly,

$$\Delta C_X = -\frac{1}{q_o}\int_o^{c/2} \frac{r}{c}\,\frac{d\delta_1}{dx}\cdot\frac{dp}{dx}\,dy \quad \text{from 2.3.9}$$

$$= -\frac{1}{q_o}\,\frac{r}{c}\int_1^{c}\frac{d\delta_1}{dx}\,\frac{dp}{dx}\,\frac{dy}{dx}\,dx$$

Since $\frac{dy}{dx}$ changes sign at $x = c/2$, the integral must be split into $\int_{c/2}^{c} + \int_o^{c/2}$ before the mean value theorem can be applied.

Hence

$$\Delta C_X = -\frac{1}{q_o}\,\frac{r}{c}\left(\overline{\frac{dy}{dx}}\right)_1\left\{-\left(\overline{\frac{dp}{dx}}\right)_2\left[(\delta_1)_{T.E.} - (\delta_1)_{x=\frac{c}{2}}\right] + \left(\overline{\frac{dp}{dx}}\right)_1 (\delta_1)_{x=\frac{c}{2}}\right\}$$

.....2.3.16

where the suffices 1 and 2 refer to conditions at $0 \leqslant x \leqslant c/2$ and $c/2 \leqslant x \leqslant c$, respectively.

The sign and value of ΔC_X depend on the relative magnitudes of the terms in the 'curly' brackets. If the rate of growth of the displacement thickness downstream of the point of maximum thickness is sufficiently large

$$\left(\overline{\frac{dp}{dx}}\right)_2\left[(\delta_1)_{T.E.} - (\delta_1)_{x=\frac{c}{2}}\right] > \left(\overline{\frac{dp}{dx}}\right)_2 (\delta_1)_{x=\frac{c}{2}}$$

and ΔC_X is negative. Such a state of affairs may arise when the boundary layer is partly turbulent and the transition point is near or at the point of maximum thickness, since for the corresponding points $(\delta_1)_{turbulent} \gg (\delta_1)_{laminar}$.

Thus, with transition near the mid-chord point one can expect that $\Delta C_{D_w} < 0$. This was actually found to be the case in ref. 13 for a 6 per cent bi-convex aerofoil at $M_o = 1.5$.

The order of magnitude of the individual terms in eqn. 2.3.16 can be found by noting that $0 \leqslant \left|\frac{dy}{dx}\right| \leqslant 2\,t/c$ for a thin circular arc profile and hence,

$$\frac{c}{q_o}\left|\left(\frac{dp}{dx}\right)\left(\frac{dy}{dx}\right)\right| = O(C_X)$$

so that $\frac{\Delta C_X}{C_X} = O\left[\frac{r}{c}\left(\frac{\delta_1}{c}\right)_{T.E.}\right]$

/that is, ...

that is, $\frac{\Delta C_Y}{C_Y}$ and $\frac{\Delta C_X}{C_X}$ are of the same order of magnitude. One must remember, however, that the increments ΔC_Y on the upper and lower surfaces are of the opposite sign, whilst the corresponding increments ΔC_X are of the same sign (c.f.fig. 4), consequently, the resultant $\frac{\Delta C_Y}{C_Y}$ will tend to be much smaller than $\frac{\Delta C_X}{C_X}$.

2.3.4. Flat plate at incidence

For a flat plate $\frac{\gamma p M^2}{\sqrt{M^2-1}}$ in eqn. 2.3.7 is constant along the surface, and is a function of the angle of incidence and the free stream conditions only, so that we can write:

$$\Delta p = f(M_o, \alpha) \frac{d\delta_1}{ds} = f(M_o, \alpha) \frac{d\delta_1}{dx}$$

where $f(M_o, \alpha) = \frac{\gamma p M^2}{\sqrt{M^2-1}}$

Hence $$\Delta C_Y = \frac{1}{q_o} \left\{ f_L(M_o, \alpha) \left[\int_o^1 \frac{d\delta_1}{dx} \, d\left(\frac{x}{c}\right) \right]_L - f_U(M_o, \alpha) \left[\int_o^1 \frac{d\delta_1}{dx} \, d\left(\frac{x}{c}\right) \right]_U \right\}$$

or $$\Delta C_Y = \frac{1}{q_o} \left[f_L(M_o, \alpha) \left(\frac{\delta_{1L}}{c}\right)_{T.E.} - f_U(M_o, \alpha) \left(\frac{\delta_{1U}}{c}\right)_{T.E.} \right] \quad 2.3.17$$

and $$\Delta C_L = \Delta C_Y \cos \alpha \; ; \; \Delta C_{D_w} = \Delta C_Y \sin \alpha$$

On a flat plate, the displacement thickness is a function of M_o, α , and R_o and 2.3.17 can be written

$$\Delta C_Y = g_L(M_o, \alpha, R_o) - g_U(M_o, \alpha, R_o)$$

where $$g(M_o, \alpha, R) = \frac{f(M_o, \alpha)}{q_o} \left(\frac{\delta_1}{c}\right)_{T.E.}$$

For the laminar boundary layer with Prandtl number of unity and $\mu \propto T$,

$$\frac{\delta_1}{c} = \frac{1.7208}{R_o} (1 + 0.277 M^2) \sqrt{\frac{x}{c}}$$

/see ...

(see e.g. Refs. 12, 27 and 28), and for given M_o and α

$$\Delta C_Y \propto \frac{1}{\sqrt{R}}$$

2.4. Skin Friction Drag

The total skin friction drag is obtained simply by integrating the local skin friction coefficient over the aerofoil.

Let $\beta = \tan^{-1} \frac{dy}{dx}$, where $y = f(x)$ is the aerofoil contour,

$c_f = \dfrac{\tau_w}{\frac{1}{2}\rho_o U_o^2} \equiv \dfrac{\tau_w}{q_o}$, the local skin friction coefficient.

Then, contribution to the friction drag from the lower surface is

$$\left[C_{D_f}\right]_L = \int_o^1 \cos(\beta+\alpha)\ c_f\ d\left(\frac{s}{c}\right) \qquad \text{.....2.4.1}$$

$$= \int_o^1 (\cos\alpha \cos\beta - \sin\alpha \sin\beta)\ c_f\ d\left(\frac{s}{c}\right)$$

or,
$$\left[C_{D_f}\right]_L = \cos\alpha \int_o^1 c_f\ d\left(\frac{x}{c}\right) - \sin\alpha \int_o^{\frac{1}{2}t/c} c_f\ d\left(\frac{y}{c}\right) \qquad \text{....2.4.2}$$

Unless the incidence is high ($\alpha \gtrsim 15\text{-}20^o$) and the aerofoil thick ($t/c \gtrsim 0.1$), the second term in the above equation is much smaller than the first and we can write without any significant loss of accuracy

$$\left[C_{D_f}\right]_L \doteq \cos\alpha \int_o^1 c_f\ d\left(\frac{x}{c}\right)$$

so that

$$C_{D_f} = \cos\alpha \left[\left(\int_o^1 c_f\ d\bar{x}\right)_U + \left(\int_o^1 c_f\ d\bar{x}\right)_L\right] \qquad \text{.....2.4.2a}$$

In incompressible flow the skin friction drag is usually determined together with the form drag from the momentum thickness of the wake at infinity downstream (c.f. eqn. 2.2.3a). In the supersonic case, this method would only give the skin friction drag and a part of the form drag. To determine the whole of the form drag (which in this case is equal to the change in wave drag due to the presence of the boundary layer),

/losses ...

losses of the total head caused by the shock waves outside the wake must also be considered. Inside the wake itself, two effects are combined: losses of the total head due to the rotational character of flow in the boundary layer, and those caused by shock waves, as streamlines which enter the boundary layer from the main stream have already suffered losses of stagnation pressure across the leading edge shock waves.

Furthermore, there is the additional difficulty of determining what effects the trailing edge shock waves have on the momentum thickness and what is the variation of the momentum thickness between the trailing edge and infinity downstream. In ref. 35 the latter is assumed to be the same as for turbulent wakes in incompressible flow, and a relation suggested by Tetervin is used to account for the effect of the shock waves. As the validity of these assumptions is dubious, it is believed more accurate to estimate the profile drag by calculating the skin friction drag and the change in wave drag separately from the local skin friction and the local changes of pressure distribution, respectively.

2.5. Heat Transfer

Unless otherwise stated, all the considerations of the present study are based on the assumption that the aerofoil surface is a perfect thermal insulator and no heat is transferred from the boundary layer.

In actual fact, with Mach numbers of the order of 2 or higher, heat transfer may be of considerable importance, particularly from the point of view of the stability of the laminar boundary layer (c.f. para.5). However, owing to the manner in which the coefficients of viscosity and heat transfer enter the boundary layer equations, the thermal and viscous effects are qualitatively similar and do not fundamentally affect the nature of the boundary layer phenomena. Consequently, it was considered that, for the present purpose, neglecting the heat transfer was justified by the resulting simplification of the mathematical treatment and it is hoped that quantitative results are not unduly affected.

2.6. Vorticity

Another effect which has been neglected is that of vorticity generated by the leading edge shock waves. When the surface of an aerofoil is curved, the expansion waves interact

/with the ...

with the leading edge shock wave which is then curved and the flow downstream of the shock wave is rotational. The simple-wave flow relations then hold only approximately, and for a more accurate determination of the surface pressure distribution the method of characteristics for rotational flow (refs. 18 and 19) should be used. However, as this method involves a laborious process of successive approximations and since in most cases of practical interest the effects of vorticity are very small, they are usually neglected.

The vorticity behind a curved shock can be shown to be given by (e.g. ref. 39): $\zeta = \frac{p}{R} \frac{dS}{d\psi}$ where R is the universal gas constant and ψ is Crocco's stream function. Along the aerofoil surface ψ = const., hence ζ is proportional to the static pressure. On a convex aerofoil the static pressure is highest at the leading edge and decreases towards the rear, therefore, the effects of vorticity are greatest near the leading edge. The pressure gradient immediately downstream of the leading edge shock wave can be determined analytically from the curved-shock relations first obtained by Crocco (L'Aerotechnica, 17, 1937), and, more recently, by Lin and Rubinov (ref. 39):

$$\frac{\partial p_1}{\partial s} = - \frac{\gamma p_o M_o^2 \left[\sin 2\xi - \frac{\gamma+1}{\gamma} \frac{\sin 2\xi}{\cos^2(\xi-\delta)} \right]}{1 + \sin^2(\xi-\delta)(M_1^2-2) - \frac{\gamma+1}{4} \frac{\sin 2\delta}{\sin 2\xi}} K$$

where the suffix 1 refers to conditions just downstream of the shock

δ = deflection of flow across the shock at that point

ξ = local angle of inclination of the shock relative to the free stream direction

$K \equiv \frac{\partial \delta}{\partial s}$ = curvature of the streamline just downstream of the shock.

s = length of arc of the streamline

If simple wave flow is assumed downstream of the shock, with the streamline having the same curvature K, we have from the Prandtl-Meyer relation

$$\frac{dp_1}{p_1} = - \frac{\gamma M_1^2}{\sqrt{M_1^2-1}} d\delta$$

/hence ...

hence $$\left(\frac{\partial p_1}{\delta s}\right)_{S.W.} = -\frac{\gamma\, p_1\, M_1^2}{\sqrt{M_1^2 - 1}}\, K = -\frac{\gamma\, p_o M_o^2 (\gamma+1) M_1^2 \sin^2\xi}{\left[(\gamma-1)M_1^2 \sin^2(\xi-\delta)+2\right]\sqrt{M_1^2-1}}\, K$$

so that

$$\frac{\partial p_1}{\partial s}\Big/\left(\frac{\partial p_1}{\partial s}\right)_{S.W.} = \frac{\left[\sin 2\xi - \frac{\gamma+1}{\gamma}\frac{\sin 2\xi}{\cos^2(\xi-\delta)}\right]\left[(\gamma-1)M_1^2 \sin^2(\xi-\delta)+2\right]\sqrt{M_1^2-1}}{\left[1 + \sin^2(\xi-\delta)(M_1^2-2) - \frac{\gamma+1}{4}\frac{\sin 2\delta}{\sin 2\xi}\right](\gamma+1)\, M_1^2 \sin^2\xi}$$

For the particular case of a 10 per cent circular arc profile at $M_o = 2.13$, the following values were obtained for the ratio of the pressure gradient behind the curved shock at the top surface, to that given by the simple-wave flow theory:

α	12.5°	10°	7.3°	0.1°	-10°	-11.4°
M_1	1.10	1.27	1.40	1.70	2.07	2.13
$\frac{\partial p}{\partial s}\Big/\left(\frac{\partial p}{\partial s}\right)_{S.W.}$	1.053	1.024	1.012	1.003	1.001	1.0000

Thus, the simple-wave flow gives a very good approximation even at the leading edge, except when the Mach number there (M_1) approaches unity and $-\left(\frac{\partial p}{\partial s}\right)_{S.W.} \to \infty$; the approximation becomes progressively better downstream, as $\zeta \propto p$.

On wedge sections, conditions at the surface are not affected by the vorticity, since regions where the shock waves become curved are well away from the surface, provided that the shock waves are attached. The shock-expansion theory is then an exact inviscid theory.

3. EXAMINATION OF LOCAL FLOW CONDITIONS

We now turn our attention to a more detailed examination of the local flow conditions, to which the considerations of the preceding section do not strictly apply.

3.1. Conditions at the Leading Edge

As was already mentioned in para. 2.1, the flow patterns found in practice near the leading edges of supersonic aerofoils differ appreciably from those predicted theoretically. The most striking discrepancies are found in cases when, according to the inviscid theory, the flow should undergo a Prandtl-Meyer expansion round the sharp edge. In practice, there is always a weak shock wave preceding the expansion and, in some cases, this expansion is associated with a local separation of

/the ...

the boundary layer, followed by another weak shock (figs. 5a,b,c). Such patterns have been observed in many experimental investigations, the details of which will be found in ref. 4,5,10,14-16.

If one attemps to explain this phenomenon, two alternatives suggest themselves: the effect of bluntness of the leading edge which, of course, cannot be made perfectly sharp, or, the effect of the initial high rate of growth of the boundary layer. Bardsley (ref. 16) claims that the first alternative is the only possible explanation, and that the existence of the shock wave cannot be explained by considerations of viscous effects. His argument is based on the fact that at the point where the rate of growth of the boundary layer displacement thickness is sufficiently high to cause a compression of the stream at the leading edge instead of an expansion, the displacement thickness would be of the same order of magnitude as the thickness of the leading edge, so that its effect on the formation of the shock would be negligible compared to that of the leading edge itself. Now, whilst it is obvious that the mere fact of the leading edge being blunt does explain the formation of the shock wave without any considerations of the viscous effects, it is not true to say that this is the only possible explanation. It can be shown just as easily that, were it possible to have a perfectly sharp leading edge, one should still expect the formation of a shock wave preceding the Prandtl-Meyer expansion.

Consider the idealised case of an infinitely thin flat plate (fig. 6a), so that the question of the finite thickness of the leading edge does not enter into the argument. ABC is the streamline just outside the surface of the plate. Along AB the flow is uniform and has the supersonic free stream velocity u_o. At B, according to the usual boundary condition at the surface of a body in a real fluid, the velocity is zero. In actual fact, there will probably be initially some slip at the surface, but even so, the flow along ABC would have to decelerate violently at B to reach at least a subsonic velocity within a very short distance from B. This is very much like the change that flow undergoes inside a shock wave. If there is to be no shock wave formed, this process would have to occur at constant pressure. The difficulty of imagining a process in which an almost discontinuous decrease of velocity in the direction of flow is not associated with a corresponding pressure increase, is obviated if one postulates the existence of a stagnation point at the leading edge, preceded by a normal shock (fig. 6b).

/The ...

The velocity at D (just downstream of the shock) would then be subsonic; from D to B the flow would be gradually compressed and brought to rest at the stagnation point, and the boundary layer would start there with a finite thickness. Outside the boundary layer, the flow would accelerate to sonic velocity and then expand to return the main stream to the required direction. The strong expansion waves would interact with the bow-wave, reducing its strength, so that within a short distance from the leading edge it would become a weak compression wave.

This qualitative argument is supported by some of the results of the fundamental investigation of the theory of viscous compressible fluids, which is being carried out at the C.I.T. by Lagerstrom, Cole and Trilling (ref. 17). Since the existing theory of differential equations appears to be inadequate for the general solution of the full Navier-Stokes equations for viscous compressible fluids, the approach adopted in ref. 17 is to deal with the linearised form of these equations and to consider their application to certain idealised cases. So far, no complete analytic solution has been obtained even for the simple problem of a flat plate at zero incidence in supersonic flow, but general properties of the solution are fairly clear. It is found that transverse and longitudinal waves are propagated by the plate into the stream. The longitudinal waves are of maximum strength near the leading edge and consist of compression waves followed by expansion waves. Moreover, there are also pressure disturbances propagated upstream even in the supersonic case, though they are subject to heavy exponential damping. The boundary layer theory applied to the Navier-Stokes equations accounts only for a part of the transverse wave component, and the application of the concept of the displacement thickness - for some of the longitudinal waves. Far downstream (on a semi-infinite flat plate), the full solution approaches asymptotically the boundary layer solution.

The possibility just considered, that the viscous effects alone can cause the formation of a shock wave in front of the Prandtl-Meyer expansion round a perfectly sharp leading edge, though interesting in itself, is of rather academic importance, as in practice no perfectly sharp leading edge can be made; on the other hand, it does demonstrate that even when the bluntness of the leading edge is the primary cause of the presence of the shock wave, one can still expect the boundary layer to have at least some important modifying effects on the flow pattern. In particular, it helps to explain why a local flow separation just downstream of the leading edge is sometimes

/observed ...

observed.

For simplicity consider a leading edge of a regular shape (fig. 5IIa,b), with square corners and of thickness ℓ. The position of the stagnation point on ℓ will depend on the incidence, but for the present purpose it can be taken to be situated halfway between the two corners A and B. The boundary layer has some finite displacement thickness at A and B, $(\delta_1)_\ell$, say. If ℓ is of the same order of magnitude as $(\delta_1)_\ell$, the effective thickness of the leading edge is considerably increased and results in the formation of a stronger shock wave than would be the case if there were no boundary layer. For $\ell \gg (\delta_1)_\ell$, this effect will be obviously negligible. On the other hand, when conditions at the corner A or B are considered, it will be seen that as on the surface the velocity of flow is zero, the region of flow in a thin layer next to the surface must have subsonic velocity. Now, subsonic compressible flow round a sharp corner is impossible, as according to the incompressible flow theory the velocity would be infinite there, which in turn implies that compressible flow would become supersonic. Thus, if the flow is to remain subsonic near the surface, as it must, it has to separate at some distance from the corner and continue along a finite radius (figs. 7a,b). Physically, the separation can be explained as induced by the suction, which is created by the high curvature of the streamlines of the subsonic flow round the corner.

The extent of the separated region will be much smaller than ℓ, as in incompressible flow the region in which the velocity tends to infinity is confined to the immediate vicinity of the sharp corner. Hence, when ℓ is of the same order of magnitude as $(\delta_1)_\ell$ or smaller, the separation will hardly influence the outer edge of the boundary layer and the external flow (fig. 5IIb). When $\ell > (\delta_1)_\ell$, the size of the separated region may well be of the same order as the boundary layer thickness, and a flow pattern as in fig. 5IIa would result. The extent of the separation will also depend on the amount of expansion that the main stream undergoes outside the separated boundary layer. Expansion to a high supersonic Mach number would create a further suction effect and enhance separation.

This suggests that the boundary layer has a considerable influence on the conditions near the leading edge and may explain why the local separation has been observed in some

/cases ...

cases and not in others. Thus e.g., on the wedge used by Bardsley, with $\ell \doteq 8 \times 10^{-4}$cm, no evidence of separation was found, whilst Valensi and Pruden observed separation on a wedge which had a relatively much thicker leading edge ($\ell \doteq 5 \times 10^{-3}$cm).

Fig. 8 shows shadowgraphs and a schlieren photograph taken at the N.P.L. in the course of investigations reported in refs. 6 and 7, and illustrating typical flow patterns near the blunt noses of thick flat plates. In (a), the flow pattern corresponds to that described above (c.f. fig. 5IIa), but (b) and (c) exhibit some novel features. In (b) separation followed by a weak shock can be observed, though the nose of the plate is elliptic and there are no sharp corners; in (c) there is no evidence of separation, but the weak compression wave does not disappear. It is suggested that this is probably caused by the high favourable pressure gradient inducing a local thinning of the boundary layer. That such thinning is possible, can be readily demonstrated for the case of the self-induced pressure gradient on a flat plate.-

According to the concept of the displacement thickness, the flow is displaced from the surface by an angle θ, such that $\theta = -\frac{d\delta_1}{dx}$. Combining this with the Prandtl-Meyer relation we have

$$\frac{d^2\delta_1}{dx^2} = \frac{\sqrt{M^2 - 1}}{\gamma M^2} \frac{1}{p} \frac{dp}{dx} \qquad \ldots\ldots\ldots 3.1.1$$

Integrating 3.1.1 once

$$\left(\frac{d\delta_1}{dx}\right)_2 = \frac{1}{\gamma} \left(\frac{\sqrt{M^2 - 1}}{M^2}\right) \log \frac{p_2}{p_1} + \left(\frac{d\delta_1}{dx}\right)_1 \qquad \ldots\ldots\ldots 3.1.2$$

where the suffices 1 and 2 refer to two stations on the surface of the plate (2 is downstream of 1), and $\left(\frac{\sqrt{M^2-1}}{M^2}\right)$ is evaluated somewhere between 1 and 2. Now, with a favourable pressure gradient $p_1 > p_2$ and if this gradient is sufficiently high (i.e. $\frac{d\theta}{dx} = \frac{d^2\delta_1}{dx^2}$ sufficiently large),

$$-\frac{1}{\gamma} \left(\frac{\sqrt{M^2 - 1}}{M^2}\right) \log \frac{p_2}{p_1} > \left(\frac{d\delta_1}{dx}\right)_1$$

so that at station 2 the rate of growth of the boundary layer is negative and a flow pattern similar to that shown in fig. 9

/may ...

may result. In general, the curvature of the boundary layer would have to be high to induce sufficiently high pressure gradients, and the concept of the displacement thickness would not strictly apply. However, at Mach numbers near 1 (as is the case with flow round blunt noses) flow is very sensitive to changes of direction and high pressure gradients can be induced by only small curvatures.

To explore this possibility further, calculations were made using pressure distributions obtained on elliptical nosed flat plates at the N.P.L. (fig. 10). It was assumed that the direction of flow at the body sonic point was the same as that just downstream of the bow-wave sonic point, and that downstream of the body sonic point simple-wave flow relations hold. The slope of the equivalent surface (θ) was then calculated from the experimental pressure distributions and the rate of growth of the boundary layer displacement thickness found from the relation

$$\frac{d\delta_1}{dx} = \tan(\theta-\beta)$$

where $\beta \equiv \tan^{-1}\frac{dy}{dx}$ is the slope of the surface of the plate. Finally, the development of the displacement thickness in terms of δ_1 at the sonic point was obtained by a numerical integration of the above relation. As will be seen from fig. 10, the result appears to confirm the possibility of the thinning of the boundary layer. The actual numerical values should not be taken too literally, as in calculating the flow direction from the pressure distribution no account was taken of the possibility of transverse pressure gradients in the boundary layer. This, combined with the assumption of simple-wave flow probably makes the thinning of the boundary layer appear far more drastic than it actually is, but the result is believed to be at least qualitatively correct.

An attempt was made to improve on these calculations by applying the method of characteristics for the rotational flow on the lines suggested by Meyer and by Ferri (references 18 and 19), which involves a somewhat complicated iterative procedure. Unfortunately, it was found that owing to the proximity of the sonic line (whose shape has to be assumed) the iterative process is very slowly convergent and depends critically on the assumed form of the sonic line, so that its results would be of doubtful accuracy.

/Effect ...

Effect of flow pattern at the leading edge on conditions downstream.

Analytic treatment of the effects so far discussed in this section appears to be, at present, out of reach. The difficulties are two-fold: the boundary layer theory which is, of course, an asymptotic theory for high Reynolds numbers obviously does not apply near the leading edge, and the problem of the flow outside the boundary is, essentially, a transonic one. Nevertheless, if one is to assess the overall boundary layer effects one must try to investigate how the leading edge flow pattern affects the conditions downstream.

In ref. 13 it was found that although the leading edge shock is, strictly speaking, detached at all angles of incidence, the surface pressure distribution calculated assuming an attached shock or an expansion (as may be the case), shows a very much better agreement with experiment than that obtained by applying the approximate method for flow behind detached shocks given in ref. 20.

To confirm this, pressure distributions were calculated for the wedge sections tested by Liepmann (ref. 15) and at the R.A.E. (ref. 10). Leading edge shock angles were assumed to be these given by the inviscid shock-expansion theory, and allowance for the boundary layer was made as indicated in para. 2.3., using Young's flat plate solution for laminar boundary layer (ref. 12). Fig. 11 shows that there is a very good agreement between the calculated and the experimental pressure distributions except very near the leading edge and near the sharp shoulder, and that the allowance for the boundary layer displacement thickness results in a definite improvement on the inviscid theory. It is, therefore, concluded that for the purpose of assessing the boundary layer effects on the surface pressure distribution, the shock-expansion theory should be used to determine the flow conditions outside the boundary layer.

Considerations of para. 2.2. suggest, however, that the local increase in shock strength at the leading edge may have a measurable effect on the wave drag. Magnitude of this effect can be assessed by assuming that the full stagnation pressure behind a normal shock acts on the leading edge. This somewhat crude assumption is justified by the fact that for a supersonic aerofoil the thickness of the leading edge, though by necessity finite, will be very small compared with the chord length and the maximum thickness of the profile. The contribution

/of the ...

of the leading edge to the wave drag is then given by

$$(\Delta D_w)_{L.E.} \doteq (p_{s1} - p_o)\ell$$

where p_{s1} = the stagnation pressure behind the normal shock,
p_o = the free stream static pressure,

to that

$$\left.\begin{aligned}(\Delta C_{D_w})_{L.E.} &\doteq \frac{2}{\gamma M_o^2}\left(\frac{p_{s1}}{p_o} - 1\right)\frac{\ell}{c} \\ &= f(M_o)\,\frac{\ell}{c}\end{aligned}\right\} \quad \ldots\ldots\ldots 3.1.3$$

From the normal shock relations we find that, with $\gamma = 1.4$,

$$\frac{p_{s1}}{p_o} = \frac{p_{s1}}{p_{so}} \times \frac{p_{so}}{p_o} = \left(\frac{7}{6}M_o^2 - \frac{1}{6}\right)^{-2.5}\left(\frac{M_o^2 + 5}{6\,M_o^2}\right)^{-3.5}\left(1 + \frac{M_o^2}{5}\right)^{3.5}$$

and the numerical values of $f(M_o)$ are

M_o	1	2	3	4	∞
$f(M_o)$	1.28	1.66	1.76	1.79	1.84

Hence for Mach numbers between 2 and 3 the value of $f(M_o)$ can be taken as 1.7, say. Then,

$$(\Delta C_{D_w})_{L.E.} \doteq 1.7\,\frac{\ell}{c} \qquad \ldots\ldots\ldots 3.1.4$$

Thus, e.g., for a 2-inch chord aerofoil with $\ell/c = 0.001$ as a typical value, $(\Delta C_{D_w})_{L.E.} = 0.0017$ which can be a considerable percentage of the total wave drag (e.g. at $M = 2.13$, $\alpha = 0^\circ$ and $t/c = 10$ per cent, $C_{D_w} = 0.0288$, so that $\dfrac{(\Delta C_{D_w})_{L.E.}}{C_{D_w}} = 0.06$, or 6 per cent).

It is possible to develop a more elaborate treatment for estimating $(\Delta C_{D_w})_{L.E.}$, based on the approximate methods for detached shocks, but since in practice the shape of the leading edge is irregular (c.f. ref. 16), some arbitrary assumptions must, in any case, be made.

/3.2. ...

3.2. Conditions at Shoulders of Wedge Sections

Flow conditions at sharp shoulders of wedge sections are in many respects similar to those near the leading edge. Although far less experimental evidence is available, the flow patterns appear, in most cases, to be rather like that shown diagrammatically in fig. 12b. The expansion fan which theoretically should originate from the vertex, starts a little upstream of the shoulder. The boundary layer appears to thin immediately downstream of the shoulder, becomes concave and causes a local compression (also c.f. fig. 17).

The latter effect can be explained in terms of the thinning of the boundary layer caused by the high negative pressure gradient, as in the case of flow near the leading edge (c.f. p. 26 above). It is also suspected that there is a small region of local separation in the immediate vicinity of the vertex, for reasons stated in the preceding section (p. 25), and it is believed that this could be observed experimentally, if the flow configurations were examined on a sufficiently large scale.

Experiments show that the expansion influences the surface pressures by diffusion of pressure through the subsonic part of the boundary layer. The extent of this diffusion will, of course, depend on the state of the boundary layer and the Reynolds number. At $R \approx 0.5\text{-}1.0 \times 10^6$ and with a laminar boundary layer, the region affected by the expansion is, in each direction, of the order of 5-10 boundary layer thicknesses just upstream of the shoulder (see e.g. refs. 10 and 15). Two typical examples of observed pressure distributions are given in fig. 11. As will be seen from the diagram 12d, the modified pressure distribution will have little effect on lift, but it may cause a noticeable reduction in wave drag.

In addition to influencing the local surface pressures, the conditions at the shoulder may have important effects on the subsequent development of the boundary layer downstream of the shoulder. Until more experimental evidence is available, it is not possible to say on the basis of the existing theories, what these effects are likely to be. For the purpose of calculating the boundary layer development on the aft part of a double-wedge profile, an acceptable assumption would be to consider the momentum thickness as being continuous across the shoulder, as a discontinuity in the momentum thickness there would imply, if taken literally, the existence of an infinite force.

/As to ...

As to the possibility of the shoulder causing transition, the little experimental evidence available seems to indicate that this is not the case. In the course of some tests at the N.P.L. it was observed that the spread of turbulence caused by a disturbance on the surface of a double-wedge aerofoil was, in fact, suppressed by the expansion at the shoulder (fig. 12c).

3.3. Conditions at the Trailing Edge

The neighbourhood of the trailing edge of a two-dimensional supersonic aerofoil is another region where flow configurations observed in wind-tunnel tests very often differ vastly from those predicted by the inviscid theory.

The actual flow patterns depend on the particular test conditions and the aerofoil geometry. In general, however, at least one shock wave is formed at the trailing edge, to return the flow over the surface to approximately the free stream direction. Since in the subsonic part of the boundary layer no discontinuity of pressure can occur, the pressure rise across the shock is diffused upstream. This results in an adverse pressure gradient, the boundary layer thickens rapidly and in some cases separation of flow occurs at a point upstream of the shock.

In fig. 13 are shown diagrammatically some typical flow patterns associated with the boundary layer separation. In general, the following possibilities exist:

(i) separation on both surfaces,
(ii) separation on one surface only,
(iii) no observable separation.

Which of these possibilities does in fact occur, depends primarily on the shock strength, the state and thickness of the boundary layer, the shape of the aerofoil contour near the trailing edge and - since the flow near the surface is subsonic - on the conditions at the other surface.

Effects of state of boundary layer, shock strength and pressure gradient

Experiments on reflection of shock waves from boundary layers on plane surfaces (refs. 21 and 22) have indicated that with the boundary layer laminar, even very weak shock waves with pressure ratios of the order of 1.01 cause the boundary layer to separate upstream and that it is, in fact, extremely difficult to obtain a reflection of an incident shock without

/the ...

the separation taking place (c.f. ref. 21). On the other hand, with turbulent boundary layers, shock waves of pressure ratios up to 1.8 have been found to cause no separation (refs. 21 - 23). In a similar manner, the extent of the upstream influence shock waves exert through the subsonic part of a laminar boundary layer is found to be roughly 10 times that for the turbulent boundary layer, typical figures being 100 and 10 displacement thicknesses respectively. Two suggestions have been put forward by various writers to explain these different reactions - first, the difference in the thickness of the subsonic region of laminar and turbulent boundary layers, this thickness being relatively smaller in the case of the turbulent layer, and second - the difference in the velocity profiles of the two layers. The latter alternative appears to be more plausible, as for given external flow conditions, the turbulent boundary layer is much thicker than the laminar and their subsonic sub-layers are, in fact, of similar thickness.

Towards the rear of a convex supersonic aerofoil, the pressure gradient is favourable and one would expect the region of interaction to be more restricted in size than would be the case with a wedge aerofoil or a flat plate. However, the greater the curvature of the surface near the trailing edge, the greater is the trailing edge angle and, consequently, the greater the strength of the shock wave formed there for a given incidence and free stream Mach number, which in turn tends to increase the extent of the shock wave - boundary layer interaction. Similarly with a concave trailing edge the shock strength is reduced but the pressure gradient is adverse. Thus, these two effects are interconnected and tend to cancel out, so that one might expect the separation to be governed mainly by the angle of incidence and the free stream conditions. Moreover, once the boundary layer has separated, the actual shape of the trailing edge region cannot have much influence on the conditions of flow there, because of the presence of a 'dead-water' region between the main stream and the surface of the aerofoil, except at small angles of incidence, when the dead-water region is small and mixing takes place. This is, of course, only a crude and greatly oversimplified representation of the actual flow conditions, but the little experimental evidence that is at present available seems to support it.

In figure 14 is shown the variation of the pressure in the separated region with the angle of incidence. The data are collected from the experimental results for a 10 per cent circular arc profile presented in refs. 4 and 10, and from some

/unpublished ...

unpublished results of tests on a 9 per cent thick symmetrical aerofoil with a concave trailing edge of 4° angle. The Mach number range is 1.6 to 2.5 and the average Reynolds number is of the order of 0.7×10^{6}; the boundary layer is laminar in all cases. It is seen that p_{sep}/p_{o}, the ratio of the pressure in the separated region to the free stream static pressure (which is also approximately equal to the reciprocal of the pressure rise across the trailing edge shock), is practically independent of the free stream Mach number, and that for angles of incidence greater than about 6° the trailing edge angle has no appreciable effect. With $\alpha < 6^{\circ}$, p_{sep}/p_{o} is higher for the concave trailing edge section than for the circular arc profile, but the difference is far less than one would expect from comparison of the theoretical shock strengths in the two cases. It must be emphasized, however, that these results do not include the effects of the Reynolds number, which was of the same order of magnitude in all cases. Likewise, the apparently negligible effect of the Mach number is probably due to the small range of variation of M, and to the fact that M and R were not varied independently. To obtain a true picture of the effects of these two parameters, tests should be made in which these effects are separated.

In addition to the trailing edge shock wave, there is usually a weak shock formed at the point of separation of the boundary layer (fig. 13). This shock is usually more pronounced in the case of a bi-convex profile than that of a double-wedge, where the compression is more gradual and spread over a larger distance. It is thought that on a convex surface this shock is the immediate cause of separation. The process through which flow stabilises itself might be as follows. The trailing edge shock initiates the separation and at the point of breakaway, where the boundary layer turns through some small angle to leave the surface, a weak shock is formed. This, in turn, induces further separation and the point of breakaway moves upstream until it reaches a region where the external pressure gradient is sufficiently high and the boundary layer sufficiently thin to prevent any further separation.

Fig. 15 shows the variation of the pressure rise across this shock, for the 10 per cent circular arc profiles referred to above. It is seen that the strength of the shock increases both with the angle of incidence and free stream Mach number, but is subject to unknown Reynolds number effects.

An attempt is made in ref. 10 to obtain an

/empirical ...

empirical estimate of the strength of this shock wave, and also of the pressure in the separated region, by considering supersonic flow over forward and backward facing steps, which are claimed to be simplified models of the flow conditions near the trailing edge. In actual fact, there seems to be no direct analogy between the two problems, other than perhaps a superficial similarity in the real flow patterns. If one considers supersonic flow past a right-angled backward facing step, the necessity for a separation of flow in the corner ABC arises

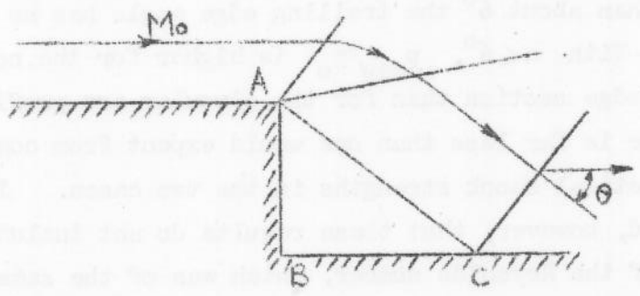

even in the inviscid case, as there is an absolute maximum on the shock deflection θ, for a given upstream Mach number, M_o. In addition to the limiting solution, when $\theta = \theta_{max}$, there is an infinite number of possible solutions, all satisfying the boundary conditions far downstream. The inviscid solution not being unique one is led, in trying to find a guide to the choice of a particular solution, to the consideration of the viscous effects. Thus, the boundary layer cannot be said to cause the separation of flow, which must occur in any case, but on the other hand it is to be expected to have a governing influence on the flow pattern, which is otherwise indeterminate. This is fundamentally quite different from the phenomena occuring near the trailing edge, where the inviscid solution is unique and viscosity can only have a modifying influence. Therefore, it is not surprising that, as concluded in ref. 10, the flow over steps does not appear to have sufficient resemblance to the separation of flow from aerofoils.

Pressure distributions in the separated region

For aerofoils with either convex or concave trailing edges, experiments (refs. 4 and 10) show that the pressure in the separated region remains approximately constant along the surface, between a point downstream of the separation point and the trailing edge (c.f. fig. 25). This indicates that there is little mixing in the dead-water region, except perhaps near the point of breakaway, where the static pressure is lower than it is downstream. In fig. 16 is shown the variation of the extent of the separation, x_s, with the angle of incidence, for the 10 per cent circular arc aerofoils. x_s is

/arbitrarily ...

arbitrarily defined as the distance upstream of the trailing edge within which the pressure is approximately constant. These data are subject to the limitations already mentioned in connection with figs. 14 and 15.

When the trailing edge is straight, as in the case of a double-wedge profile, appreciable pressure gradients are sometimes observed in the separated region, at small or moderate angles of incidence (a typical example of such a pressure distribution is shown in fig. 17). This implies that there is some considerable mixing and reversed flow in the separated region, and it is thought that this is caused by the proximity of the separated jet to the aerofoil surface. With the trailing edge convex or concave, or with straight trailing edges at high incidences, the jet separates clear of the surface within a short distance from the point of breakaway and the reversed flow is less pronounced. There is also a possibility of the separated jet becoming turbulent and re-attaching itself to the surface before it reaches the trailing edge.

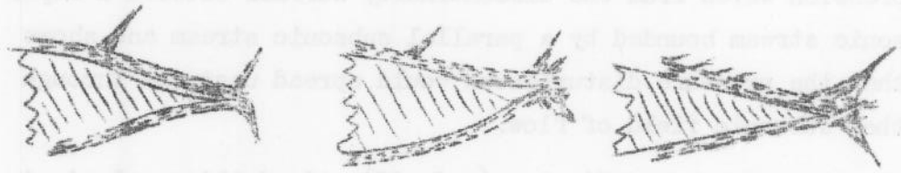

In addition to decreasing the wave drag and lift, the pressure in the dead-water region has important effects on the conditions on the other surface. If this pressure is lower than that just upstream of the trailing edge on the other surface, an expansion must occur there (as the pressure in the dead-water region must be continuous), and no separation takes place on the other surface; if it is higher, separation is likely to occur on both surfaces.

Review of theoretical studies

Even in the comparatively simple case of an oblique shock incident on a plane surface, little progress has been made with theoretical analysis of the shock wave - boundary layer interaction. The basic difficulty derives from the fact that some of the fundamental assumptions of the boundary layer and of the shock wave theories are incompatible; for instance, the former assumes changes of velocity and pressure in the direction of flow to be negligible compared with those

normal to the direction of flow, whereas in the latter the reverse is assumed to be the case. It would appear that one has to use the full equations of motion of a viscous compressible fluid in the regions where both the boundary layer and the shock wave effects are important. Whilst it may be possible to develop some sort of a numerical process to solve these equations, such approach, apart from being of doubtful validity, would give no insight into the nature of the phenomena and their mechanism. Consequently, all the attempts at analytical treatment have so far been based on assumptions which are not, strictly speaking, justified and deal with idealised cases and flow models which have little immediate application to real flow problems.

Howarth (ref. 24) considers the reflection of compression waves from the discontinuity surface between a supersonic stream bounded by a parallel subsonic stream and shows that the pressure disturbances would spread upstream through the subsonic field of flow.

Tsien and Finston (ref. 25) extend this analysis to the case in which the subsonic stream is bounded on the other side by a solid surface, but neither of these investigations takes account of viscosity.

Oswatitsch and Wieghardt (ref. 26) consider the interaction between the boundary layer and the main supersonic stream, by making use of the concept of the equivalent boundary defined by the boundary layer displacement thickness, and by satisfying von Karman's momentum equation for flow within the boundary layer. They find that under these conditions, small pressure disturbances propagated along the surface grow exponentially with the distance along the surface in the limiting case of a vanishingly small pressure gradient.

Lees (ref. 41) applies this approach to the problem of an oblique shock incidence on a flat plate. He uses the standard Pohlhausen method for laminar boundary layers, as modified by Dorodnitzyn to allow for the effects of compressibility, and finds that:

(i) the pressure rise across the shock diffused upstream of the foot of the shock decreases exponentially with the distance from the foot,

(ii) the relaxation distance, $\frac{l}{(\delta_1)_o}$, defined as the distance in which the pressure rise decreases to 1/e of its original value, increases with the Reynolds number based on $(\delta_1)_o$ and decreases with the Mach number M_o (the suffix o

/refers ...

refers to conditions far upstream, where the boundary layer can be considered to be undisturbed by the shock wave),

(iii) for $M_o > 1.25$, all incident shocks with deflections greater than about 1^o will cause separation.

Now, whilst these results are, in themselves, of considerable interest and appear to agree qualitatively with experiment, it is doubtful whether they are very reliable quantitatively, owing to the nature of the assumptions and simplifications involved in the analysis. To begin with, the Pohlhausen approximation is known to give unreliable results for boundary layers in adverse pressure gradients even in the incompressible case, and there is no reason to expect it to be any more accurate for compressible flow. Further, Lees assumes that the pressure gradient is small and linearises the differential equation for the modified Pohlhausen parameter

$$\lambda = \delta^{*2} \frac{1}{1 - u_1^2} \frac{du_1}{dx} .$$

This linearisation is a fairly good approximation for $0 < (-\lambda) < 6$, but becomes progressively worse as $(-\lambda)$ approaches its value of 12 (or 10, as arbitrarily assumed by Lees) at the separation. In common with other boundary layer methods, the transverse pressure gradients across the boundary layer are neglected, though they may have important effects near the point of separation, where the curvature of streamlines is large.

While all these approximations may be conceivably justified in the case of a shock wave of moderate strength incident on a plane surface, up to a point fairly close to the foot of the wave, their validity would be more than doubtful if one tried to apply Lees method, as it stands, to the more general case of strong shocks on curved surfaces, where external pressure gradients would be high. When one drops the assumptions as to the magnitude of these gradients, the resulting equations become unamenable to analytical treatment and an iterative numerical process becomes necessary. It was felt that such computations would not be justified until Lees' analysis is supported by experiment, but some calculations were made to test the validity of such a procedure, for one particular case of a 6 per cent double-wedge aerofoil at $M_o = 1.57$ and $\alpha = 8^o$. From the experimental pressure distribution obtained at the N.P.L. the shape of the equivalent surface was deduced using the process already described in para. 3.1. It is seen from fig. 17 that the pressure gradient at the rear of the upper surface is fairly

/high and ...

high and that between the shoulder and the trailing edge the equivalent surface is displaced by about 2 per cent of the chord length. If the boundary layer were completely separated, there would have to be a very considerable amount of reversed flow in the dead-water region with speeds up to, in this case, 20 per-cent of the free stream velocity. As such high velocities of the reversed flow are unlikely, it appears more reasonable to assume that the boundary layer was turbulent and had not separated. In that case, if the equivalent surface is taken to be the contour of the displacement thickness, the actual boundary layer thickness at the trailing edge would be of the order of 15 - 20 per cent of the chord length. This shows clearly that the static pressure cannot be assumed to be constant across the boundary layer, and that the pressure gradient outside the boundary layer is probably much smaller than that indicated by the surface pressures.

4. SUGGESTED METHOD FOR ESTIMATING BOUNDARY LAYER EFFECTS

4.1. Summary of the Method

On the basis of the considerations described so far, one can attempt to devise a method for an approximate assessment of the boundary layer effects on the aerodynamic characteristics of two-dimensional supersonic aerofoils. The method suggested here will be restricted to aerofoils with sharp leading and trailing edges ('sharp' is used here in the sense 'sharpest possible') and at incidences such that the leading edge shock waves are attached.

4.1.1. Theoretical pressure distribution and aerodynamic characteristics

The pressure distribution on both surfaces is obtained from the standard shock-expansion theory, assuming simple-wave flow along the surface.

The force and moment coefficients (lift, wave drag and pitching moment) can then be obtained from equations 2.3.1. to 2.3.6. by numerical or graphical integration of pressure distributions. For wedge aerofoils these are simple to calculate since pressures are constant along straight surfaces. For other shapes, the numerical integration is straightforward but somewhat tedious. In the case of circular arc profiles of maximum thickness up to 10 - 12 per cent of chord, it was found that

/the pressure ...

the pressure distribution can be approximated with a very good accuracy by an interpolating polynomial of the third degree and the force coefficients can then be expressed in terms of the angle of incidence, the leading edge angle and the values of pressure at four equally spaced points on the surface (just downstream of the leading edge, just upstream of the trailing edge and at two intermediate points). The derivation is given in the Appendix III and results in the following expressions:

$$C_Y = \frac{2\beta_\ell}{q_o} \frac{r}{c} \left[\cos \beta_\ell \sum_{n=o}^{3} a_n f_n + \sin \beta_\ell \sum_{n=o}^{3} a_n g_n \right] \qquad \ldots\ldots\ldots 4.1.1$$

$$C_X = \frac{2\beta_\ell}{q_o} \frac{r}{c} \left[\sin \beta_\ell \sum_{n=o}^{3} a_n f_n - \cos \beta_\ell \sum_{n=o}^{3} a_n g_n \right] \qquad \ldots\ldots\ldots 4.1.2$$

where a_n are coefficients depending on the value of pressure at the four points (eqn. A.III.11) and f_n and g_n are functions of the leading edge angle β_ℓ (eqn. A.III.10).

4.1.2. Development of the boundary layer

Neglecting the effects of shock waves and separation (which are taken account of separately), any convenient method can be used for computing the development of the displacement thickness and the local skin friction coefficient, from the theoretical pressure distributions. The available methods are discussed and summarised in ref. 12.

For the laminar boundary layer with zero heat transfer and the Prandtl number of unity, one has e.g. the approximate methods of Howarth (ref. 27), Young (ref. 28) and Dorodnitzyn (ref. 29), all based on the standard Pohlhausen approximation for the velocity profile. However, it will be found that in the case of convex aerofoils with $t/c \geq 0.06$ and $M \geq 1.5$ approx. the methods of Howarth and Dorodnitzyn break down at some point on the aerofoil surface, owing to a singularity in the differential equation for the modified Pohlhausen parameter λ, which occurs at $\lambda = 12$. The range of validity of these methods can be extended to $\lambda \geq 12$ by assuming a quintic velocity distribution as was done by Dryden for the incompressible case (ref. 30), but this would further increase the amount of labour involved in computations, which is very considerable even with the quartic velocity distribution. The method of Young is very

/much ...

much simpler and does not cease to give results when $\lambda \geq 12$ (λ is not used explicitly in that method), but owing to the nature of its simplifying assumptions, it cannot be expected to be very accurate in the case of comparatively thick aerofoils at high incidences. Consequently, it was decided to develop a new integral relation for laminar boundary layers in supersonic flow by adopting Young's general approach but relaxing his simplifying assumptions. The resulting relations are derived in the Appendix I and discussed in section 4.2.

For turbulent boundary layers one can use e.g. one of the approximate methods developed by Young and Winterbottom (ref. 31, also see ref. 13) and Tucker (ref. 32). It should be noted that the experimental results of ref. 32 indicate that wall density used as the reference value in the relation for the shear stress at the wall gives better agreement with experiment than the main stream density at the edge of the boundary layer.

4.1.3. Effects of the boundary layer displacement thickness

Changes in the local pressure due to the displacement of flow caused by the boundary layer are obtained from the development of the displacement thickness using eqn. 2.3.7. The corresponding increments of force and moment coefficients are computed from eqns. 2.3.8 - 2.3.12, by numerical or graphical integration. As very near the leading edge the rate of growth of the displacement thickness is, according to the boundary layer theory, infinite, it is suggested that the pressure increments are calculated from the eqn. 2.3.7. up to an arbitrary point downstream of the leading edge (at, say, 2 - 3 per cent chord) and extrapolated from there to the leading edge.

If the local pressure increments are appreciable, it may be necessary to use the new pressure distribution to calculate the second approximation to the boundary layer development, but in most cases it will be found that the first approximation is sufficiently accurate.

4.1.4. Skin friction drag

The total skin friction drag is obtained from eqn. 2.4.2. by integrating the distribution of the local skin friction over the aerofoil. It should be noted that here again one is faced with a singularity at the leading edge, where $c_f \to \infty$. Now, on a flat plate with a laminar boundary layer $c_f \propto \frac{1}{\sqrt{x}}$, where x is the distance downstream of the leading

/edge, ...

edge, and the integration can be carried out right to the leading edge. On a curved surface $c_f \propto \frac{F}{\vartheta} + G.\vartheta$, where F and G are functions of the external flow conditions. Near the leading edge $\frac{F}{\vartheta} \gg G.\vartheta$, so that $c_f \propto \frac{F}{\vartheta}$, very nearly. But $\vartheta \propto \sqrt{x}$, approximately (for a laminar boundary layer), hence it is suggested that upstream of a point near the leading edge ($x/c = 0.02$, say), c_f is assumed to vary with $\frac{1}{\sqrt{x}}$, so that $\int_0^1 c_f \, d\bar{x}$ in eqn. 2.4.2. becomes

$$\int_0^1 c_f \, d\bar{x} = \int_{0.02}^1 c_f \, d\bar{x} + 0.04 \, (c_f)_{\bar{x} = 0.2} \quad \ldots.4.1.5.$$

For the turbulent boundary layer, $c_f \propto x^{-n}$, where n depends on the power law assumed for the velocity profile (and is, generally, of the order of 0.2); hence

$$\int_0^1 c_f \, d\bar{x} = \int_{0.02}^1 c_f \, d\bar{x} + \frac{0.02}{1-n} \, (c_f)_{\bar{x} = 0.02} \quad \ldots.4.1.5a$$

4.1.5. Effects of separation

Until systematic experimental results are available which would permit the derivation of an empirical relationship for the prediction of separation, or until a reliable theory is developed, it is suggested that the data presented in figs. 14 to 16 may be used tentatively for biconvex aerofoils of the maximum thickness of the order of 10 per cent, for the range of Mach numbers of 1.6 - 2.5 and Reynolds numbers of $5 \times 10^5 - 10^6$. The pressure changes due to separation, $\Delta_{sep} p$, can be estimated as shown in the diagram below.-

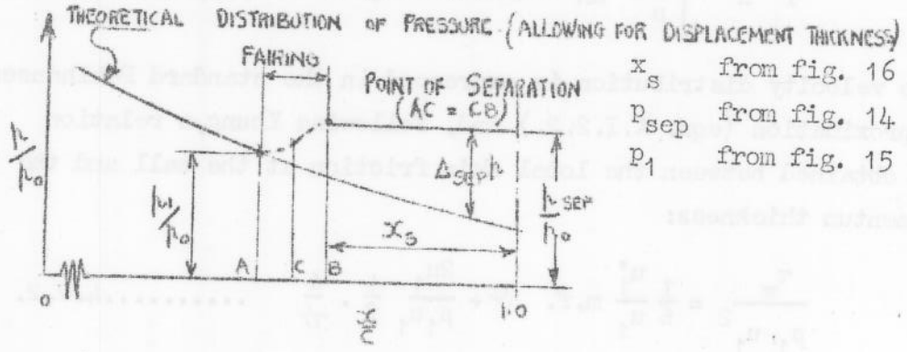

x_s from fig. 16
p_{sep} from fig. 14
p_1 from fig. 15

Increments of the lift, wave drag and pitching moment coefficients are then found, similarly to those due to the displacement thickness, by integrating $\Delta_{sep} p$ over the region of separation. The change in the skin friction drag can be estimated by assuming that the local skin friction downstream of the point of separation is zero.

/When ...

When the boundary layer is assumed to be turbulent, (e.g. at flight Reynolds numbers), the effects of separation can be altogether neglected, since even if separation does occur, its extent would generally be limited to the immediate vicinity of the trailing edge.

Nett values of the force and moment coefficients are then obtained by summing the various increments:

$$C_{L,M} = (C_{L,M})_{TH} + \Delta_{\delta_1} C_{L,M} + \Delta_{sep} C_{L,M} \quad \ldots\ldots 4.1.6.$$

$$C_D = (C_{D_w})_{TH} + \Delta_{\delta_1} C_{D_w} + \Delta_{sep} C_{D_w} + C_{D_f} + \Delta_{sep} C_{D_f} \quad \ldots\ldots\ldots 4.1.7$$

$$\frac{x_{c.p.}}{c} = \frac{(x_{c.p.})_{TH}}{c} + \frac{\Delta_{sep} x_{c.p.}}{c} + \frac{\Delta\delta_1 x_{c.p.}}{c} \quad 4.1.8.$$

4.2. New Integral Relation for Laminar Boundary Layers in Supersonic Simple-Wave Flow and Zero Heat Transfer

The method of derivation of the new relation is essentially an extension of Young's approach (ref. 28) and a compromise between his approximate method and that of Howarth (ref. 27). As in both these methods, use is made of the fact that when the Prandtl number is unity and $\omega = 1$ in the relation $\mu \propto T^{\omega}$, the velocity distribution in the laminar boundary layer with zero heat transfer is independent of the Mach number, if expressed as a function of Y, where

$$Y = \int \frac{\mu_1}{\mu} \, dn \quad \ldots\ldots\ldots 4.2.1.$$

The velocity distribution is expressed in the standard Pohlhausen approximation (eqn. A.I.2.2.) and, following Young, a relation is obtained between the local skin friction at the wall and the momentum thickness:

$$\frac{\tau_w}{\rho_1 u_1^2} = \frac{1}{6} \frac{u_1'}{u_1} \, m.f. \, \vartheta + \frac{2\mu_1}{\rho_1 u_1} \frac{1}{f} \cdot \frac{1}{\vartheta} \quad \ldots\ldots\ldots 4.2.2.$$

where $f = \frac{\delta^*}{\vartheta}$ and $m = \frac{\mu_w}{\mu_1}$.

However, at this point Young assumes that m, f and also $H = \frac{\delta_1}{\vartheta}$ are constant along the surface and functions only of the free stream conditions; in Howarth's analogue of Pohlhausen's

/method ...

method these ratios are, of course, functions of the main stream conditions at the edge of the boundary layer and of the boundary layer thickness in terms of Y, whereas in the present method they are assumed to be unique but arbitrary functions of the local main stream conditions only. Then, for the case of supersonic simple-wave flow

$$\frac{\delta^*}{\vartheta} = f(\theta) \; ; \; \frac{\mu_w}{\mu_1} = m(\theta) \; ; \; H = \frac{\delta_1}{\vartheta} = k(\theta) \qquad \ldots\ldots 4.2.3.$$

where θ is the direction of flow at the edge of the boundary layer, measured from some datum direction (taken as $\theta = 0$ at $M = 1$).

von Karman's momentum equation then becomes

$$\frac{d\,\tilde{\vartheta}}{d\theta} + j(\theta)\,\tilde{\vartheta} = \frac{1}{\kappa} k(\theta) \qquad \ldots\ldots 4.2.4$$

where $\tilde{\vartheta} \equiv \rho_1^2 \vartheta^2$ and $\kappa \equiv \frac{\partial \theta}{\partial s}$ = curvature of the surface, and $j(\theta)$, $k(\theta)$ are functions of the local main stream conditions defined in eqn. A.I.2.10b.

This equation can be either solved by a step-by-step process, or integrated directly to yield

$$\left[\tilde{\vartheta}\right]_{\theta_1} = \frac{e^{-\frac{1}{2}\int_{\theta_L}^{\theta_1} j(\theta)d\theta}}{\rho_1} \left[\int_{\theta_L}^{\theta_1} \frac{k(\theta)}{\kappa} e^{\int_{\theta_L}^{\theta} j(\theta)d\theta}\, d\theta\right]^{\frac{1}{2}} \qquad \ldots\ldots 4.2.5$$

In the case of a circular arc profile, this integral assumes a particularly simple form:

$$\left[\tilde{\vartheta}\right]_{\theta_1} = A\, J_{\tilde{\vartheta}}(\theta_1) \sqrt{K(\theta_1) - K(\theta_L)} \qquad \ldots\ldots 4.2.6$$

whilst the displacement thickness and the skin friction are given by

$$\left[\delta_1\right]_{\theta_1} = H \left[\tilde{\vartheta}\right]_{\theta_1} \qquad \ldots\ldots 4.2.7$$

$$c_f \equiv \frac{2\tau_w}{\rho_o U_o^2} = B.L(\theta)\,\tilde{\vartheta} + C.M(\theta)\,\frac{1}{\tilde{\vartheta}} \qquad \ldots\ldots 4.2.8$$

/where ...

where A, B and C (defined in eqn. A.I.3.4a and 3.8a) depend on the aerofoil dimensions and the free stream conditions and are constant along the surface; J, K, L and M are unique functions of θ only, defined in eqns. A.I.3.7a and 3.8a.

Once these functions have been computed and tabulated for a range of θ, the calculation of the boundary layer development in a particular case then involves only the determination of the quantities A, B and C and the use of tables to find the appropriate values of J, K, L and M, for the required points on the surface.

For the present purpose it was assumed that the variation of $\frac{\delta_1^*}{\vartheta}$, $\frac{\mu_w}{\mu_1}$ and $\frac{\delta_1}{\vartheta}$ with the local Mach number, M_1, is the same as for a flat plate at zero incidence with the corresponding free stream Mach number $M_o = M_1$. Young's flat plate solution (refs. 12, 31) was used, so that

$$H = k(\theta) = 2.59\ (1 + 0.277\ M_1^2)$$

$$\frac{\delta^*}{\vartheta} = 9.072\ \left[1 + 0.365\ (\gamma-1)\sigma^{\frac{1}{2}}\ M_1^2\right]^{(1-\omega)}$$

$$\frac{\mu_\omega}{\mu_1} = \left[1 + \frac{\gamma-1}{2}\ \sigma^{\frac{1}{2}}\ M_1^2\right]^{\omega}$$

with $\omega = 8/9$, $\sigma = 0.72$ and $\gamma = 1.4$.

The variation of these functions and also of $\bar{j}$, $\bar{k}$, J_ϑ, K, L and M with θ is shown in fig. 18, and their values are tabulated in table I.

Fig. 19 shows a comparison of the results of the present method with those obtained by the methods of Howarth[*] and Young, for the momentum and the displacement thickness on the lower surface of a 10 per cent circular arc aerofoil, with $M_o = 2.13$ and $R = 0.64 \times 10^6$. It will be seen that the development of the displacement thickness calculated from eqn. 4.3.8. compares better with Howarth's method, than does that obtained by using Young's method; the agreement is not so good in the case of the momentum thickness, but even there the discrepancies are generally less than about 5 per cent.

/The obvious ...

---

[*] functions of λ used in Howarth's method are tabulated in table II for the range of λ from 0 to 11.5.

The obvious advantage of the new relation is the minimum amount of labour involved in computing and the ease with which δ_1, ϑ and c_f can be obtained at discrete points on the surface of a circular arc profile.

The method can be easily adapted to other forms of relations for H, $\frac{\delta^*}{\vartheta}$ and $\frac{\mu_w}{\mu_1}$, provided they are uniquely determined by the local flow conditions. This allows the possibility of using empirical relations for the functions f, m and h, should such relations be found to give better agreement with experiment.

4.3. Comparison with Experiment; Discussion of Results.

The method of estimating the boundary layer effects, suggested in para. 4.1., was applied to the particular case of a 10 per cent symmetrical circular arc profile at $M_o = 2.13$ and $R = 0.64 \times 10^6$, for a range of incidence from 0° to 10°. The new integral relation was used for the development of the boundary layer, which was assumed to be laminar throughout.

4.3.1. Boundary layer displacement thickness; local pressure increments; skin friction.

The development of the displacement thickness is shown in fig. 20a and its rate of growth in fig. 20b. It is seen that for any given point on the surface, the displacement thickness increases almost linearly with the incidence and so does its rate of growth. At $\alpha = 10^\circ$, the values of δ_1 on the top surface are nearly twice as large as those at the corresponding points on the bottom surface.

The resulting increments of the local pressure vary only little with incidence for $x/c \geq 0.4$ (fig. 21), but towards the leading edge increase fairly rapidly with increasing incidence.

The local skin friction (fig. 22) is seen to decrease with increase of the local Mach number, but the rate of variation is small.

4.3.2. Effects of displacement thickness on force and moment coefficients

The increments of lift and wave drag coefficients due to the displacement of flow by the boundary layer are.-

α	0°	4°	8°	10°
ΔC_{D_w}	.000486	.000528	.000581	.000641
ΔC_L	0	.00029	.00047	.00054

The increments of pitching moment coefficient and the movement of the centre of pressure are negligible $\left[0(10^{-5})\right]$.

When expressed as percentages of the theoretical values of the coefficients, $\frac{\Delta C_L}{C_L}$ and $\frac{\Delta C_{D_w}}{C_{D_w}}$ are found to decrease with incidence (fig. 23a) and are of the order of 0.2 per cent and 1 per cent respectively.

4.3.3. Skin friction drag

The total skin friction drag is found to be practically independent of the incidence, the values of C_{D_f} being.-

α	0°	4°	8°	10°
C_{D_f}	.00461	.00460	.00460	.00466

It is of interest to note, that in ref. 13 the value of C_{D_f} for the same section at the same Mach number and $\alpha = 0^\circ$, obtained by Young's method, is 0.00465.

4.3.4. Effects of separation

These effects were estimated from the empirical data of figs. 14 - 16, as suggested in para. 4.1.5. The changes in force and moment coefficients are given in table III(c), and are plotted in fig. 23(b) as percentages of the corresponding theoretical values of the coefficients.

It will be seen that the effects of separation are most marked in the case of the pitching moment, whose value is reduced by as much as 26 per cent at $\alpha = 4^\circ$, falling to just under 14 per cent at $\alpha = 10^\circ$.

The lift coefficient is reduced by amounts varying from 12 per cent at $\alpha = 4^\circ$ to 7 per cent at $\alpha = 10^\circ$. The reduction in the wave drag varies only little with incidence and is of the order of 10 per cent.

Separation also results in a forward shift of the centre of pressure position, varying from 6.5 per cent chord at $\alpha = 4^\circ$ to 3.2 per cent chord at $\alpha = 10^\circ$.

/The ...

The decrease of skin friction drag was estimated as 4.4 per cent at $\alpha = 0^{\circ}$ rising to 9.2 per cent at $\alpha = 10^{\circ}$.

4.3.5. Comparison with experiment

The Mach number and Reynolds number were chosen so that the above results can be compared directly with the experimental results obtained by Ferri (ref. 4). The final calculated values of the aerodynamic coefficients are given in table III(d), together with the theoretical values obtained from the inviscid shock-expansion theory (table IIIa) and the averaged results of Ferri's experiments (table IIIe); they are also shown plotted in fig. 24.

The inviscid shock-expansion theory appears to be in very poor agreement with the experiment. The greatest discrepancies occur in the lift and moment coefficients and the L/D ratio. At $\alpha = 10^{\circ}$, the theoretical values of C_L, C_M and L/D are respectively 19 per cent, 30 per cent, and 17 per cent higher than the experimental values determined by force measurements. Taking account of the boundary layer effects, reduces these differences to 11 per cent, 12 per cent and 12 per cent, respectively, which are still very considerable amounts. It is not known what is the probable experimental error, but scatter of the experimental points is large and some of the numerical results are quoted, in ref. 4, to two figures only. Further, there are large discrepancies between the lift and moment coefficients obtained from integration of the pressure distributions and those determined from force measurements (see table IVa) (the values of drag cannot be so compared, as C_D calculated from the pressure distributions obviously does not include the skin friction drag). Therefore, it is suggested that the force measurements in ref. 4 are subject to serious experimental error. Moreover, there is also some doubt as to the precise geometrical characteristics of the aerofoil tested. It is stated in ref. 4 that the dimensions of the 10 per cent circular arc profile were: 60 mm chord, 6 mm maximum thickness, 150 mm radius of curvature and $22^{\circ}40'$ leading edge angle. Taking the chord length as the datum dimension, the correct value of the radius of curvature is 151.5 mm and the correct leading edge angle is $22^{\circ}50'$. Though perhaps not very significant, these differences cast doubt on the accuracy of the other experimental data. It will also be seen from table IVb that numerical values of the pitching moment coefficient at positive angles of incidence are consistently higher than those at the corresponding negative incidences, which indicates that either the aerofoil was not exactly

/symmetrical ...

symmetrical, or that the distribution of flow in the tunnel working-section was not uniform.

This view is supported by the comparison of lift coefficients and one typical example of pressure distributions obtained by Ferri for the 10 per cent circular arc profile at M = 1.85 ($R = 0.72 \times 10^6$), with those given in ref. 10 for the same profile at M = 1.86 ($R = 0.66 \times 10^6$) - fig. 25. The slight differences in the pressure distribution cannot possibly account for the large difference in the lift coefficients for the two cases, which is some 24 per cent at $\alpha = 6^\circ$, so that Ferri's force measurements again appear to be in error. The differences in the pressure distributions, though only small, can be explained by neither the slightly different Mach numbers, nor by the boundary layer effects, but can be accounted for by asymmetry of the aerofoil, or non-uniformity of flow in the working-section.

Results of ref. 10 appear to be far more reliable, but unfortunately they were not available until after the present calculations had been completed for the Mach number of 2.13. An attempt was made to interpolate some of the results for M = 1.85 and M = 2.48 to M = 2.13, assuming that C_L and $\left(C_{D_W}\right)_{C_L=0}$ are proportional to $\frac{1}{\sqrt{M^2 - 1}}$. As can be seen from fig. 24 and table V, the agreement with the corresponding calculated values is very good. However, it should be noted that the results of ref. 10 may be subject to a certain amount of error, owing to the fact that C_L and C_D were calculated from the pressure distributions, which were extrapolated over some 20 per cent of chord.

4.3.6. Assessment of the Method

The method suggested here cannot be properly assessed until reliable experimental data are available, comprising both pressure and force measurements. The obviously weak point of the present method, as it stands, is the empirical correction for separation based on inadequate data, but here again the fault lies with the lack of comprehensive experimental results.

With the laminar boundary layer, the effects of separation are of much greater importance than the effects of the displacement thickness, but with the turbulent boundary layer, when separation is unlikely to occur, the latter effects become predominant and the method should give a reasonable estimate of the viscous effects.

/5. ...

5. SOME NOTES ON CHOICE OF AEROFOIL SECTIONS FOR SUPERSONIC WINGS

5.1. Inviscid Characteristics

According to the two-dimensional inviscid theory, a symmetrical double-wedge section has a lower wave drag coefficient than sections of any other shape at the same Mach number and with the same maximum t/c ratio. However, since the minimum limit on the thickness of a wing is governed by considerations of the structural strength and of storage capacity, drag in terms of the cross-section area or the 2nd moment of area (in the case of thin solid wings) rather than in terms of the t/c ratio is a more appropriate criterion for comparing drag properties of various wing sections.

Determination of the optimum shape of section using the shock-expansion theory cannot, unfortunately, be carried out analytically. However, the linearised theory is amenable to analytical treatment and whilst its results cannot be claimed to be very accurate, it affords at least a qualitative guide to the relative merits of various aerofoil sections.

Using the linear theory, it can be shown quite simply by the calculus of variations that the section having the least wave drag for a given cross-section area is composed of two symmetrical parabolic arcs. Now, within the approximations of the linearised theory the wave drag of the parabolic profile is exactly the same as that of a circular arc profile of the same t/c ratio, since the equations of the two profiles are identical to the first order in y/c.

The table below shows some first order estimates of the wave drag coefficients of symmetrical parabolic and circular arc profiles as compared with the symmetrical double wedge of equal thickness/chord ratio, cross-section area or 2nd moment of area:

$\frac{C_{D_{C.A.\&P.A.}}}{C_{D_{D.W.}}}$ for	equal t/c	equal area	equal 2nd moment
$\alpha = 0^\circ$	1.33	0.750	0.892
$\alpha = 10^\circ$	1.07	0.897	0.950

The drag of the double-wedge can of course, be further reduced without altering the section area or its 2nd moment by moving the point of maximum thickness beyond the mid-chord.

/Moreover, ...

Moreover, for a more accurate comparison the shock-expansion theory should be used, and the above ratios will then also depend on the Mach number. Nevertheless, even the simple example considered here shows that when the structural strength is the primary consideration, the circular arc profile may be expected to offer a wave drag saving as compared with the corresponding double wedge profile.

5.2. Effects of Aerofoil Shape on Stability of Laminar Boundary Layer

A further important factor which should be considered is that of the viscous effects from the point of view of the stability of the laminar boundary layer. The recent work of Lees (ref. 33), shows that favourable pressure gradients may have important stabilising effects at Mach numbers up to about 2.

Fig. 27 (adapted from ref. 33) shows the stability limit in terms of the minimum critical Reynolds number based on the displacement thickness, for a 6 per cent circular arc profile at $M_o = 1.5$ and zero incidence, for a range of Reynolds numbers based on the chord length. It is seen that with $R_o > 5 \times 10^5$ there is a region of instability near the leading edge, the size of which increases with R_o. Fig. 26 shows the corresponding limits for a 6 per cent double-wedge section at the same Mach number and incidence (the values of $R_{\vartheta_{crit}}$ were obtained from ref. 34), calculated assuming the momentum thickness to be continuous at the shoulder. The boundary layer is almost completely unstable even at $R_o = 5 \times 10^5$.

Whilst the considerations of stability cannot determine the probable position of the transition point, it is clear that transition is more likely to occur when the boundary layer is unstable than when it is completely stabilised. In fig. 28a is shown a comparison of the wave and skin friction drag coefficients of the two aerofoils for various transition positions. Transition was assumed to occur suddenly and the skin friction drag calculated by integrating the local skin friction coefficient along the surface, neglecting the effect of the trailing edge shock waves. Assuming that transition occurs at a point where $R_{\delta_1 \text{ or } \vartheta} = n \left(R_{\delta_1 \text{ or } \vartheta} \right)_{crit_{min}}$, the values of $C_{D_w} + C_{D_f}$ obtained with $n = 4$ and $n = 12$ are shown in fig. 28b. It will be observed that with R_o between 10^6 and 10^7 the drag of the circular arc is only slightly higher than that of the double-

/wedge. ...

wedge.

Similar calculations for aerofoils at other Mach numbers had been carried out in ref. 35, before Lees completed his analysis for the effects of pressure gradients on stability of the laminar boundary layer, and appear to indicate that at M = 1.6 the drag of the circular arc profile can actually be less than that of the double-wedge of the same thickness.

At Mach numbers higher than 2, the effect of aerodynamic heating becomes predominant (c.f. ref. 33) and cancels out the effect of the favourable pressure gradient, hence the circular arc profile no longer has the advantage over the double-wedge on the grounds of stability of the boundary layer. As suggested by Lees, withdrawal of heat from the surface may help to restore the stabilising effects of the favourable pressure gradients.

5.3. Effects of Separation

From the point of view of separation, there is little to choose between the various profiles, as with the boundary layer laminar, separation is just as likely to occur in one case as in another (c.f. para. 3.3., page 32). Effects of separation are not serious in the case of plain wings, since loss of lift is associated with a decrease of drag, but may cause disastrous losses of control effectiveness. An obvious method of preventing or limiting separation at low Reynolds numbers is to induce turbulent flow over the rear part of the wing, but this would result in a serious increase of drag. An alternative might be to have blunt trailing edges, in which case the shock waves would move downstream of the trailing edge and would be preceded by expansions, which may suppress separation. This again would result in an increased drag, caused by a suction force on the blunt edge.

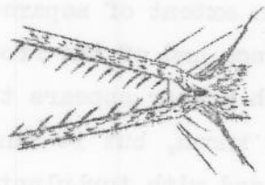

5.4. Concluding Remarks

The above considerations are only tentative and, in any case, concern only two-dimensional aerofoils. On finite wings the phenomena discussed may be even qualitatively different. Much experimental and theoretical research is needed, before it is possible to say with any degree of certainty, what aerofoil sections should be used for supersonic wings in any particular case.

/6. ...

6. SOME SUGGESTIONS FOR EXPERIMENTAL RESEARCH

As there seems to be little hope of a complete theory of the shock wave - boundary layer interactions being developed in the immediate future, there is need for a systematic experimental investigation of this phenomenon, particularly as it affects the conditions at the trailing edges of supersonic aerofoils. It is believed essential to explore as fully as possible the scale effects, as it is reasonable to expect that at high Reynolds numbers the effects of separation at the trailing edge may well become of minor importance only. In the first instance, such experiments should be limited to two or three representative aerofoil sections tested over a wide range of Mach numbers, Reynolds numbers and the angle of incidence. It is thought that interferometry would prove very useful in exploring regions of flow, where static pressure measurements are difficult or impossible. Force measurements should also be made, both as a check on the pressure and optical measurements and as a means of determining the total drag.

7. CONCLUSIONS

Experiments show that real flow patterns observed on two-dimensional supersonic aerofoils differ appreciably from those predicted by inviscid theory.

The most striking discrepancies are found near the trailing edges, where separation of flow is often observed. This separation is caused by the interaction of the trailing edge shock waves with the boundary layer and, on general grounds, it can be shown to result in a loss of lift and a decrease of wave drag. Examination of available experimental results shows that the pressure in the separated region and the extent of separation are mainly functions of the angle of incidence and of the free stream static pressure; the effect of the Mach number appears to be negligible. The scale effects are not known, but it can be expected that at high Reynolds numbers and with turbulent boundary layers, the effects of separation should be of only minor importance.

At the leading edges, at incidences when according to the inviscid theory the flow should undergo a simple Prandtl-Meyer expansion, a weak shock wave is always observed. Though the bluntness of the leading edge appears to be the primary cause of the formation of the shock wave, the viscous effects have at least an important modifying influence and, in the case of appreciably thick leading edges, may result in a local separation of flow. The effect of the flow pattern at the leading

/edge on ...

edge on the pressure distribution downstream is believed to be negligible and, as calculations show, is confined to the first few per cent of the chord length.

At sharp shoulders of wedge sections, the flow patterns observed are found to be fundamentally similar to those at the leading edge. It is believed that a very small region of locally separated flow exists at the sharp corner. The surface pressure distributions are affected by the diffusion of pressure through the subsonic part of the boundary layer within a distance of the order of 5 - 10 boundary layer thicknesses from the shoulder.

In the regions of flow which are unaffected by shock waves boundary layer effects can be estimated by applying the concept of the equivalent profile, formed by the addition of the boundary layer displacement thickness to the contour of the aerofoil, and by computing the potential flow round the new shape (using the standard shock-expansion theory). The relative increments of lift and wave drag coefficients are found to be of the order of $\frac{r}{c}\left(\frac{\delta_1}{c}\right)_{T.E.}$ and vary approximately as $1/\sqrt{R_o}$ for the laminar boundary layer, and as $1/R_o^n$ for the turbulent boundary layer, where $n = 0(0.2)$. The lift increment is generally positive, but the drag increment may be negative if there is transition occuring near the point of the maximum thickness.

In the absence of a general theory of the shock wave - boundary layer interaction, the effects of separation of flow have to be allowed for empirically, on the basis of the available experimental data.

For the particular case of a 10 per cent circular arc profile at $M = 2.13$ and $R_o = 0.64 \times 10^6$ with a laminar boundary layer, it is found that the effects of separation are far more important than those of the displacement thickness. At $\alpha = 10^o$ the separation results in a reduction of C_L, C_M and C_{D_w} of approx. 7 per cent, 14 per cent and 8 per cent respectively, with a forward shift of the centre of pressure of 6.5 per cent chord. The displacement of flow by the boundary layer increases C_{D_w} by amounts of the order of 1 per cent, whilst the increments of the lift coefficient are only of the order of 0.2 per cent. The skin friction drag coefficient is 0.00461 at $\alpha = 0^o$ and is practically independent of the angle of incidence. The calculated nett values of the aerodynamic coefficients appear to be in poor agreement with the experimental results of Ferri (ref. 4). It is believed that those results are subject to serious experimental error, as they exhibit a

/number ...

number of inconsistencies. Interpolation of some of the results obtained at the R.A.E. (ref. 10) gives a good agreement with the present calculations.

A short examination of the relative merits of supersonic aerofoil sections indicated that there is a real possibility of the total drag of a double-wedge profile being higher than that of a circular arc profile of the same maximum thickness to chord ratio, owing to the stabilising effect of the favourable pressure gradients on the laminar boundary layer at low supersonic Mach numbers (< 2) and moderate Reynolds numbers ($10^6 - 5 \times 10^7$).

The new integral relation for laminar boundary layers in supersonic simple-wave flow with zero heat transfer is found to give results in good agreement with those obtained by the approximate method of Howarth.

ACKNOWLEDGEMENTS

The author wishes to thank the Director of the National Physical Laboratory for permission to reproduce the pictures shown on Figures 8, 10 and 17.

/APPENDIX I ...

APPENDIX I

A NEW INTEGRAL RELATION FOR LAMINAR BOUNDARY LAYERS ON TWO-DIMENSIONAL CYLINDERS IN SIMPLE-WAVE SUPERSONIC FLOW WITH ZERO HEAT TRANSFER

1. Boundary Layer Equations

With the usual approximations of the laminar boundary layer theory the equations of motion are (ref. 12).-

$$\rho u \frac{\partial u}{\partial s} + \rho v \frac{\partial u}{\partial n} = \frac{\partial}{\partial n}\left(\mu \frac{\partial u}{\partial n}\right) \qquad \ldots\ldots\ldots 1.1.$$

$$0 = \frac{\partial p}{\partial n} \qquad \ldots\ldots\ldots 1.2.$$

$$\frac{\partial}{\partial s}(\rho u) + \frac{\partial}{\partial n}(\rho v) = 0 \qquad \ldots\ldots\ldots 1.3.$$

1.3 is the equation of continuity and is exact. von Karman's momentum equation is

$$\vartheta' + \left[(H+2)\frac{u_1'}{u_1} + \frac{\rho_1'}{\rho_1}\right]\vartheta = \frac{\tau_w}{\rho_1 u_1^2} \qquad \ldots\ldots\ldots 1.4$$

where dashes denote differentiation with respect to s, the suffix 1 refers to the main stream conditions at the edge of the boundary layer, and

$$\vartheta = \int_0^\infty \frac{\rho u}{\rho_1 u_1}\left(1 - \frac{u}{u_1}\right) dn, \quad \text{the momentum thickness,}$$

$$\delta_1 = \int_0^\infty \left(1 - \frac{\rho u}{\rho_1 u_1}\right) dn, \quad \text{the displacement thickness,}$$

$$\tau_w = \mu_w \left(\frac{\partial u}{\partial n}\right)_{n=0}$$

= value of the local skin friction at the surface, and s,n are coordinates parallel and normal to the surface.

2. Development of the Method

We transform the coordinate n to Y, where

$$Y = \int \frac{\mu_1}{\mu} dn \qquad \ldots\ldots\ldots 2.1.$$

Now, when w = 1 in the relation $\mu \propto T^w$ and σ, the Prandtl number is unity, the velocity distribution in the

laminar ...

laminar boundary layer is independent of the Mach number, if expressed as a function of Y. Hence, using the standard Pohlhausen velocity distribution for incompressible flow, we have

$$\bar{w} \equiv \frac{u}{u_1} = a_1 \left(\frac{Y}{\delta^*}\right) + a_2 \left(\frac{Y}{\delta^*}\right)^2 + a_3 \left(\frac{Y}{\delta^*}\right)^3 + a_4 \left(\frac{Y}{\delta^*}\right)^4$$

$$= a_1 \eta + a_2 \eta^2 + a_3 \eta^3 + a_4 \eta^4 \quad \ldots\ldots\ldots 2.2.$$

where δ^* is the boundary layer thickness in terms of Y, and

$$\eta = Y/\delta^*$$

The boundary conditions are

$$\left.\begin{aligned} &\bar{w} = 1, \ \frac{\partial \bar{w}}{\partial \eta} = \frac{\partial^2 \bar{w}}{\partial \eta^2} = 0 \quad \text{at } \eta = 1 \\ &\bar{w} = 0, \ \frac{\partial T}{\partial \eta} = 0 \ \text{(no heat transfer) at } \eta = 0 \\ &\frac{\partial^2 \bar{w}}{\partial \eta^2} = -\lambda, \ \text{at } \eta = 0 \end{aligned}\right\} \quad \ldots 2.3.$$

From 1.1 $\frac{\partial}{\partial n}\left(\mu \frac{\partial u}{\partial n}\right)_{n=0} = \frac{\partial p}{\partial s} = -\rho_1 u_1 u_1' \quad \ldots\ldots\ldots 2.4.$

but from 2.1. $\frac{\partial Y}{\partial n} = \frac{\mu}{\mu_1}$, and $\left(\frac{\partial u}{\partial n}\right)_{n=0} = 0$ by the second eqn. 2.3.

hence 2.4. yields $\frac{\partial^2 \bar{w}}{\partial \eta^2} = -\delta^{*2} u_1' \rho_1 \frac{\mu_w}{\mu_1^2}$

where μ_w is the value of μ at $n = 0$,

so that $\lambda = \delta^{*2} u_1' \rho_1 \frac{\mu_w}{\mu_1^2} \quad \ldots\ldots\ldots 2.5.$

Using the boundary conditions 2.3. to solve 2.2. for the coeffi-cients 'a', we have

$$a_1 = 2 + \frac{\lambda}{6}; \quad a_2 = -\frac{\lambda}{2}; \quad a_3 = -2 + \frac{\lambda}{2}; \quad a_4 = 1 - \frac{\lambda}{6}$$

$$\ldots\ldots\ldots 2.6.$$

The skin friction at the wall is, by definition

$$\tau_w = \mu_w \left(\frac{\partial u}{\partial n}\right)_{n=0}$$

/hence ...

hence $$\tau_w = \frac{\mu_1 u_1}{\delta^*}\left(\frac{\partial \bar{w}}{\partial \eta}\right)_{\eta=0} = \frac{\mu_1 u_1}{\delta^*}\left(2 + \frac{\lambda}{6}\right)$$ by 2.2. and 2.6.

and $$\frac{\tau_w}{\rho_1 u_1^2} = \frac{\mu_1}{\rho_1 u_1 \delta^*}\left(2 + \frac{\lambda}{6}\right)$$

or, substituting for ,

$$\frac{\tau_w}{\rho_1 u_1^2} = \frac{1}{6}\frac{\mu_w}{\mu_1}\frac{u_1'}{u_1}\delta^* + \frac{2\mu_1}{\rho_1 u_1}\frac{1}{\delta^*} \qquad \ldots\ldots\ldots 2.7.$$

We shall now assume that the ratios $\frac{\delta^*}{\vartheta}$, $H = \frac{\delta_1}{\vartheta}$ and $\frac{\mu_w}{\mu_1}$ are functions only of the local flow conditions in the main stream at the edge of the boundary layer and are independent of δ^*. Then, for the case of simple-wave supersonic flow, we can write

$$\frac{\delta^*}{\vartheta} = f(\theta)\ ;\quad H = \frac{\delta_1}{\vartheta} = h(\theta)\ ;\quad \frac{\mu_w}{\mu_1} = m(\theta) \qquad \ldots\ldots 2.8.$$

where θ is the direction of flow at the edge of the boundary layer, measured from some datum direction.

Eqn. 2.7. then becomes

$$\frac{\tau_w}{\rho_1 u_1^2} = \frac{1}{6}\frac{u_1'}{u_1} m(\theta)\, f(\theta). \quad + \quad \frac{2\mu_1}{\rho_1 u_1}\frac{1}{f(\theta)} \cdot \frac{1}{\vartheta} \qquad \ldots\ldots\ldots 2.9.$$

Substituting this into the momentum equation, we have

$$\vartheta' + \left[(h(\theta) + 2)\frac{u_1'}{u_1} + \frac{\rho_1'}{\rho_1}\right]\vartheta = \frac{1}{6}\frac{u_1'}{u_1} m(\theta).f(\theta).\vartheta + \frac{2\mu_1}{\rho_1 u_1}\frac{1}{f(\theta)}\frac{1}{\vartheta}$$

or, multiplying both sides by $\rho_1^2 \vartheta$ and rearranging

$$\frac{d}{ds}(\rho_1^2 \vartheta^2) + (\rho_1^2 \vartheta^2)\frac{u_1'}{u_1} \cdot 2\left[(h+2) - \frac{1}{6} f.m\right] = \frac{4\mu_1 \rho_1}{u_1 f} \qquad \ldots 2.10.$$

We note that the expression in the square brackets involves only the functions h, f and m and thus is, itself, a unique function of θ, and we can write

$$2\left[(h+2) - \frac{1}{6} f\, m\right] = g(\theta) \qquad \ldots\ldots\ldots 2.11.$$

(as far as possible the notation of ref. 28 is used, so that a direct comparison with Young's method can be made).

/Now, ...

Now, $\frac{d}{ds} \equiv \left(\frac{\partial\theta}{\partial s}\right) \frac{d}{d\theta}$

hence $\frac{d}{ds} = \mathcal{K} \frac{d}{d\theta}$ .....2.12.

where $\mathcal{K} = \frac{\partial\theta}{\partial s}$ is the curvature of the wall.

To simplify notation we shall write $\rho_1^2 u^2 \equiv \textcircled{\sim}$.
Then, using 2.11. and 2.12, eqn. 2.10 becomes

$$\frac{d}{d\theta}\left[\textcircled{\sim}\right] + \textcircled{\sim} \frac{g}{u_1} \frac{du_1}{d\theta} = \frac{4\mu_1\rho_1}{\mathcal{K} u_1} \frac{1}{f} \qquad \text{.....2.10a.}$$

Now, both $\frac{g}{u_1} \frac{du_1}{d\theta}$ and $\frac{\mu_1\rho_1}{u_1 f}$ are unique functions of θ, hence 2.10a can be written in the form

$$\frac{d\textcircled{\sim}}{d\theta} + j(\theta)\textcircled{\sim} = \frac{1}{\mathcal{K}} k(\theta) \qquad \text{.....2.10b.}$$

where $j(\theta) = \frac{g(\theta)}{u_1} \frac{du_1}{d\theta}$, and $k(\theta) = \frac{4\mu_1\rho_1}{u_1 f(\theta)}$.

If the functions f and g are known, together with the velocity distribution along the surface, we can integrate 2.10b by a step-by-step process and obtain the distribution of $\textcircled{\sim}$ along the surface, whence ϑ, δ_1 and τ_w can be readily evaluated.

Alternatively, if we express $\mathcal{K}$, the curvature of the surface, as a function of the angle of inclination of the tangent to the surface, β, we shall have

$$\begin{aligned} \theta &= \text{const.} + \beta \\ d\theta &= d\beta \\ \mathcal{K} &= \mathcal{K}(\theta) \end{aligned} \qquad \text{.....2.11.}$$

2.10b can then be integrated to yield

$$\textcircled{\sim} = e^{-\int j(\theta)d\theta} \left[\int \frac{k(\theta)}{\mathcal{K}(\theta)} e^{\int j(\theta)d\theta} d\theta + C\right] \qquad \text{.....2.12.}$$

where C is a constant of integration and we require one boundary condition to determine its value. If the flow at the leading edge is not supersonic outside the boundary layer, the present method does not apply and some other method must be used

/to determine ...

to determine the value of $\tilde{\omega}$ at the sonic point and supply the necessary boundary condition. When the potential flow is supersonic at the leading edge, where $\theta = \theta_L$, say, we must have $[\tilde{\omega}]_{\theta_L} = 0$ since $[u_1]_{\theta_L} \neq 0$ and as we cannot have a finite loss of momentum there, $[\vartheta]_{\theta_L} = 0$. Eqn. 2.12 then becomes

$$[\tilde{\omega}]_{\theta_1} = e^{-\int_{\theta_L}^{\theta_1} j(\theta)\,d\theta} \int_{\theta_L}^{\theta_1} \frac{k(\theta)}{\kappa(\theta)}\, e^{\int_{\theta_L}^{\theta} j(\theta)\,d\theta}\, d\theta \qquad \ldots\ldots\ldots 2.12a.$$

so that

$$[\vartheta]_{\theta_1} = e^{-\frac{1}{2}\int_{\theta_L}^{\theta} j(\theta)\,d\theta} \left[\int_{\theta_L}^{\theta_1} \frac{k(\theta)}{\kappa(\theta)}\, e^{\int_{\theta_L}^{\theta} j(\theta)\,d\theta}\, d\theta\right]^{\frac{1}{2}} \qquad \ldots\ldots\ldots 2.13.$$

---

3. Laminar Boundary Layer on a Circular Arc Profile

When the surface is a circular arc, the present method is considerably simplified.

First, we note that for a circular arc profile

κ = constant

and the solution of 2.10b is then

$$\tilde{\omega} = \frac{e^{-\int j\,d\theta}}{\kappa}\left[\int K\, e^{\int j\,d\theta}\, d\theta + C\right] \qquad \ldots\ldots\ldots 3.1.$$

where C is again a constant of integration.

Referring to fig. 3, let O be the centre of curvature of the top surface of a circular arc profile; ϕ is the angular distance from the leading edge along the surface, r is the radius of curvature of the surface, c is the chord length and θ is the angle which the direction of the tangent to the surface makes with some datum direction; suffix 1 refers to the values of ϕ and θ at some point P on the surface.

We then have $\theta = \phi + \theta_L$

$$d\theta = d\phi \qquad \ldots\ldots\ldots 3.2.$$

/where ...

where θ_L is the value of θ at the leading edge.

Further, we have $\kappa_L \equiv \frac{\partial\theta}{\partial s} = \frac{\partial\phi}{\partial s} = \frac{180}{\pi}\frac{1}{r}$

(θ and ϕ measured in degrees).

To express eqn. 2.11 in a non-dimensional form, we introduce the following dimensionless quantities:

$$\left.\begin{aligned} \bar{u} = \frac{u}{q^*} \;;\; \bar{\rho} = \frac{\rho}{\rho_s} \;;\; \bar{\mu} = \frac{\mu}{\mu_s} \;;\; \bar{\vartheta} = \frac{2\vartheta}{c} \;;\; \bar{\delta}_1 = \frac{\delta_1}{c} \\ R_o = \frac{U_o \rho_o c}{\mu_o} \;;\; \bar{\textcircled{\sim}} = (\bar{\rho}\,\bar{\vartheta})^2 \end{aligned}\right\} \quad \ldots 3.3.$$

where q^* is the critical velocity, and the suffices o, 1 and s denote the free stream conditions ahead of the aerofoil, the main stream conditions at the edge of the boundary layer, and the stagnation (reservoir) conditions, respectively.

Eqn. 2.10b is then transformed into

$$\frac{d\bar{\textcircled{\sim}}}{d\phi} + \bar{j}(\theta)\bar{\textcircled{\sim}} = A^2 \bar{k}(\theta) \qquad \ldots\ldots\ldots 3.4.$$

where $\bar{j}(\theta) = \frac{g(\theta)}{\bar{u}_1}\frac{d\bar{u}_1}{d\phi}$; $\bar{k}(\theta) = \frac{\bar{\mu}_1\bar{\rho}_1}{\bar{u}_1 f(\theta)}$

$$A^2 = \frac{\pi}{45}\,\frac{r}{c}\,\frac{p_{so}}{p_{s1}}\,\frac{\bar{\rho}_o\bar{u}_o}{R_o}\,\frac{1}{\bar{\mu}_o} \qquad \ldots\ldots\ldots 3.4a.$$

We note that A^2 is a function of M_o and the incidence α only and is, therefore, constant along the surface.

We shall now restrict the solution of 3.4. to the case of an attached shock or an expansion at the leading edge, so that $\left[\bar{\textcircled{\sim}}\right]_{\phi=0} = 0$, as before.

Solving 3.4. we have

$$\left[\bar{\textcircled{\sim}}\right]_{\phi_1} = A^2\, e^{-\int_o^{\phi_1} \bar{j}\, d\phi} \int_o^{\phi_1} \bar{k}\, e^{\int_o^{\phi} j\, d\phi}\, d\phi \qquad \ldots\ldots\ldots 3.5.$$

If we now let $\theta = 0$ when $M = 1$, as is usual when dealing with the simple-wave flow relations, we find it convenient to define some datum $\theta_D > 0$, to avoid the singularity at $\theta = 0$,

/where ...

where $\frac{du}{d\theta} \to \infty$. Eqn. 3.5. can then be written

$$\left[\bar{\omega}\right]_{\theta_1} = A^2 \, e^{-\int_{\theta_L}^{\theta_1} \bar{j}\, d\theta} \int_{\theta_L}^{\theta_1} \bar{k}\, e^{\int_{\theta_L}^{\theta} \bar{j}\, d\theta} \, d\theta, \text{ by 3.2.,}$$

or,
$$\left[\bar{\omega}\right]_{\theta_1} = A^2 \, e^{-\int_{\theta_D}^{\theta_1} \bar{j}\, d\theta} \left[\int_{\theta_D}^{\theta_1} \bar{k}\, e^{\int_{\theta_D}^{\theta} \bar{j}\, d\theta} \, d\theta - \int_{\theta_D}^{\theta_L} \bar{k} e^{\int_{\theta_D}^{\theta} d\theta} \, d\theta \right] \quad \ldots\ldots\ldots 3.6.$$

or,
$$\left[\bar{\omega}\right]_{\theta_1} = A^2 \, e^{-\int_{\theta_D}^{\theta_1} \bar{j}\, d\theta} \left[K(\theta_1) - K(\theta_L) \right] \quad \ldots\ldots 3.6a.$$

where
$$K(\theta_1) = \int_{\theta_D}^{\theta_1} \bar{k}\, e^{\int_{\theta_D}^{\theta} \bar{j}\, d\theta} \, d\theta$$

But,
$$\bar{\vartheta} = \sqrt{\frac{\bar{\omega}}{\bar{\rho}^2}}$$

hence,
$$\bar{\vartheta}_1 = A \, J_{\vartheta}(\theta_1) \sqrt{K(\theta_1) - K(\theta_L)}$$

and
$$\delta_1 = A \, J_{\delta}(\theta_1) \sqrt{K(\theta_1) - K(\theta_L)} \quad \ldots\ldots\ldots 3.7.$$

$$-\tfrac{1}{2} \int_{\theta_D}^{\theta_1} \bar{j}\, d\theta$$

where
$$J_{\vartheta}(\theta_1) = \frac{e}{\bar{\rho}_1} \quad \text{and} \quad J_{\delta}(\theta) = H \, J_{\vartheta}(\theta) \quad \ldots\ldots\ldots 3.7a.$$

From eqn. 2.9. the local skin friction coefficient can be determined and we find that

$$c_f \equiv \frac{2\,\tau_w}{\rho_o U_o^2} = B. \, L(\theta) \bar{\vartheta} + C. \, M(\theta) \, \frac{1}{\bar{\vartheta}} \quad \ldots\ldots\ldots 3.8.$$

/where ...

where
$$L(\theta) = \frac{\bar{p}_1 M_1^2}{\bar{u}_1} \frac{d\bar{u}_1}{d\theta} m(\theta) f(\theta)$$
$$M(\theta) = \frac{\bar{\mu}_1 \bar{u}_1}{f(\theta)}$$
$$B = \frac{60}{\pi} \frac{c}{r} \frac{1}{\bar{p}_o M_o^2} \frac{p_{s1}}{p_{so}} ; \quad C = \frac{4}{\bar{\mu}_o \bar{u}_o} \frac{1}{R_o} \qquad \text{..3.8a.}$$

We note that the functions J, K, L and M do not involve the aerofoil dimensions and are unique functions of the flow direction. Once evaluated, these functions can be used to compute ϑ, δ_1 and c_f for any circular arc profile, provided that the leading edge shocks are attached.

So far, the method has been quite general and the only condition we have imposed on the functions f, h, and m was that they must be unique functions of θ. It is now suggested that the variation of these functions with the local Mach number M_1 can be taken to be the same as for a flat plate at zero incidence with the corresponding free stream Mach number $M_o = M_1$. We could choose the flat plate solution for which $w = \sigma = 1$, to be consistent with the coordinate transformation 2.1. but it is believed more accurate to use the flat plate solution as given by Young in ref. 31. Young obtained.-

$$H = 2.59 \ (1 + 0.277 M_o^2)$$
$$\frac{\delta^*}{\vartheta} = 9.072 \left[1 + 0.365 \ (\gamma-1)\sigma^{\frac{1}{2}} M_o^2\right]^{(1-w)} \qquad \text{.....3.9.}$$
$$\frac{\mu_w}{\mu_o} = \left[1 + \frac{\gamma-1}{2} \sigma^{\frac{1}{2}} M_o^2\right]^w$$

so that, taking $w = 8/9$, $\sigma = 0.72$ and $\gamma = 1.4$, we have

$$h(\theta) \equiv H = 2.59 \ (1 + 0.277 M_1^2)$$
$$f(\theta) \equiv \frac{\delta^*}{\vartheta} = 9.072 \left[1 + 0.12388 M_1^2\right]^{1/9} \qquad \text{....3.10.}$$
$$m(\theta) \equiv \frac{\mu_w}{\mu_1} = (1 + 0.1697 M_1^2)^{8/9}$$

Expressions for functions g, k, J, K, L and M then follow from their definitions.

/APPENDIX II ...

APPENDIX II

DERIVATION OF DRAG-ENTROPY AND LIFT RELATIONS FROM MOMENTUM THEOREM; VORTICITY TRANSPORT

1.

Consider a two-dimensional aerofoil in a uniform supersonic stream, enclosed by a simple-connected boundary C (fig.2a). The momentum theorem, which is a direct consequence of Newton's laws of motion, states that:

Force exerted by a body on fluid in the positive direction = force exerted by the boundary C on the fluid inside it in the positive direction,

- the nett flow of momentum across the boundary C,

provided the flow is steady and body forces negligible. This can be written

$$\underline{R} = \underline{F} - \int \rho \, q_n \, ds. \, \underline{q} \qquad \text{.....1.1.}$$

where $\underline{q}$ is the resultant velocity vector at some point P on C,

q_n is the velocity component normal to the length of arc element of C, and

$\underline{R}$ is the resultant force on the body.

It will be easily seen from fig. 2a that this results in the following expressions for lift and drag:

$$-D = \int_C \rho u(u\,dy - v\,dx) + \int_C (p_{yx}\,dx - p_{xx}\,dy) \qquad \text{.....1.2.}$$

$$-L = \int_C \rho v(u\,dy - v\,dx) + \int_C (p_{yy}\,dx - p_{yx}\,dy) \qquad \text{.....1.3.}$$

where p_{xx}, p_{yx}, p_{yy} are the stress components given in the case of a compressible viscous fluid by

$$\left.\begin{aligned} p_{xx} &= -\left(p + \tfrac{2}{3}\mu\triangle\right) + \mu\, e_{xx} = -\left(p + \tfrac{2}{3}\mu\triangle\right) + 2\mu\,\frac{\partial u}{\partial x} \\ p_{yy} &= -\left(p + \tfrac{2}{3}\mu\triangle\right) + \mu\, e_{yy} = -\left(p + \tfrac{2}{3}\mu\triangle\right) + 2\mu\,\frac{\partial v}{\partial y} \\ p_{yx} &= p_{xy} = \mu\, e_{xy} = \mu\left(\frac{\partial v}{\partial x} + \frac{\partial u}{\partial y}\right) = 2\mu\,\frac{\partial u}{\partial y} + \mu\,\zeta \end{aligned}\right\} \quad 1.4.$$

/with ...

with p = the static pressure,

$\Delta \equiv \frac{\partial u}{\partial x} + \frac{\partial v}{\partial y}$, the 'dilation',

$\zeta = \frac{\partial u}{\partial y} - \frac{\partial v}{\partial x}$, the vorticity,

μ = the coefficient of viscosity.

2. Entropy-Drag Relation

Let the boundary C_1 be a rectangle with its horizontal sides parallel to the free stream direction (fig. 2b) and enclosing a two-dimensional aerofoil. AB is taken to be far downstream ($x = \infty$) and the sides AD and BC at $y = \infty$ and $y = -\infty$, respectively.

The following assumptions are now made:

(i) pressure on AB is equal to the free stream static pressure;

(ii) velocity on AB has the free stream direction.

These assumptions rest on the fact, supported by both the theory and the experimental evidence, that even immediately downstream of the trailing edge shocks, the downwash is very small (angle of downwash $\ll 1^\circ$, c.f. ref. 40), and the static pressure is very nearly equal to the free stream static pressure.

Now, on DC $dx = 0$, $v = \zeta = 0$, $u = u_o$, $\rho = \rho_o$, $p_{xx} = -p_o$; on AD and BC $dy = 0$, and since at ∞ the shock waves become Mach waves, the flow is irrotational and $\zeta = 0$, $\frac{\partial u}{\partial y} = 0$, hence $p_{yx} = 0$; on AB $dx = 0$, $\frac{\partial v}{\partial y} = 0$ by (ii) above, $\frac{\partial u}{\partial x}$ is at most of the order of $\frac{u}{x}$ and $\to 0$ as $x \to \infty$, hence $p_{xx} = -p_o$.* The eqn. 1.2. then reduces to

$$D = \int_{DC} \rho_o u_o^2 \, dy - \int_{AB} \rho u^2 \, dy - \int_{DA-CB} \rho uv \, dx \quad \ldots 2.1.$$

since $\int_C p_o \, ds = 0$

Now along AD and BC the flow is isentropic with the entropy having its free stream value and since $u \to u_o$,

/$v \to 0$

---

* Accepting the usual boundary layer approximations for flow in the wake, this also holds on W, i.e. that part of AB which is in the wake.

$v \to 0$ and $\rho \to \rho_o$ as $y \to \pm\infty$, we can write

$$u = u_o + u', \quad v = v', \quad \rho = \rho_o + \rho' \qquad \ldots\ldots\ldots 2.2.$$

where the suffix o refers to the free stream conditions and ρ', u', v', are the usual perturbation quantities whose products and powers higher than 1 can be neglected. Then,

$$\rho uv \doteq \rho_o u_o v'$$

and eqn. 2.1 becomes

$$D = \int_{DC} \rho_o u_o^2 \, dy - \int_{AB} \rho u^2 \, dy - \int_{DA-CB} \rho_o u_o v' dx \qquad \ldots\ldots\ldots 2.1a.$$

Continuity of mass flow in ABCD gives

$$\int_{DC} \rho_o u_o \, dy - \int_{AB} \rho u \, dy = \int_{DC-CB} \rho_o v' dx \qquad \ldots\ldots 2.3.$$

Hence, substituting for $\rho_o v'$ in 2.1a we have

$$D = \int_{AB} \rho u \, (u_o - u) dy \qquad \ldots\ldots\ldots 2.4.$$

or,
$$D = \int_{AB-W} \rho u (u_o - u) dy + \int_{W} \rho u (u_o - u) dy \qquad \ldots\ldots\ldots 2.5.$$

where W denotes integration across the wake.

In the case of incompressible flow, or shock-free compressible flow, $u = u_o$ at infinity outside the wake, and 2.5. reduces to the familiar expression for the profile drag of an aerofoil.-

$$D_p = \int_W \rho_\infty u_\infty (u_o - u_\infty) dy \qquad \ldots\ldots\ldots 2.6.$$

where ∞ denotes conditions on AB $(x = \infty)$. This implies that the first integral in 2.5. gives the wave drag of the aerofoil in supersonic flow, i.e.

$$D_W = \int_{\infty(-W)-\infty} \rho_\infty u_\infty (u_o - u_\infty) dy \qquad \ldots\ldots\ldots 2.7.$$

/where ...

where $\infty(-W)-\infty$ indicates integration excluding the wake.

We shall now assume that viscosity in the main stream is negligible, and that there is no heat transfer. The equation of energy is then

$$\tfrac{1}{2} q^2 + \frac{\gamma}{\gamma-1} \cdot \frac{p}{\rho} = \text{const.} = J C_p T_{so}$$

so that for conditions on DC and AB we have (ouside the wake):

$$\tfrac{1}{2} u_o^2 + \frac{\gamma}{\gamma-1} \frac{p_o}{\rho_o} = \tfrac{1}{2} u^2 + \frac{\gamma}{\gamma-1} \frac{p_o}{\rho} = J C_p T_{so} \quad \ldots\ldots 2.8.$$

dropping the suffix ∞ and remembering that u and ρ refer to conditions at $x = \infty$.

2.8. yields $\frac{u}{u_o} = \sqrt{(k+1) - k \frac{\rho_o}{\rho}}$, where $k = \frac{2}{\gamma-1} \frac{1}{M_o^2}$ ..2.9.

From 2.7.

$$C_{D_w} = \frac{D_w}{\frac{1}{2} \rho_o u_o^2 c} = 2 \int_{\infty(W)-\infty} \frac{\rho u}{\rho_o u_o} \left(1 - \frac{u}{u_o}\right) d\left(\frac{y}{c}\right)$$

.....2.10.

Substituting 2.9 into 2.10 and rearranging, we have

$$C_{D_w} = 2 \int_{\infty(W)-\infty} \left[k - \frac{\rho}{\rho_o} (k+1) + \sqrt{(k+1)\left(\frac{\rho}{\rho_o}\right)^2 - k\left(\frac{\rho}{\rho_o}\right)} \right] d\bar{y}$$

.....2.11

where $\bar{y} = y/c$.

Now, along a streamline the change of entropy between DC and AB is

$$\triangle S \equiv S - S_o = C_p \frac{\gamma-1}{\gamma} \log\left(\frac{p_{so}}{p_{s1}}\right) \quad \ldots\ldots 2.12.$$

But $$\frac{p_{so}}{p_{s1}} = \left[\frac{p}{p_o} \left(\frac{\rho_o}{\rho}\right)^{\gamma} \right]^{1/\gamma-1} = \left(\frac{\rho_o}{\rho}\right)^{\gamma/\gamma-1}, \quad \text{as } p = p_o.$$

Hence $$\triangle S = - C_p \log\left(\frac{\rho}{\rho_o}\right)$$

or, $$\frac{\rho}{\rho_o} = e^{-\triangle S/C_p} \quad \ldots\ldots 2.13.$$

/Substituting ...

substituting this into 2.11, we get

$$C_{D_w} = 2\int_{\infty(W)-\infty} \left[k - (k+1)e^{-\Delta S/C_p} + \sqrt{(k+1)e^{-\Delta S/C_p} - ke^{-\Delta S/C_p} \cdots} \right] d\bar{y} \quad \ldots\ldots\ldots 2.14.$$

Eqn. 2.14. relates the pressure drag of a supersonic aerofoil to the entropy change across the shock system associated with the aerofoil. For thin aerofoils at small incidences and moderate supersonic Mach numbers, ΔS will, in general be small and we can simplify the above relation considerably by expanding $e^{-\Delta S/C_p}$ and neglecting powers of $\frac{\Delta S}{C_p}$ greater than 1. Eqn. 2.14 then reduces to

$$C_{D_w} = k\int_{\infty(W)-\infty} \frac{\Delta S}{C_p}\, d\bar{y} = \frac{2}{(\gamma-1)\,M_o^2}\int_{\infty(W)-\infty} \frac{\Delta S}{C_p}\, d\left(\frac{y}{c}\right) \quad \ldots\ldots 2.15.$$

or
$$C_{D_w} = \frac{2}{(\gamma-1)M_o^2}\,\frac{1}{C_p}\int_{\infty(W)-\infty} (S-S_o)\, d\left(\frac{y}{c}\right) \quad \ldots\ldots\ldots 2.15a.$$

i.e., the pressure drag of a supersonic aerofoil is approximately proportional to the integral of entropy round the aerofoil. This is equivalent to the result obtained by Liepmann in ref. 11, viz.:

$$\frac{D\,u_o}{m\,R\,T_o} \doteq \frac{\gamma}{\gamma-1}\,\frac{\Delta S}{C_p} \quad ; \quad \text{where } m = \text{mass flow.}$$

Since the above derivation was obtained independently and the method of approach is somewhat different from Liepmann's, it was thought that its details would not be out of place in the present report.

It is to be noted that the approximation involved in obtaining 2.15 from 2.14 is equivalent to assuming that the linearised relations 2.2 hold not only at $y = \pm\infty$, but also for finite y at $x = \infty$, for then

$$\rho u\,(u_o - u) \doteq -\rho_o u_o u'$$

$$u_o u' \doteq \frac{\gamma}{\gamma-1}\,\frac{p_o}{\rho_o}\,\frac{\rho'}{\rho_o} \quad , \text{ from the linearised form of}$$

the energy equation, and the result 2.15 readily follows.

3. Lift

Consider now an aerofoil at an incidence enclosed by

/a rectangular ...

a rectangular boundary C_2, as shown in fig. 2c. FA is not necessarily far downstream, so that GF and HA are at finite distances from the aerofoil.

On FA $dx = 0$. FGHA lies in the undisturbed uniform stream, hence in eqn. 1.3. $\int_{FGHA} = 0$, and 1.3 reduces to

$$L = -\int_{AF} (\rho uv - p_{yx})\,dy = -\int_{AF} (\rho uv - 2\mu \frac{\partial u}{\partial y} - \mu\zeta)\,dy \quad 3.1.$$

If the viscosity can be neglected outside the wake, 3.1. yields

$$L = -\int_{AC,DF} \rho uv\,dy - \int_{Wake} \mu\,\zeta\,dy \quad \ldots\ldots\ldots 3.2.$$

since in the wake $2\mu \frac{\partial u}{\partial y} \doteq -2\mu\zeta$

The first term in 3.2 is the result obtained for inviscid flow in ref. 36. The second term can be shown to be either zero or negligibly small by the following argument.

Integrating the second term of 3.2 and applying the mean value theorem

$$-\int_W \mu\,\zeta\,dy = \int_W \mu \frac{\partial u}{\partial y}\,dy = \int_W \mu\,du = \mu_m (u_D - u_C) \quad \ldots\ldots\ldots 3.2a.$$

where μ_m is a mean value of μ in the wake, and u_D, u_C are the velocities just outside the wake, below and above it. If the wake is symmetrical, $u_D = u_C$ and $\int = 0$. If it is not symmetrical, we can estimate the order of magnitude of $\int_W \mu\,\zeta\,dy$ as follows. From 2.9 the velocity far downstream is, outside the wake

$$u = (k+1 - ke^{\Delta S/C_p})^{\frac{1}{2}}\, u.$$

Hence, to first order of $\Delta S/C_p$

$$\frac{u}{u_o} = 1 - \tfrac{1}{2}\, k\, \frac{\Delta S}{C_p} = 1 - \tfrac{1}{2}\, k\, (S - S_o)$$

so that $u_D - u_C = \frac{u_o k}{2C_p} \left[S_C - S_D\right] = \frac{u_o k}{2} \frac{\Delta S_W}{C_p}$

where ΔS_W = the difference in entropy between the streamlines just outside the wake.

/The ...

The contribution of $-\int_W \mu\,\zeta\,dy$ to the lift coefficient is then,

$$\Delta C_{L_W} = \tfrac{1}{2} u_o\, k\, \frac{\Delta S_W}{C_p}\, \mu_m\, \frac{1}{\tfrac{1}{2}\rho_o u_o^2 c} = \frac{2}{\gamma-1}\,\frac{\mu_m}{\mu_o}\,\frac{1}{M_o^2}\,\frac{\Delta S_W}{C_p}\,\frac{1}{R_o}$$

where $R_o = \dfrac{\rho_o u_o c}{\mu_o}$.

Hence, in general $\Delta C_{L_{wake}} = 0\ (R_o^{-1})$

and the effect of wake on lift is clearly negligible.

Eqn. 3.2. then becomes

$$L = -\int_{AC,DF} \rho u\, v\, dy \qquad \ldots\ldots\ldots 3.3.$$

We now take C_2 to be any simply-connected boundary enclosing the aerofoil and use the linear relations 2.2. Further, we neglect viscosity and changes of entropy. We then have $\rho v\,(u\,dy - v\,dx) \doteq \rho_o u_o\, v'dy$

Bernoulli's eqn. is $dp + \rho q\, dq \equiv dp + \rho(u\,du + v\,dv) = 0$ 3.4.

Substituting for u, v and ρ in 3.4. from 2.2, together with a corresponding relation for p, viz.: $p = p_o + p'$, we have

$$p' + \rho_o u_o u' = 0 \qquad \ldots\ldots\ldots 3.5.$$

Eqn. 1.3. then becomes

$$L = -\int_C \left[\rho_o u_o v'dy - (p_o + p')dx\right]$$

$$= -\int_C \left[\rho_o u_o (v'dy + u'dx) - (\rho_o u_o u' + p')dx\right],$$

since $\int_C p_o dx = 0$

Hence $L \doteq -\int_C \rho_o u_o (v'dy + u'dx)$ by 3.5.

Now $v'dy + u'dx = \underline{q}'.\ d\underline{s} = d\Gamma$ by the definition of circulation, and

$$L \doteq \rho_o u_o \Gamma_c \qquad \ldots\ldots\ldots 3.6.$$

/where ...

where Γ_c is the circulation round C (in the clockwise sense). Thus, in supersonic flow the lift-circulation theorem is true to the first order only, i.e. if the flow outside the wake is assumed isentropic. The same result was obtained by Lighthill in ref. 36, by considering pressure distribution on a two-dimensional supersonic aerofoil as given by the linearised theory.

Relation 3.6. can also be deduced directly from Temple's result for compressible subsonic flow (ref. 38), as neglecting changes of entropy amounts to treating the flow as isentropic. There is, however, one important difference in the argument - Temple shows that by expanding the boundary C to infinity, the relation $L = \rho_o u_o \Gamma_c$ becomes exact for the subsonic compressible case, as the terms neglected in the exact momentum equation are of the order of $1/r$, where r is the distance from the aerofoil. This is not longer true for the supersonic case with shock waves present, since the change of entropy along the streamlines is independent of x, the distance downstream of the aerofoil, and does not become zero as $x \to \infty$. The terms in the momentum equation which depend on entropy are, in general, $O\left(\frac{1}{y^n}\right)$ and as one cannot have $y = \infty$ everywhere on C, the relation 3.6. does not become exact even at infinity.

/APPENDIX III ...

APPENDIX III

INTERPOLATION FORMULAE FOR FORCE COEFFICIENTS ON TWO-DIMENSIONAL SUPERSONIC CIRCULAR ARC PROFILES

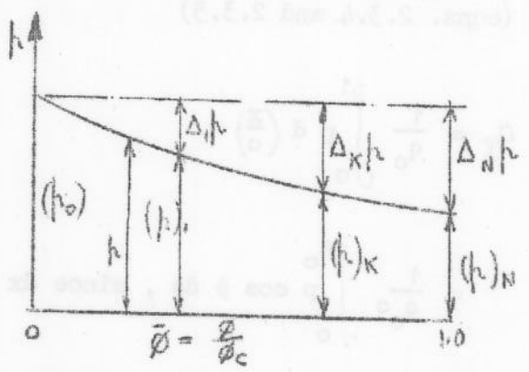

Let the pressure p at any point P on the surface be expressed as a polynomial of degree n in $\bar{\phi}$, with constant coefficients:

$$p = \sum_{j=0}^{n} a_j \bar{\phi}^j \qquad \ldots\ldots\ldots 1$$

To determine the coefficients 'a', n equations are required. Choosing n equally spaced intervals of $\bar{\phi}$ we shall have

$$\bar{\phi}_k = k/n, \quad k = 0, 1, 2, \ldots\ldots, n \qquad \ldots\ldots\ldots 2$$

so that $$(p)_k = \sum_{j=0}^{n} a_j \bar{\phi}_k^j = \sum_{j=0}^{n} a_j \left(\frac{k}{n}\right)^j, \qquad \ldots\ldots\ldots 3$$

But for $k = 0$, $(p)_0 = a_0$

hence $$\Delta_k p \equiv (p)_k - (p)_0 = \sum_{j=1}^{n} a_j \left(\frac{k}{n}\right)^j \qquad \ldots\ldots\ldots 4$$

$$k = 1, 2, \ldots, n$$

Solving for the coefficients 'a', we have

$$a_j = A_j/D \qquad \ldots\ldots\ldots 5$$

where $$D = \begin{vmatrix} 1/n, & (1/n)^2, \ldots, & (1/n)^j, \ldots, & (1/n)^n \\ 2/n, & (2/n)^2, \ldots, & (2/n)^j, \ldots, & (2/n)^n \\ \cdot & \cdot & \cdot & \cdot \\ \cdot & \cdot & \cdot & \cdot \\ (k/n), & (k/n)^2, \ldots, & (k/n)^j, \ldots, & (k/n)^n \\ \cdot & \cdot & \cdot & \cdot \\ 1, & 1, \ldots\ldots, & 1, \ldots\ldots, & 1 \end{vmatrix} \quad k = 1, 1, \ldots, n$$

/and ...

and A_j is the determinant D with its j^{th} column replaced by

$$\Delta_k p, \quad k = 1, 2, \ldots, n$$

Considering the lower surface only, the force coefficients are (eqns. 2.3.4 and 2.3.5)

$$C_Y = \frac{1}{q_o} \int_o^1 p \, d\left(\frac{x}{c}\right)$$

$$= \frac{1}{q_o c} \int_o^{s_c} p \cos\beta \, ds \text{ , since } dx = \cos\beta \, ds,$$

$$= \frac{1}{q_o} \frac{r}{c} \int_o^{\phi_c} p \cos\beta \, d\phi \text{ , since } s = \phi r \text{ (ϕ in radians),}$$

$$= \frac{2\beta_\ell}{q_o} \frac{r}{c} \int_o^1 p \cos(\beta_\ell - \phi) d\bar{\phi}, \text{ since } \beta = \beta_\ell - \phi = \beta_\ell - \phi_c \bar{\phi}, \quad \phi_c = 2\beta_\ell$$

Expanding and substituting for p from (1),

$$C_Y = \frac{2\beta_\ell}{q_o} \frac{r}{c} \int_o^1 (\cos\beta_\ell \cos\phi + \sin\beta_\ell \sin\phi) \sum_{j=0}^{n} a_j \bar{\phi}^j \, d\bar{\phi} \qquad \ldots\ldots\ldots 7$$

Similarly,

$$C_X = \frac{2\beta_\ell}{q_o} \frac{r}{c} \int_o^1 (\sin\beta_\ell \cos\phi - \cos\beta_\ell \sin\phi) \sum_{j=0}^{n} a_j \bar{\phi}^j \, d\bar{\phi} \qquad \ldots\ldots\ldots 8$$

Eqns. (7) and (8) involve integrals of the form

$$\int \phi^n \cos b\phi \, d\phi \; ; \quad \int \phi^n \sin b\phi \, d\phi$$

Using the reduction formulae

$$\int \phi^n \cos b\phi \, d\phi = \frac{\phi^n}{b} \sin b\phi - \frac{n}{b} \int \phi^{n-1} \sin b\phi \, d\phi$$

$$\int \phi^n \sin b\phi \, d\phi = -\frac{\phi^n}{b} \cos b\phi + \frac{n}{b} \int \phi^{n-1} \cos b\phi \, d\phi$$

eqns. (7) and (8) can be written in the form

$$C_Y = \frac{2\beta_\ell}{q_o} \frac{r}{c} \left[\cos\beta_\ell \sum_{j=0}^{n} a_j f_j(\beta_\ell) + \sin\beta_\ell \sum_{j=0}^{n} a_j g_j(\beta_\ell) \right] \qquad \ldots\ldots\ldots 9$$

/C_X ...

$$C_X = \frac{2\beta_\ell}{q_o} \cdot \frac{r}{c}\left[\sin\beta_\ell \sum_{j=0}^{n} a_j f_j(\beta_\ell) - \cos\beta_\ell \sum_{j=0}^{n} a_j g_j(\beta_\ell)\right] \quad \ldots\ldots\ldots 10$$

where $f_j(\beta_\ell) = f_o(\beta_\ell) - \frac{j}{2\beta_\ell} g_{j-1}(\beta_\ell)$; $g_j(\beta_\ell) = g_o(\beta_\ell) - \frac{1}{2\beta_\ell} + \frac{j}{2\beta_\ell} f_{j-1}(\beta_\ell)$

$$f_o(\beta_\ell) = \frac{1}{2\beta_\ell}\sin 2\beta_\ell \; ; \quad g_o(\beta_\ell) = \frac{1}{2\beta_\ell}\left[1 - \cos 2\beta_\ell\right] \quad \ldots\ldots\ldots 11$$

For aerofoils with the thickness ratio up to 10 - 12 per cent, it will in general be found sufficiently accurate to use a third degree polynomial. With $n = 3$, eqns. (5) and (6) give for the coefficients 'a'.-

$$\begin{aligned} a_o &= (p)_o \,, \\ a_1 &= 9\Delta_1 p - 4.5\Delta_2 p + \Delta_3 p \,, \\ a_2 &= -22.5\Delta_1 p + 18\Delta_2 p - 4.5\Delta_3 p, \quad \ldots\ldots\ldots 12 \\ a_3 &= 13.5\Delta_1 p - 13.5\Delta_2 p + 4.5\Delta_3 p \end{aligned}$$

For the particular case of a 10 per cent thick circular arc profile

$$\beta_\ell = 11^\circ 25' \; ; \quad r/c = 2.525$$

and the f and g functions have the following numerical values.-

n	0	1	2	3
f	.97375	.48035	.31762	.23602
g	.19663	.13074	.09800	.07847

Hence,

$$C_Y = \frac{1}{q_o}\left[.99965(p)_o + .36415\Delta_1 p + .38745\Delta_2 p + .12014\Delta_3 p\right] \quad \ldots\ldots\ldots 13$$

$$C_X = \frac{1}{q_o}\left[.04170\Delta_1 p - .04116\Delta_2 p - .01973\Delta_3 p\right] \quad \ldots\ldots\ldots 14$$

Example

At $M_o = 2.13$ and with $\alpha = 10^\circ$ it was found using the above formulae that

$$C_L = 0.3928, \quad C_{D_w} = 0.1007$$

which is in excellent agreement with the corresponding results obtained by a numerical integration of pressure distributions, viz.:

$$C_L = 0.3930, \quad C_{D_w} = 0.1004.$$

REFERENCES

1. Preston, J.H. — The approximate calculation of the lift of symmetrical aerofoils taking account of the boundary layer, with application to control problems. A.R.C., R and M. 1996, 1943.

2. Preston, J.H. — The effect of the boundary layer and wake on the flow past a symmetrical aerofoil at zero incidence. A.R.C. R. and M. 2107, 1945.

3. Preston, J.H. — The calculation of lift, taking account of the boundary layer. A.R.C. 12,747, 1949.

4. Ferri, A. — Some experimental results obtained on wing profiles in the Guidonia supersonic wind tunnel, (Atti di Guidonia No. 17, 1939). R.T.P. Translation No. 1115, also NACA TM 946.

5. Valensi, J. Pruden, F.W. — Some observations on sharp nosed profiles at supersonic speeds. A.R.C. 10,607, 1947.

6. Holder, D.W., Tomlinson, R.C., Rogers, E.W.E. — Preliminary experiments on blunt-nosed flat plates in supersonic airstreams. A.R.C. 12,418, 1949.

7. Holder, D.W., North, R.J., Chinneck, A. — Addendum to A.R.C. 12,418

8. Holder, D.W., North, R.J., Chinneck, A. — Observations of the bow-waves of blunt-nosed bodies of revolution in supersonic airstreams. A.R.C. 12,495, 1949.

9. Holder, D.W., Chinneck, A., Hurley, D.G. — Observations of the supersonic flow round a 6 per cent thick double wedge. A.R.C. 13,623, 1950.

10. Beastall, D., and Pallant, R.J. — Wind tunnel tests on two-dimensional supersonic aerofoils at M = 1.86 and M = 2.48. R.A.E. Rep. Aero. 2384, 1950.

11. Liepmann, H.W. — On the relation between drag and entropy. Douglas A.C. Rep. SM-13726, 1950.

12. Young, A.D. — Boundary layers in compressible flow. Modern Developments in Fluid Dynamics Vol. III, Chapter X, (to be published).

13. Daboo, J.E. — The profile drag of wing sections at supersonic speeds. College of Aeronautics Diploma thesis (to be published as a C. of A. report)

14. Liepmann, H.W., Ashkenas, H., Cole, J.D. — Experiments in transonic flow. GALCIT Suppl. No. 6 to W33038 ac 1717 (11592), 1947.

/15. ...

15. Liepmann, H.W., Bryson, Jr. A.E. — Transonic flow past wedge sections. J.Ae.Sc. Vol.17, No.12, 1950.

16. Bardsley, O. — The conditions at a sharp leading edge in supersonic flow. Phil. Mag. Vol.42, 1951, pp.255-63.

17. Lagerstrom, P.A., Cole, J.D., Trilling, L. — Problems in the theory of viscous compressible fluids. C.I.T. Rep. for O.N.R., 1949.

18. Ferri, A. — Method of evaluating from shadow or schlieren photographs the pressure drag in two-dimensional or axially-symmetrical flow phenomena with detached shocks. NACA TN. 1808, 1948.

19. Ferri, A. — Application of the method of characteristics to supersonic rotational flow. NACA Rep. 841, 1946.

20. Moeckel, W.E. — Approximate method for predicting form and location of detached shock waves ahead of plane or axially symmetric bodies. NACA TN 1921, 1949.

21. Liepmann, H.W., Roshko, A., Dhawan, S. — On the reflection of shock waves from the boundary layer. GALCIT Final Rep. for contr.NAw-5631 1949.

22. Fage, A., Sargent, R.F. — Shock wave and boundary layer phenomena near a flat plate. Proc. Roy. Soc. A190, 1947.

23. Bardsley, O., Mair, W.A. — The interaction between an oblique shock wave and a turbulent boundary layer. Phil. Mag. Vol. 42, 1951, pp.29-36.

24. Howarth, L. — The propagation of a steady disturbance in a supersonic stream bounded on one side by a parallel subsonic stream. Proc. Cambridge Phil.Soc. Vol. 44, 1944, pp. 380-390.

25. Tsien, H.S., Finston, M. — Interaction between parallel streams of subsonic and supersonic velocities. Jnl. of Aero. Sc. Vol. 16, 1949, pp. 515-28.

26. Oswatitsch, K., Wieghardt, K. — Theoretical analysis of stationary potential flows and boundary layers at high speeds. GDC 10/4482T, 1946.

27. Howarth, L. — Concerning the effect of compressibility on laminar boundary layers. Proc.Roy.Soc. A194, 1948, pp.16-42.

28. Young, A.D. — Skin friction in laminar boundary layers in compressible flow. College of Aeronautics Rep. No. 20, 1948.

29. Dorodnitzyn, A. — Laminar boundary layer in a compressible fluid. Comptes Rendus Acad.Sc.USSR, Vol.4, 1942, pp. 213-219.

/30.

30. Dryden, H.L. — Computation of the two-dimensional flow in a laminar boundary layer. NACA Rep. 497, 1934.

31. Young, A.D., Winterbottom, N.E. — High speed flow in smooth cylindrical pipes of circular section. R. and M. 2068, 1942.

32. Tucker, M. — Approximate turbulent boundary layer development in plane compressible flow along thermally insulated surfaces, with applications to supersonic wind tunnel corrections. NACA TN 2045, 1949.

33. Lees, L. — Stability of the supersonic laminar boundary layer with a pressure gradient. Princeton Univ. Rep. No. 167, 1950.

34. Laurmann, J.A. — Stability of laminar boundary layers in compressible flow with external pressure gradients. College of Aeronautics Rep. No. 48, 1951.

35. Ivey, H.R., Klunker, B.E. — Considerations of the total drag of supersonic aerofoil sections. NACA TN. 1371, 1947.

36. Lighthill, M.J. — Two-dimensional supersonic aerofoil theory. A.R.C. R. and M. 1929, 1944.

37. Lighthill, M.J. — The conditions behind the trailing edge of the supersonic aerofoil. A.R.C. R. and M. 1930, 1944.

38. Temple G. — Vorticity transport and theory of the wake. A.R.C. 7118, 1943.

39. Lin, C.C., Rubinov, S.I. — On the flow behind curved shocks. Jnl. of Mathematics and Physics, Vol.27, 1948, pp. 105-129.

40. Liepmann, H.W., Puckett, A.E. — Introduction to aerodynamics of a compressible fluid. New York, J. Wiley, Inc., 1948.

41. Lees, L. — Interaction between the laminar boundary layer over a plane surface and an incident oblique shock wave. Prin. Univ. Rep. No. 143, 1949.

42. Bryant and Williams — An investigation of the flow of air around an aerofoil of infinite span, with an appendix by G.I.Taylor. A.R.C. R. and M. 989, 1924.

Table I. Laminar Boundary Layer Functions

θ	$m(\theta)$	$f(\theta)$	$h(\theta)\equiv H$	$\bar{j}(\theta)$	$10^2\bar{k}(\theta)$	$J_{x\theta}(\theta)$	$K(\theta)$	$L(\theta)$	$M(\theta)$
0	1.150	9.191	3.307	∞	5.864			∞	.09461
1	1.170	9.206	3.429	.3064	5.014			.2559	.09633
2	1.191	9.218	3.510	.2416	4.516			.2078	.09794
3	1.206	9.231	3.584	.2098	4.142			.1843	.09942
4	1.221	9.243	3.655	.1895	3.830			.1694	.1006
5	1.235	9.253	3.723	.1753	3.554	1.986	0	.1584	.1016
6	1.248	9.263	3.791	.1644	3.307	1.890	.0374	.1497	.1024
7	1.267	9.274	3.857	.1560	3.071	1.810	.0784	.1426	.1032
8	1.276	9.284	3.929	.1485	2.884	1.739	.1227	.1367	.1038
9	1.291	9.294	3.995	.1425	2.697	1.677	.1711	.1316	.1042
10	1.305	9.304	4.068	.1372	2.524	1.620	.2232	.1268	.1046
11	1.324	9.314	4.144	.1326	2.358	1.569	.2770	.1225	.1049
12	1.335	9.324	4.210	.1286	2.218	1.523	.3387	.1187	.1052
13	1.349	9.334	4.281	.1252	2.081	1.481	.4024	.1148	.1054
14	1.365	9.345	4.362	.1221	1.951	1.442	.4701	.1112	.1055
15	1.380	9.356	4.439	.1193	1.832	1.407	.5419	.1080	.1056
16	1.396	9.366	4.517	.1167	1.718	1.373	.6178	.1049	.1055
17	1.413	9.377	4.598	.1143	1.611	1.347	.6977	.1019	.1054
18	1.429	9.388	4.681	.1121	1.512	1.320	.7818	.09883	.1052
19	1.445	9.410	4.765	.1102	1.420	1.296	.8701	.09595	.1050
20	1.463	9.422	4.850	.1084	1.333	1.275	.9625	.09325	.1048
21	1.481	9.434	4.941	.1068	1.249	1.254	1.059	.09083	.1045
22	1.506	9.446	5.032	.1054	1.172	1.236	1.160	.08832	.1041
23	1.518	9.458	5.126	.1040	1.099	1.219	1.265	.08568	.1037
24	1.537	9.470	5.222	.1027	1.030	1.204	1.374	.08319	.1033
25	1.553	9.482	5.321	.1014	.9647	1.190	1.487	.08061	.1028
26	1.578	9.482	5.422	.1002	.9033	1.177	1.604	.07831	.1023
27	1.598	9.495	5.527	.0992	.8450	1.167	1.726	.07602	.1017
28	1.619	9.508	5.635	.0983	.7900	1.157	1.851	.07376	.1011
29	1.641	9.521	5.745	.0974	.7391	1.148	1.980	.07153	.1004
30	1.663	9.535	5.859	.0965	.6912	1.140	2.113	.06932	.09975
31	1.687	9.549	5.976	.0957	.6447	1.135	2.250	.06718	.09900
32	1.711	9.562	6.098	.0951	.6028	1.130	2.391	.06514	.09824
33	1.735	9.576	6.222	.0945	.5626	1.125	2.535	.06305	.09742
34	1.760	9.591	6.351	.0939	.5246	1.122	2.683	.06110	.09660
35	1.791	9.605	6.483	.0932	.4900	1.120	2.834	.05919	.09571

θ	m(θ)	f(θ)	h(θ)≡H	$\bar{j}(\theta)$	$10^2\bar{k}(\theta)$	$J_{2d}(\theta)$	K(θ)	L(θ)	m(θ)
36	1.812	9.620	6.620	.0929	.4555	1.119	2.989	.05707	.09487
37	1.841	9.636	6.762	.0924	.4236	1.119	3.147	.05519	.09389
38	1.869	9.650	6.908	.0920	.3938	1.120	3.307	.05331	.09294
39	1.898	9.666	7.058	.0918	.3663	1.121	3.471	.05149	.09196
40	1.928	9.683	7.214	.0913	.3402	1.123	3.639	.04966	.09099
41	1.959	9.700	7.375	.0911	.3150	1.127	3.809	.04800	.08994
42	1.991	9.716	7.536	.0909	.2924	1.131	3.983	.04617	.08883
43	2.024	9.734	7.714	.0907	.2710	1.136	4.157	.04448	.08775
44	2.059	9.751	7.892	.0905	.2506	1.142	4.334	.04284	.08660
45	2.094	9.769	8.077	.0903	.2318	1.149	4.512	.04119	.08551
46	2.130	9.787	8.268	.0903	.2141	1.157	4.695	.03962	.08430
47	2.169	9.806	8.466	.0902	.1976	1.166	4.878	.03809	.08311
48	2.207	9.825	8.672	.0902	.1822	1.176	5.064	.03656	.08190
49	2.248	9.843	8.885	.0902	.1686	1.188	5.248	.03506	.08068
50	2.290	9.864	9.116	.0902	.1545	1.200	5.434	.03363	.07945

For the definitions of the above functions see the Appendix I.

/TABLE II ...

Table II. Functions of the Modified Pohlhausen Parameter λ used in Howarth's Approximate Method for Laminar Boundary Layers in Compressible Flow

λ	$g(\lambda)$	$k(\lambda)$	$\ell(\lambda)$	λ	$g(\lambda)$	$k(\lambda)$	$\ell(\lambda)$
0	34.05	6.811	0	7.2	-.8310	24.81	11.35
0.2	33.00	7.041	.2008	7.4	-1.992	26.04	12.01
0.4	31.94	7.276	.4032	7.6	-3.201	27.38	12.75
0.6	30.91	7.518	.6075	7.8	-4.462	28.74	13.52
0.8	29.89	7.768	.8138	8.0	-5.800	30.44	14.36
1.0	28.88	8.026	1.023				
1.2	27.98	8.291	1.234	8.2	-7.191	32.01	15.29
1.4	26.90	8.565	1.448	8.4	-8.682	34.15	16.31
1.6	25.93	8.849	1.665	8.6	-10.28	36.33	17.45
1.8	24.96	9.140	1.886	8.8	-12.01	38.77	18.71
2.0	24.00	9.442	2.110	9.0	-13.88	41.53	20.14
2.2	23.05	9.756	2.339	9.2	-15.96	44.70	21.77
2.4	22.11	10.08	2.571	9.4	-18.25	48.30	23.62
2.6	21.18	10.31	2.809	9.6	-20.84	52.52	25.77
2.8	20.25	10.77	3.052	9.8	-23.81	57.50	28.30
3.0	19.40	11.13	3.302	10.0	-27.25	63.47	31.33
3.2	18.41	11.50	3.555	10.1	-29.16	66.78	33.01
3.4	17.50	11.90	3.817	10.2	-31.37	70.74	35.01
3.6	16.59	12.31	4.086	10.3	-33.72	75.02	37.17
3.8	15.67	12.73	4.362	10.4	-36.37	79.83	39.59
4.0	14.76	13.17	4.646	10.5	-39.33	85.27	42.33
4.2	13.86	13.64	4.942	10.6	-42.66	91.49	45.47
4.4	12.94	14.13	5.246	10.7	-46.46	98.66	49.07
4.6	12.03	14.64	5.562	10.8	-50.88	107.0	53.27
4.8	11.12	15.18	5.890	10.9	-56.05	116.9	58.23
5.0	10.19	15.74	6.230	11.0	-62.20	128.8	65.28
5.2	9.345	16.34	6.586	11.1	-69.66	143.2	71.44
5.4	8.329	16.97	6.957	11.2	-78.93	161.3	80.49
5.6	7.384	17.64	7.345	11.3	-90.77	184.6	92.15
5.8	6.426	18.34	7.753	11.4	-106.5	215.6	107.7
6.0	5.450	19.09	8.182	11.5	-128.40	259.0	129.4
6.2	4.472	19.89	8.637	12.0	$-\infty$	∞	∞
6.4	3.461	20.74	9.112				
6.6	2.430	21.02	9.607				
6.8	1.369	22.63	10.16				
7.0	.2895	23.67	10.74				

The above functions are defined as (ref. 27):

/$g(\lambda)$ ...

$$g(\lambda) = \frac{15120 - 2784\lambda + 79\lambda^2 + \frac{5}{3}\lambda^3}{(12-\lambda)(37+\frac{25}{12}\lambda)}$$

$$k(\lambda) = \frac{\gamma-1}{2} j(\lambda) + \gamma \ell(\lambda)$$

$$\ell(\lambda) = \lambda + \lambda^2 h(\lambda)$$

where $$h(\lambda) = \frac{8 + \frac{5}{3}\lambda}{(12-\lambda)(37+\frac{25}{12}\lambda)}$$

$$j(\lambda) = \frac{15120 - 1008\lambda + 63\lambda^2}{(12-\lambda)(37+\frac{25}{12}\lambda)}$$

Table III. Summary of Results for the 10 per cent Symmetrical Circular Arc Profile at $M_o = 2.13$ and $R_o = 0.64 \times 10^6$

(a) Force and moment coefficients from inviscid theory (shock-expansion)

α^o	C_L	C_{D_w}	C_M	L/D	$\bar{x}_{c.p.}$
0	0	.0288	0	0	-
4	0.1521	.0390	.0645	3.90	.417
8	0.3089	.0748	.1330	4.13	.418
10	0.3930	.1004	.1691	3.91	.418

At $\alpha = 10^o$, the linear theory gives

$C_L = 0.3710$, $C_{D_w} = 0.0930$, $C_M = .0175$, $\bar{x}_{c.p.} = 0.50$

(b) Increments due to the boundary layer displacement thickness

α	0	4	8	10
ΔC_L	0	.00029	.00047	.00054
ΔC_{D_w}	.000486	.000528	.000581	.000641

ΔC_M and $\Delta \bar{x}_{c.p.}$ are negligible, $[O(10^{-5})]$.

Skin friction drag coefficient

α	0	4	8	10
C_{D_f}	.00461	.00460	.00460	.00465

/(c) ...

(c) Increments due to separation

α	ΔC_L	ΔC_{D_w}	ΔC_M	ΔC_{D_f}	$\Delta \bar{x}_{c.p.}$
0	0	-.00284	0	-.00026	-
4	-.0189	-.00426	-.01692	-.00034	-.032
8	-.0241	-.00696	-.02167	-.00042	-.039
10	-.0267	-.00845	-.02294	-.00043	-.065

(d) Nett calculated values of the coefficients

α	C_L	C_D	C_M	L/D	$\bar{x}_{c.p.}$
0	0	.0308	0	0	-
4	.1335	.0395	.0476	3.45	.350
8	.2853	.0726	.1113	3.90	.380
10	.3668	.0968	.1462	3.77	.387

(e) Averaged experimental values (Ferri - ref.4 - force measurements)

α	C_L	C_D	C_M
0	-.005	.0356	.005
4	+.123	.0436	.0395
8	.262	.0748	.0985
10	.329	.0982	.130

(f) Comparison of experimental and calculated results at $\alpha = 10^\circ$

	C_L	C_D	C_M	L/D	$\bar{x}_{c.p.}$
Experiment (average)	.329	.0982	.130	3.35	.37
Shock-expansion theory	.3930	.1004	.1691	3.91	.418
% difference	19.4	2.3	30.0	16.7	13.0
Linear theory	.3710	.0930	.175	3.99	.50
% difference	12.7	-5.3	34.6	19.0	35.0
Present method	.367	.0968	.1462	3.77	.387
% difference	11.5	-1.5	12.5	12.5	4.5

/Table IV(a) ...

Table IV(a). Comparison of pressure and force measurements of ref. 4

α		4	8	10
C_L	pressure distribution	.139	.291	.362
	force measurements	.123	.262	.392
C_M	pressure distribution	.0482	.111	.148
	force measurements	.0395	.099	.130

Table IV(b) Pitching moment coefficients at positive and negative angles of incidence (ref.4)

α	10	-10	8	-8	6	-6
100 C_M	13.0	-10.8	10.0	-9.7	7.3	-6.4

α	4	-4	2	-2	0	(-0)
100 C_M	4.1	-3.8	1.8	-1.4	0.4	-0.2

Table V .Comparison of calculated results with those interpolated from ref. 10

(i) Lift

	α	4	8	10
C_L	Interpolated	0.141	0.291	0.367
	Calculated	0.134	0.285	0.367

(ii) Drag

C_{D_w} interpolated from ref. 10 = 0.0263 (at $\alpha = 0^\circ$)

allowance for skin friction = 0.0045 (see tables III(b) and (c))

0.0309

Calculated C_D (total) = 0.0308

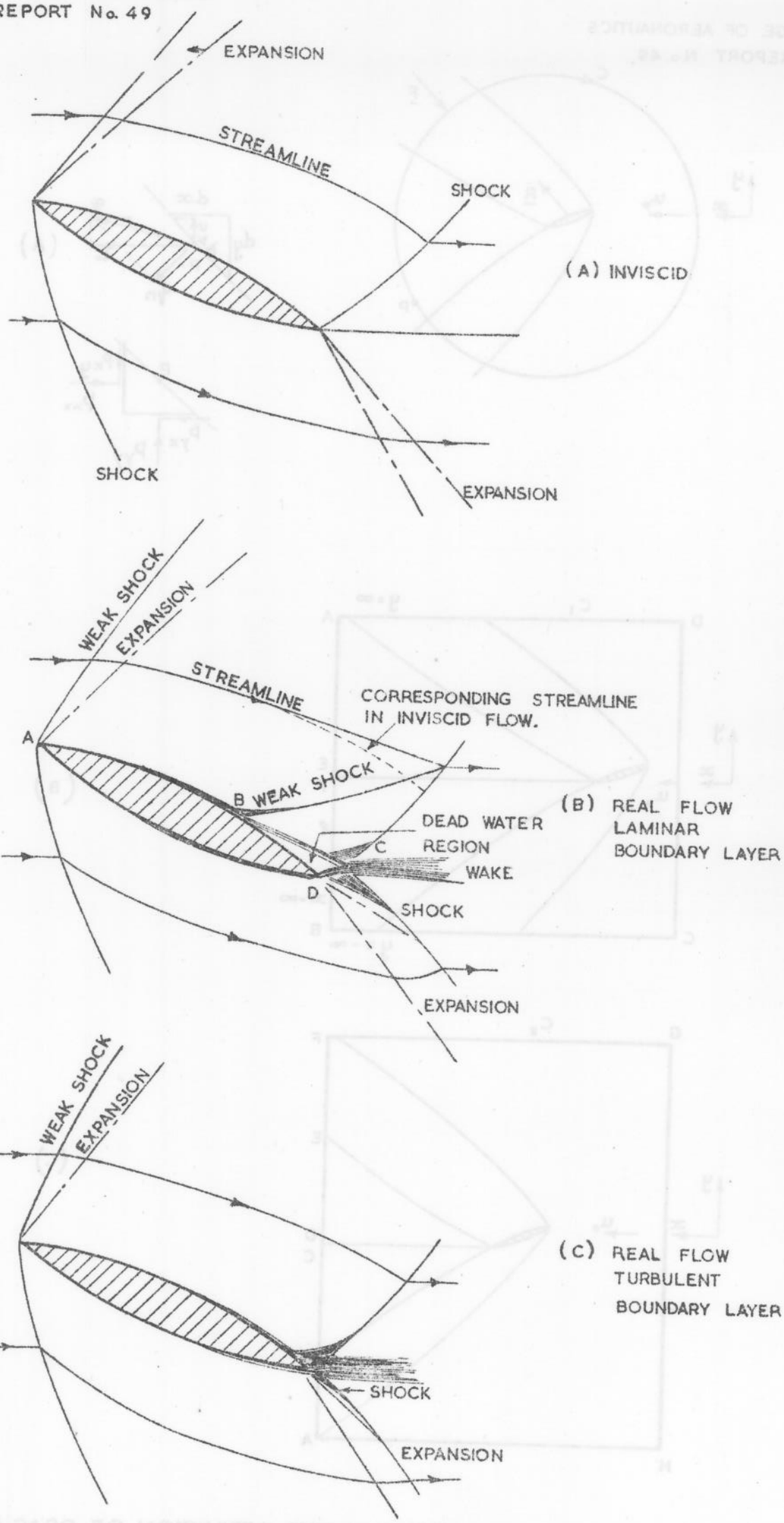

FIG. 1. TYPICAL FLOW PATTERNS ON TWO-DIMENSIONAL SUPERSONIC AEROFOILS

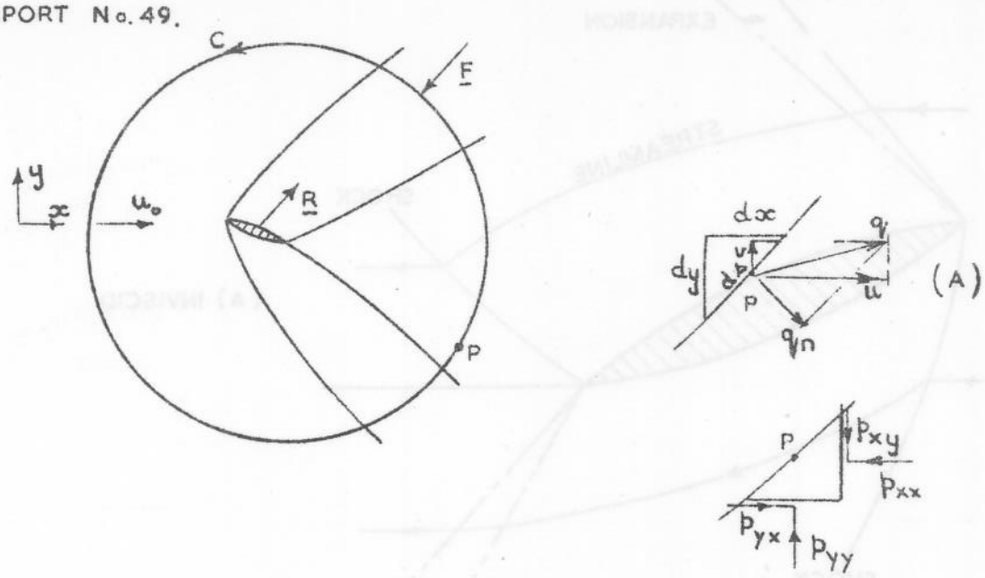

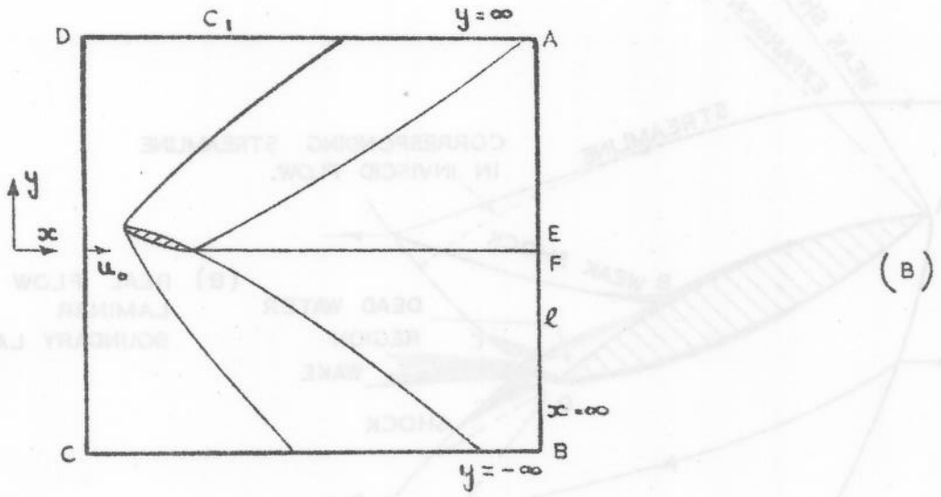

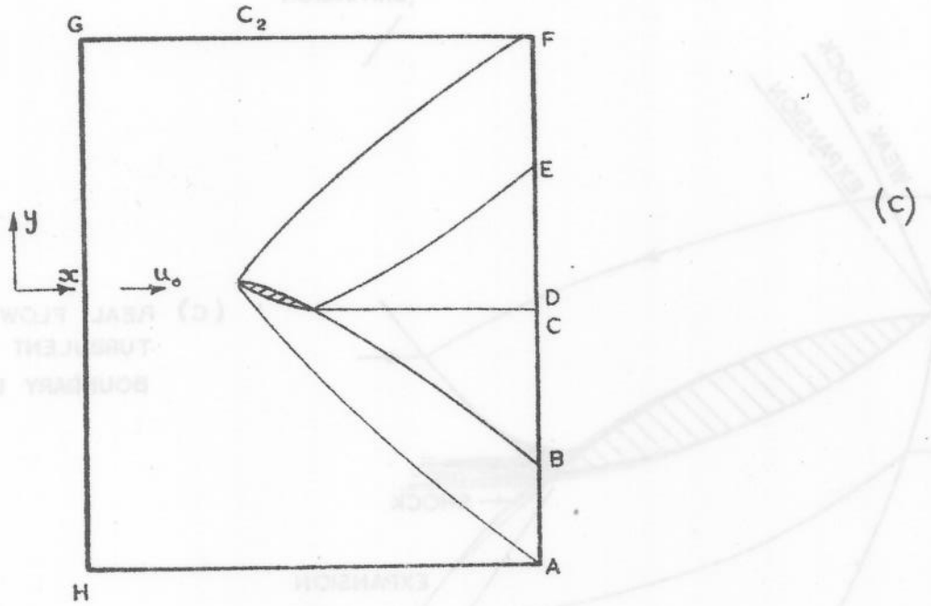

FIG. 2. CONTROL SURFACES USED IN THE DERIVATION OF DRAG-ENTROPY AND LIFT RELATIONS FROM THE MOMENTUM THEOREM

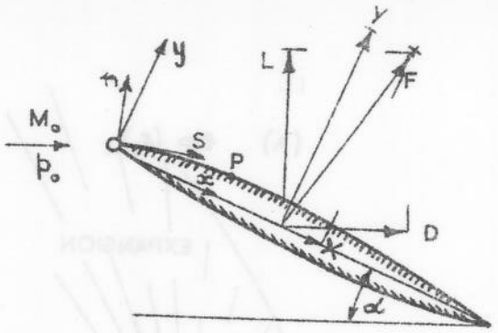

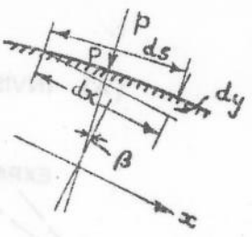

(A) PROFILES OF ARBITRARY SHAPE

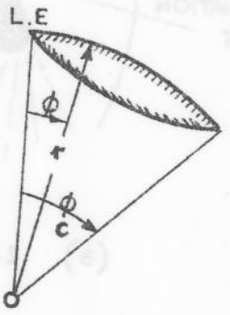

(B) CIRCULAR ARC PROFILES

FIG. 3. SYSTEMS OF COORDINATES

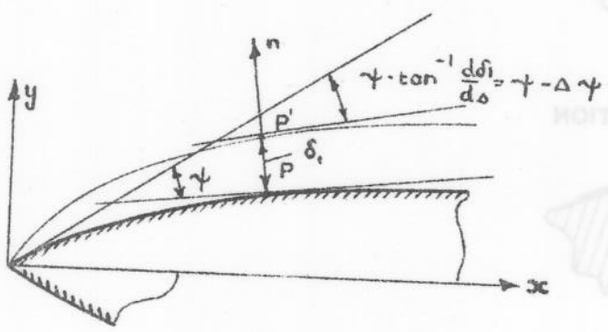

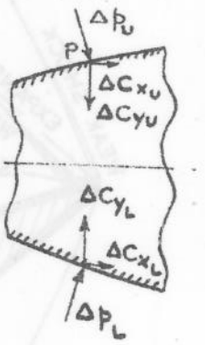

FIG. 4. THE EQUIVALENT PROFILE

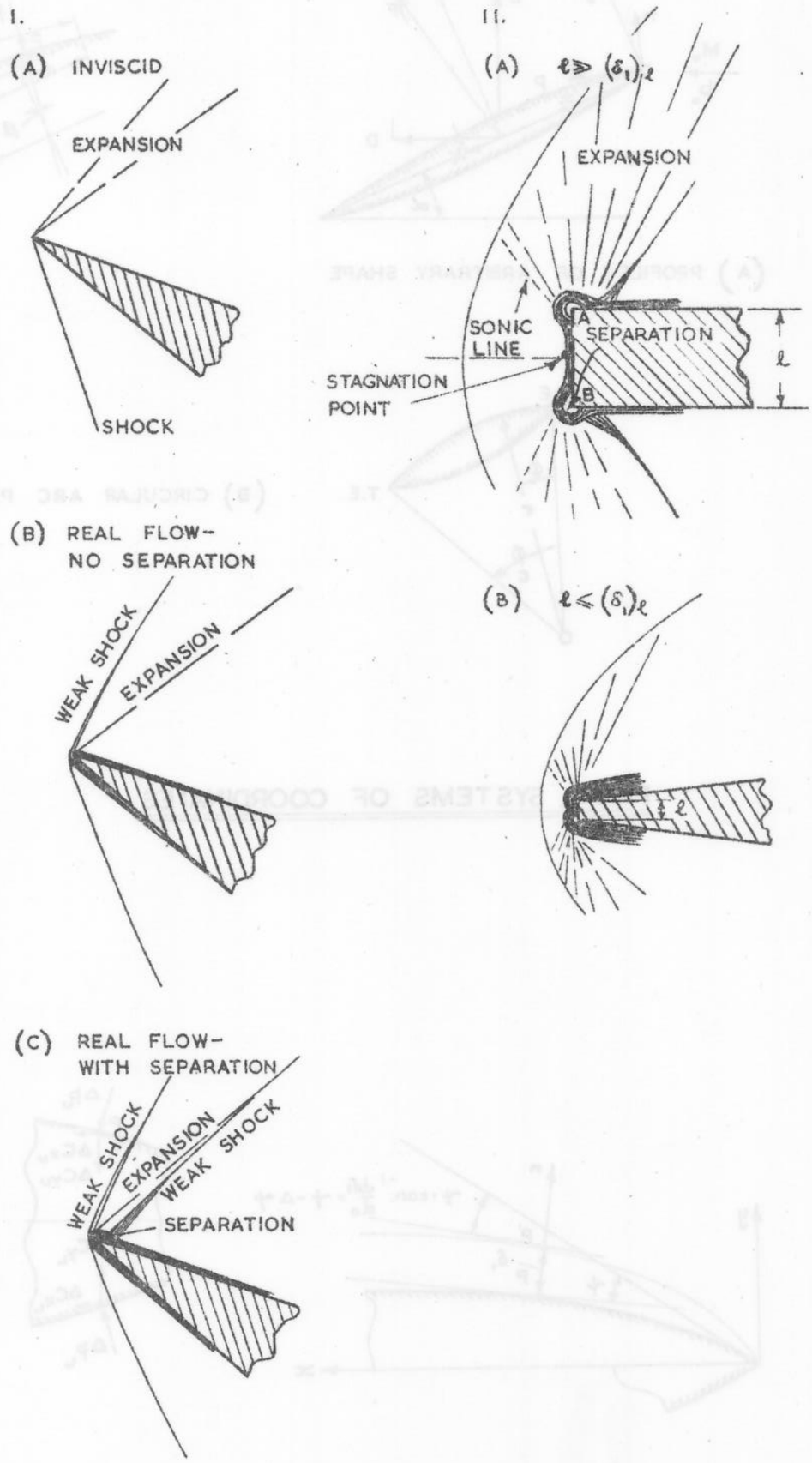

FIG. 5. FLOW PATTERNS NEAR LEADING EDGES

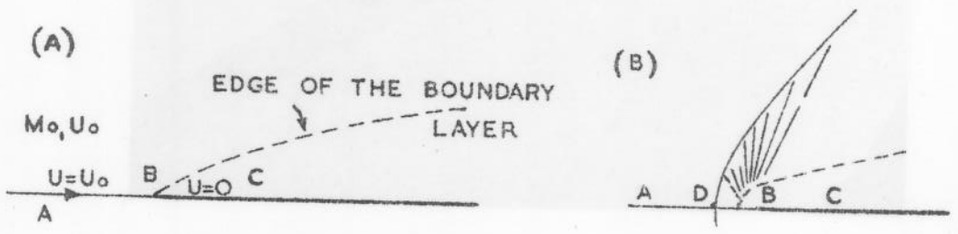

FIG. 6. VISCOUS FLOW OVER A FLAT PLATE OF ZERO THICKNESS

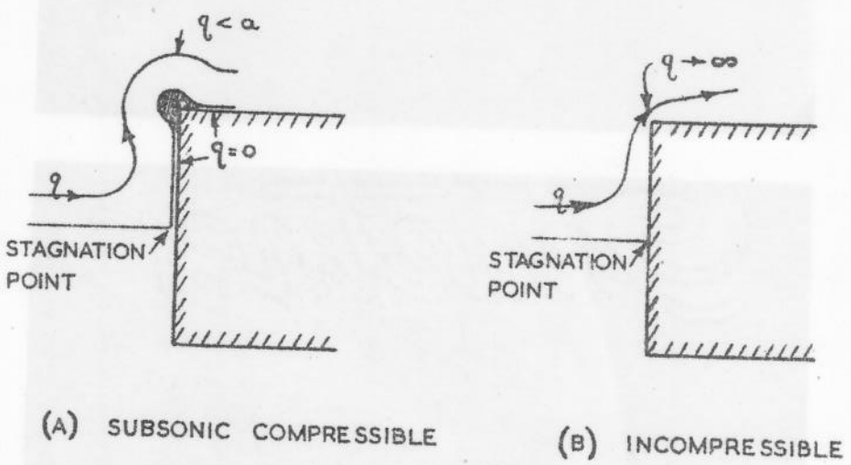

FIG. 7. FLOW ROUND A SHARP CORNER

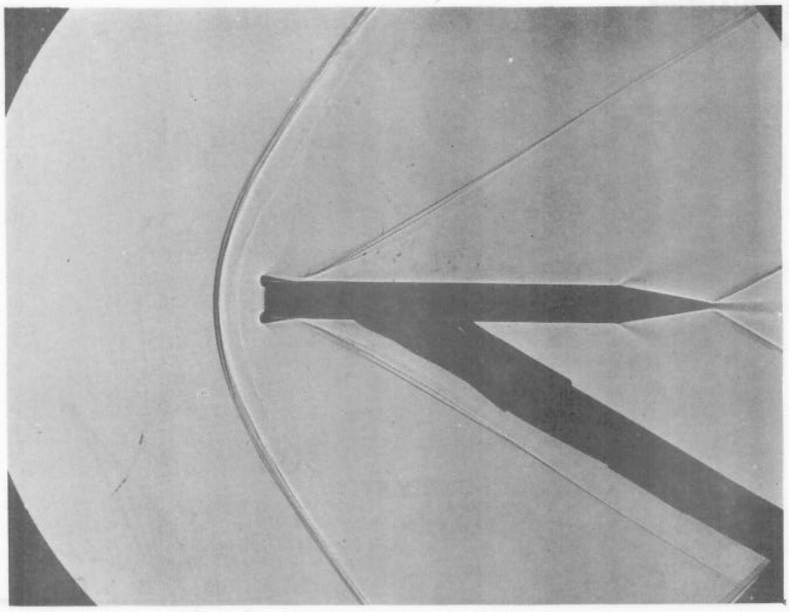

(A) M=1·8
SQUARE NOSE

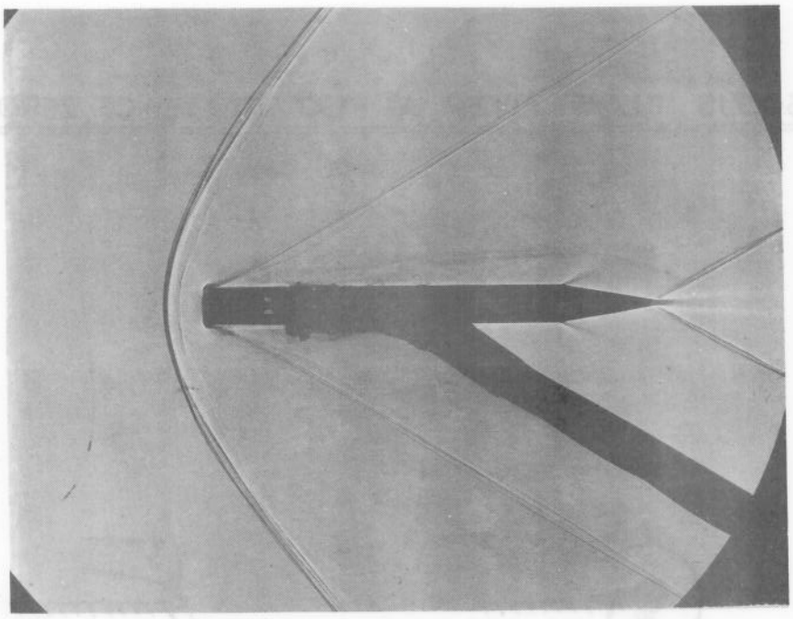

(B) M=1·8
1:2 ELLIPSE

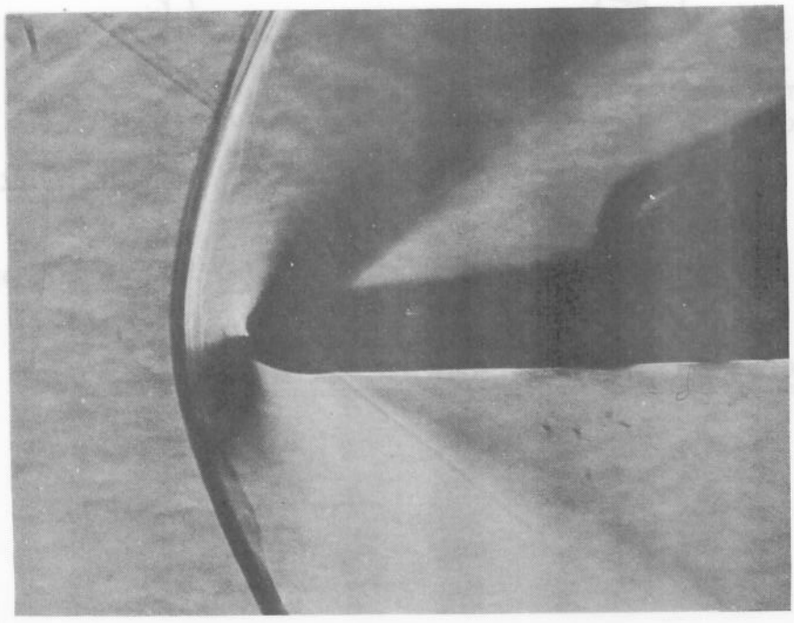

(C) M=1·6
2:1 ELLIPSE

FIG. 8. FLOW ROUND BLUNT-NOSED FLAT PLATES [N.P.L., REF. 6.]

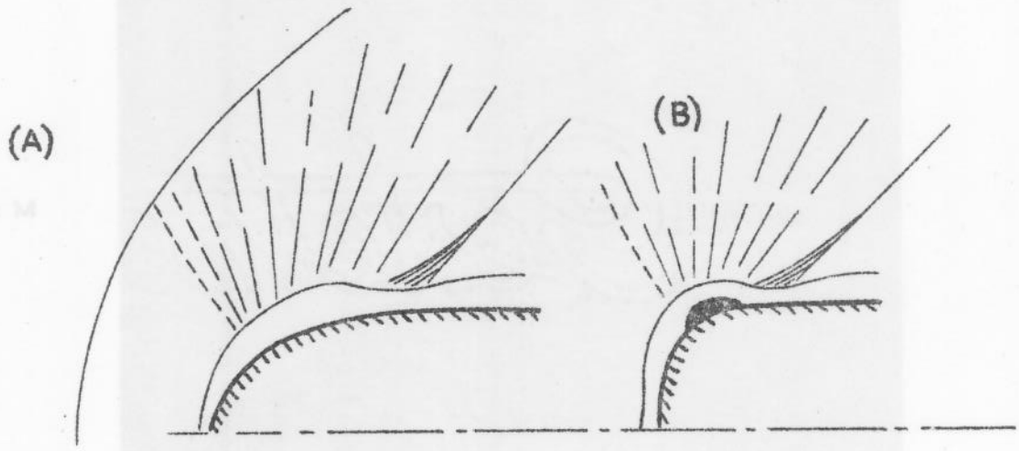

FIG. 9. BOUNDARY LAYER THINNING CAUSED BY A HIGH FAVOURABLE PRESSURE GRADIENT

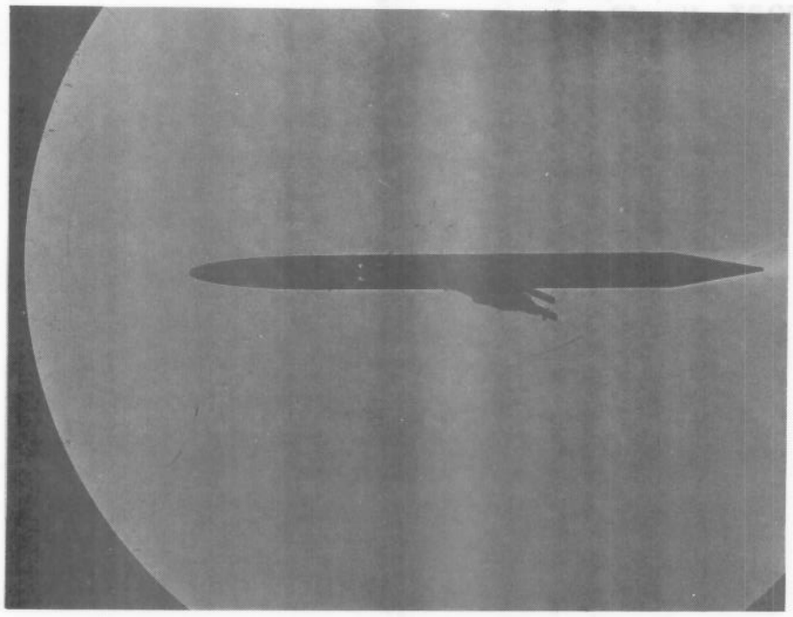

M=0

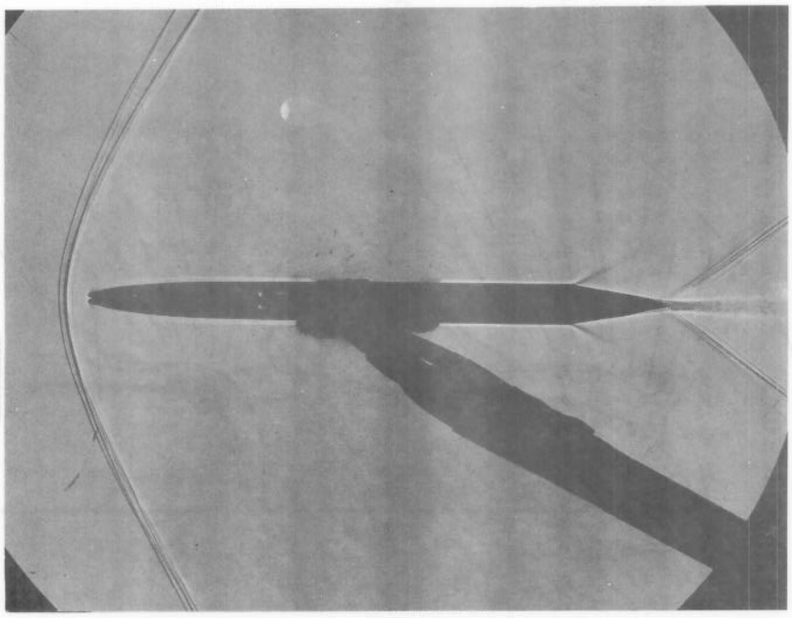

M = 1·42

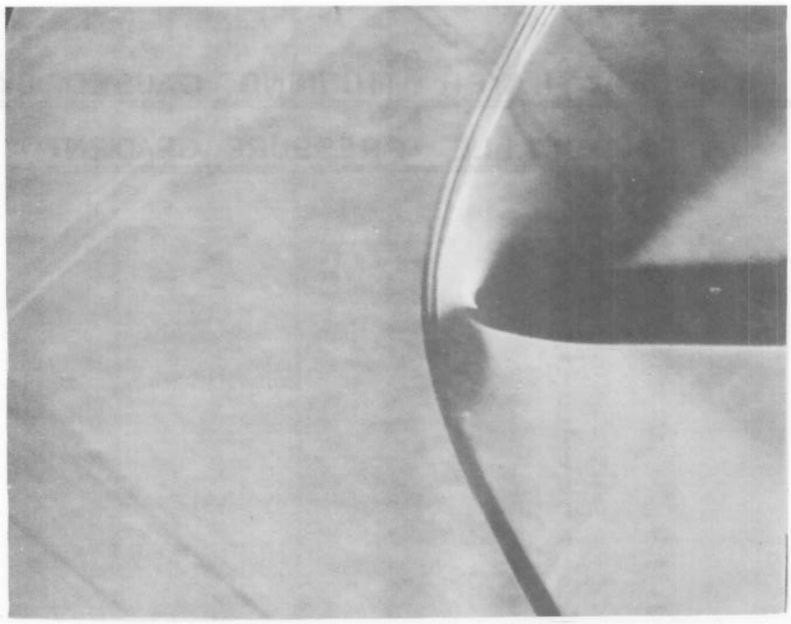

M=1·6

FIG. 10. FLOW ROUND FLAT PLATE WITH 8·1 ELLIPTICAL NOSE [N.P.L.]

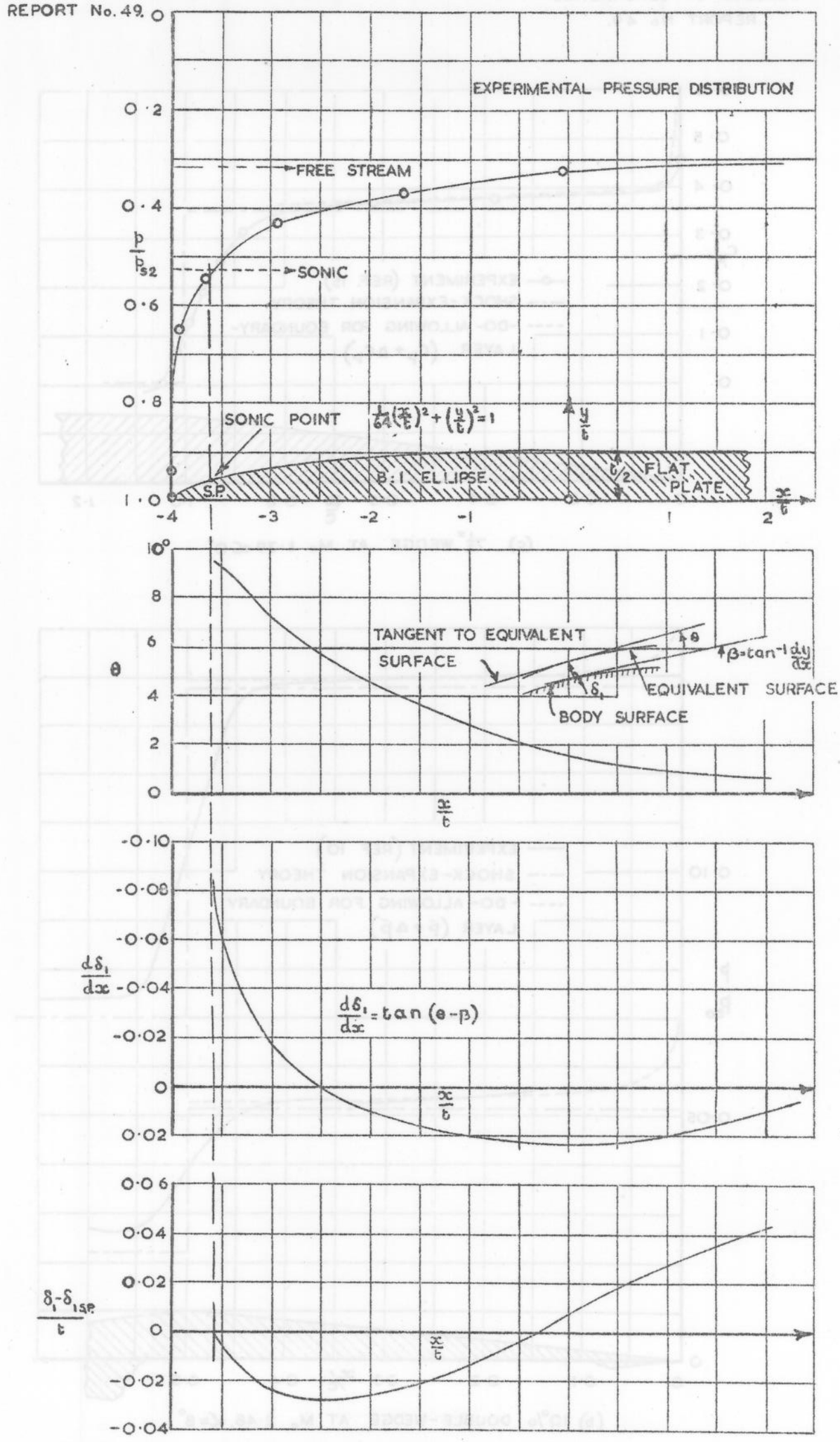

FIG. 10. (CONTINUED) DEDUCED SHAPE OF THE BOUNDARY LAYER DISPLACEMENT THICKNESS ON THE 8:1 ELLIPSE AT M=1·42

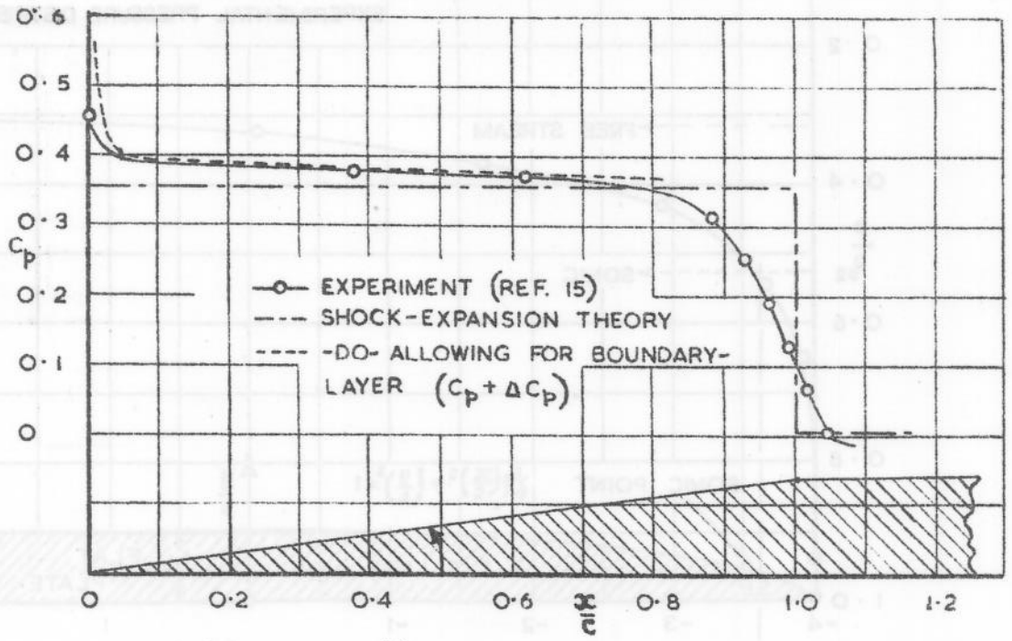

(c) $7\frac{1}{2}°$ WEDGE AT M_0 1·39 α 0°

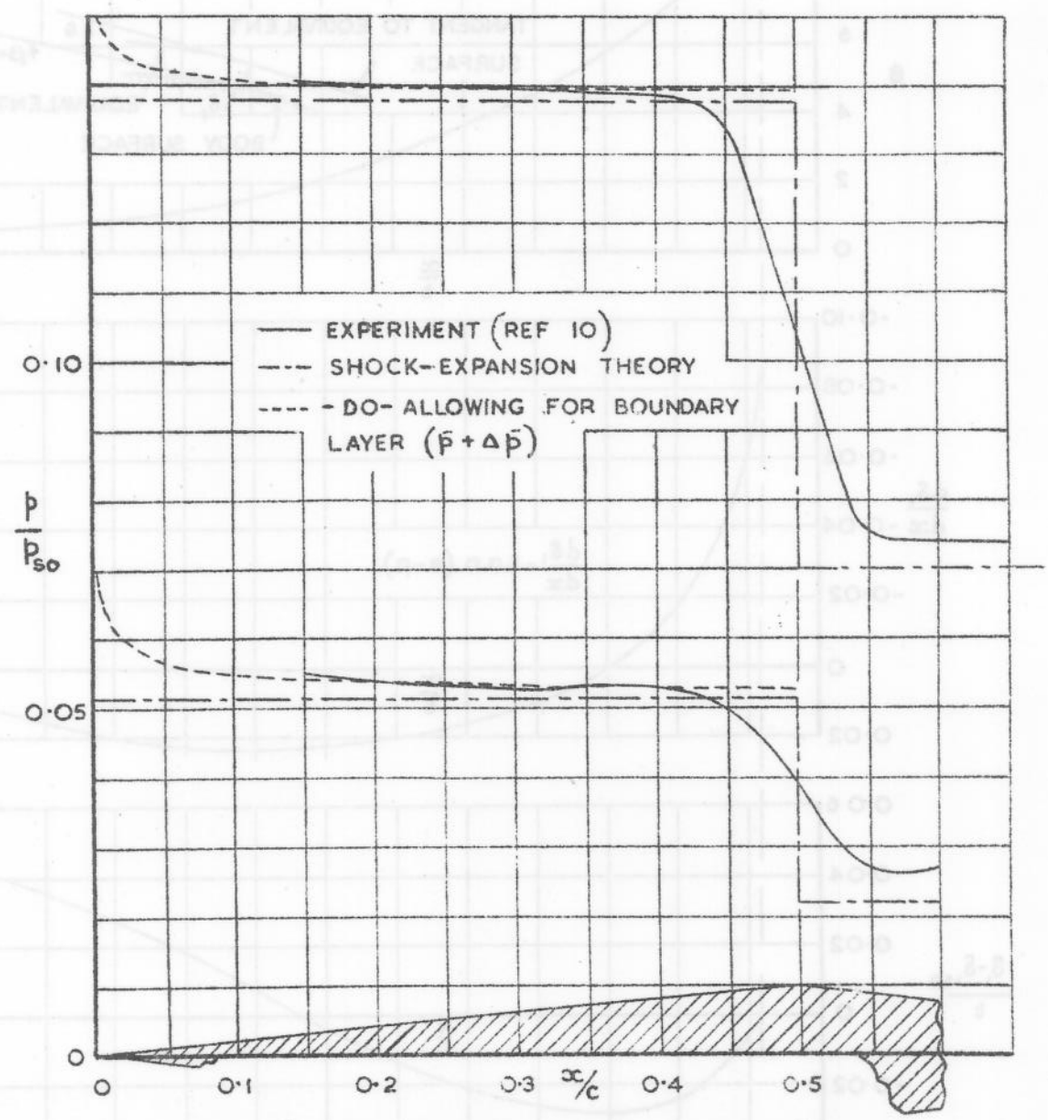

(b) 10% DOUBLE-WEDGE AT M_0 2·48, $\alpha = 8°$

FIG. 11. COMPARISON OF CALCULATED AND EXPERIMENTAL PRESSURE DISTRIBUTIONS ON WEDGE SECTIONS.

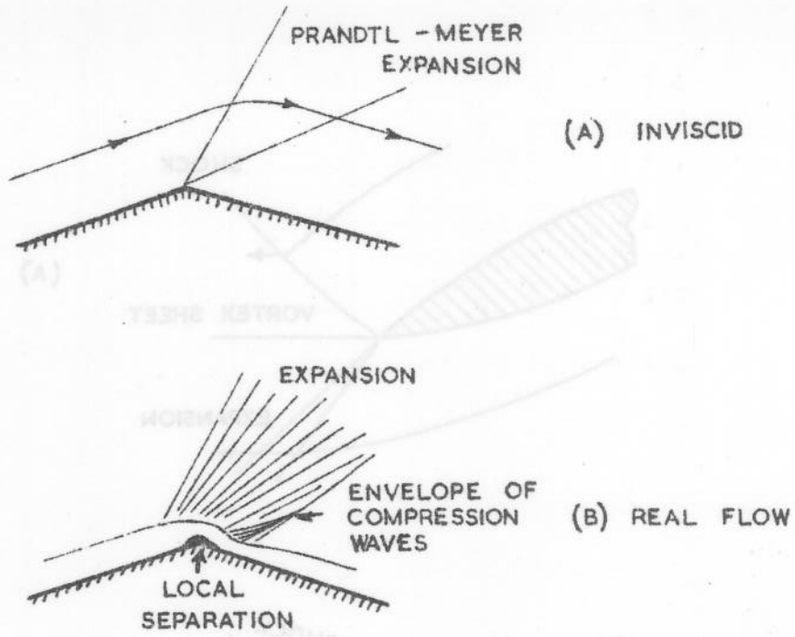

FIG. 12. TYPICAL CONDITIONS OF FLOW OVER THE SHOULDER OF A WEDGE SECTION

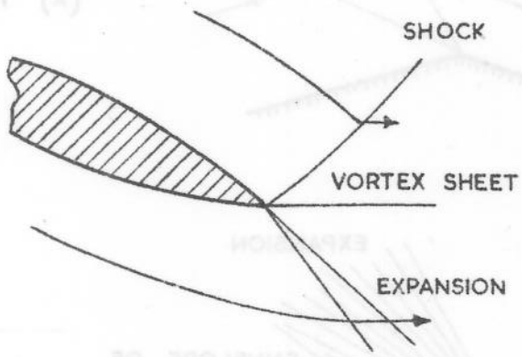

(A) INVISCID

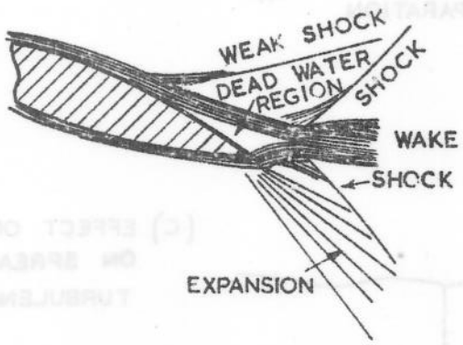

(B) LAMINAR BOUNDARY LAYER, SEPARATION ON ONE SURFACE ONLY.

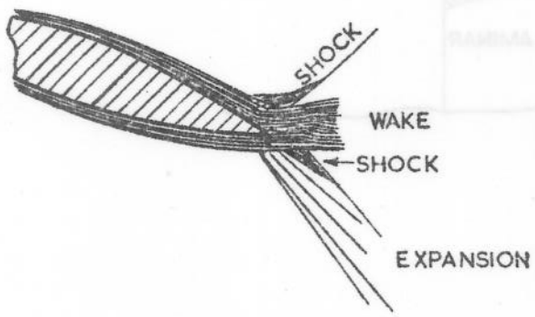

(C) TURBULENT BOUNDARY LAYER

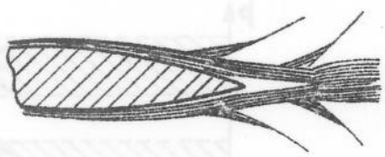

(D) LAMINAR BOUNDARY LAYER SEPARATION ON BOTH SURFACES

FIG. 13. TYPICAL FLOW PATTERNS NEAR TRAILING EDGES

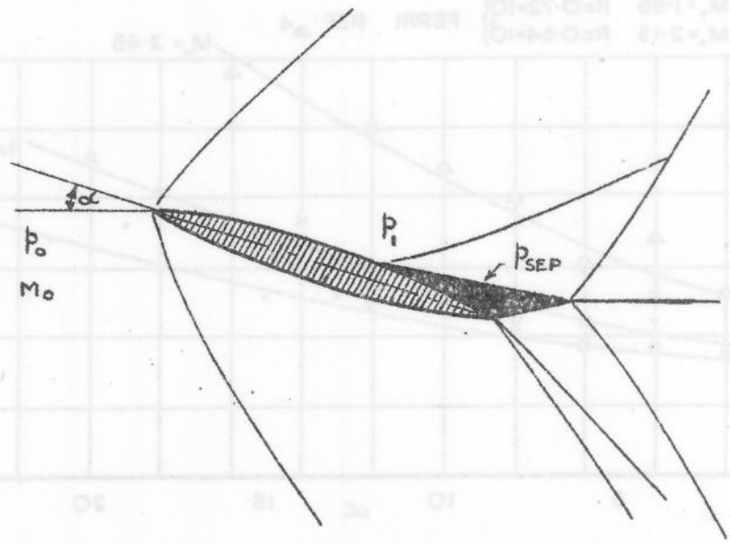

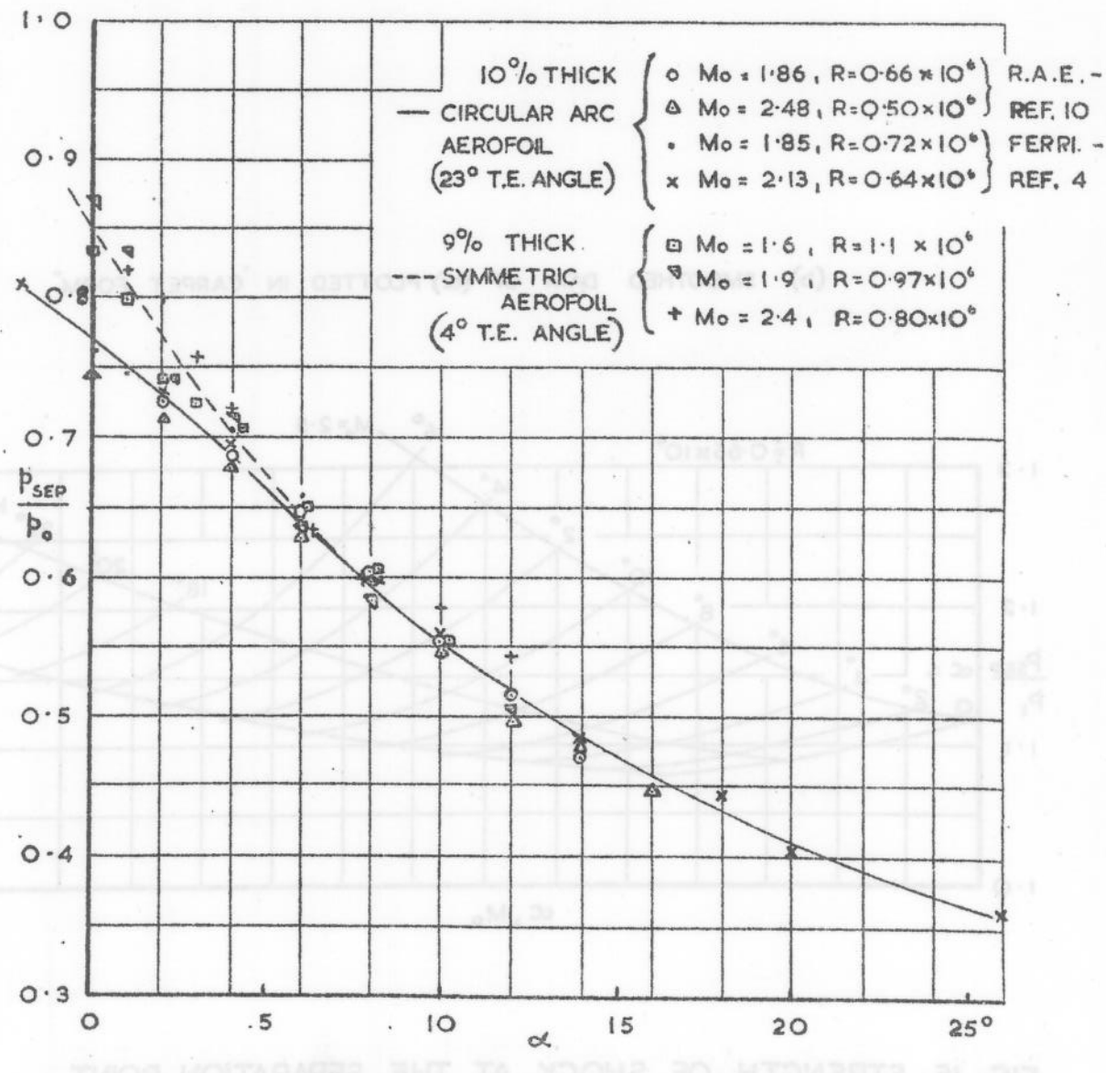

FIG. 14. VARIATION OF PRESSURE IN THE SEPARATED REGION SYMMETRICAL AEROFOILS WITH LAMINAR BOUNDARY LAYER

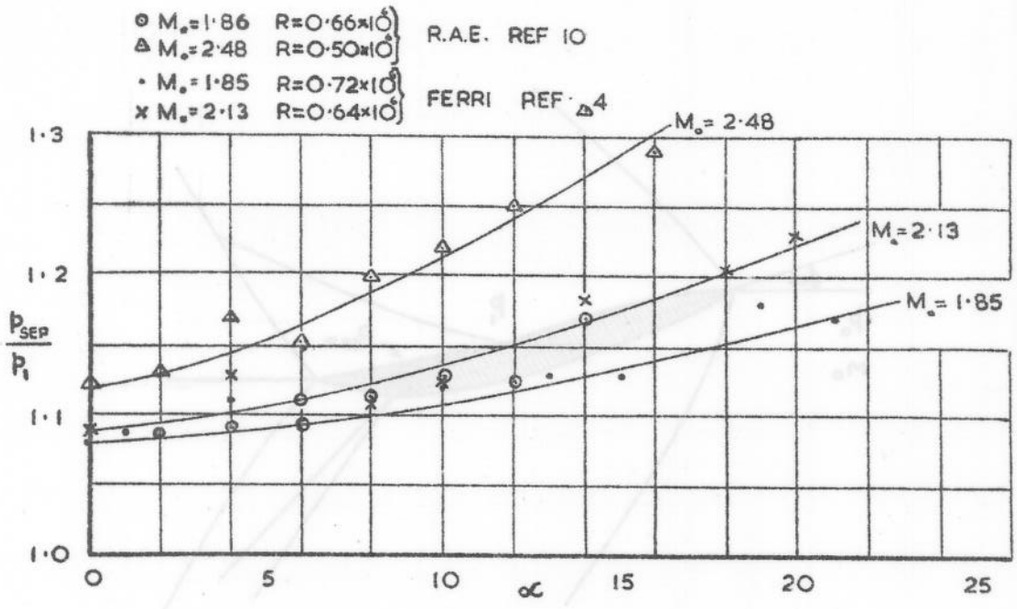

(a) EXPERIMENTAL POINTS

(b) SMOOTHED DATA OF (a) PLOTTED IN "CARPET FORM"

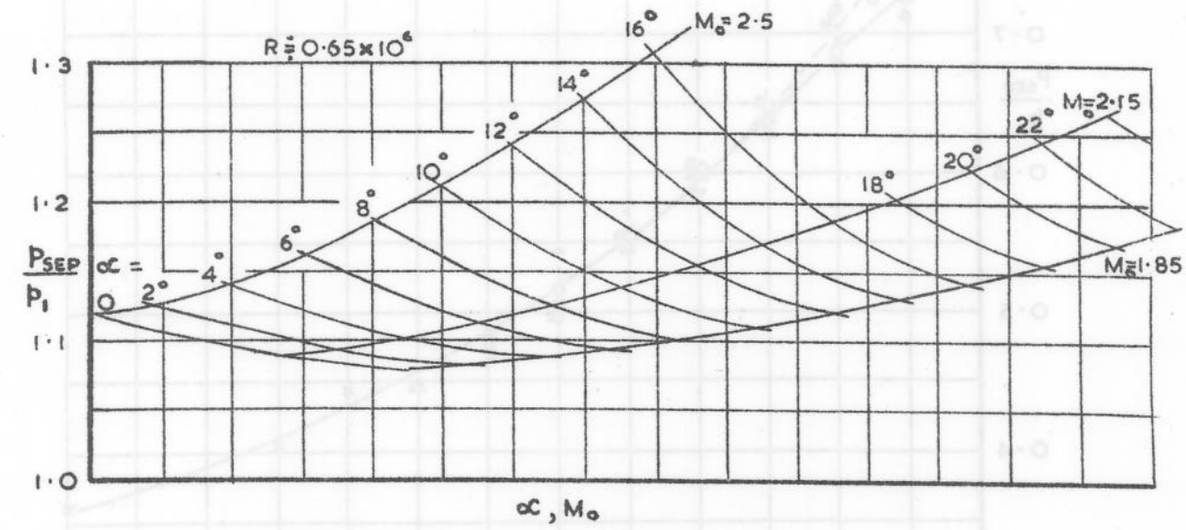

FIG. 15. STRENGTH OF SHOCK AT THE SEPARATION POINT

10% CIRCULAR ARC PROFILES; LAMINAR

BOUNDARY LAYER

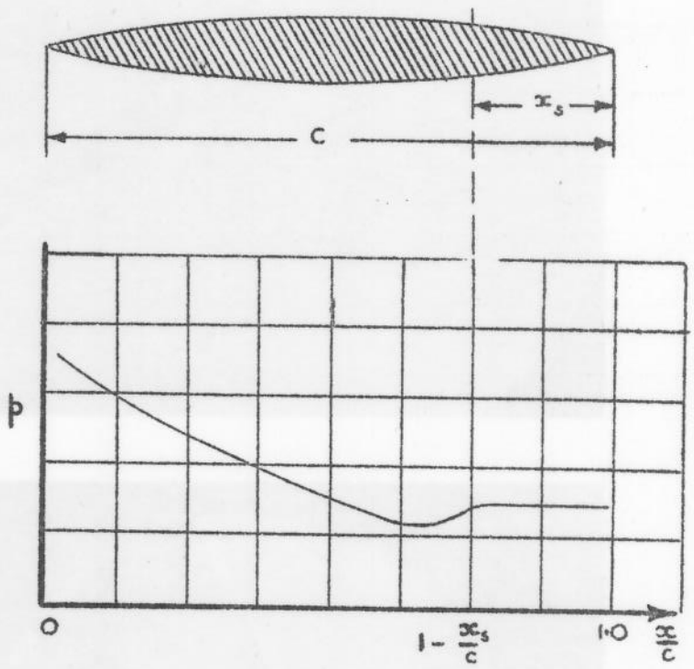

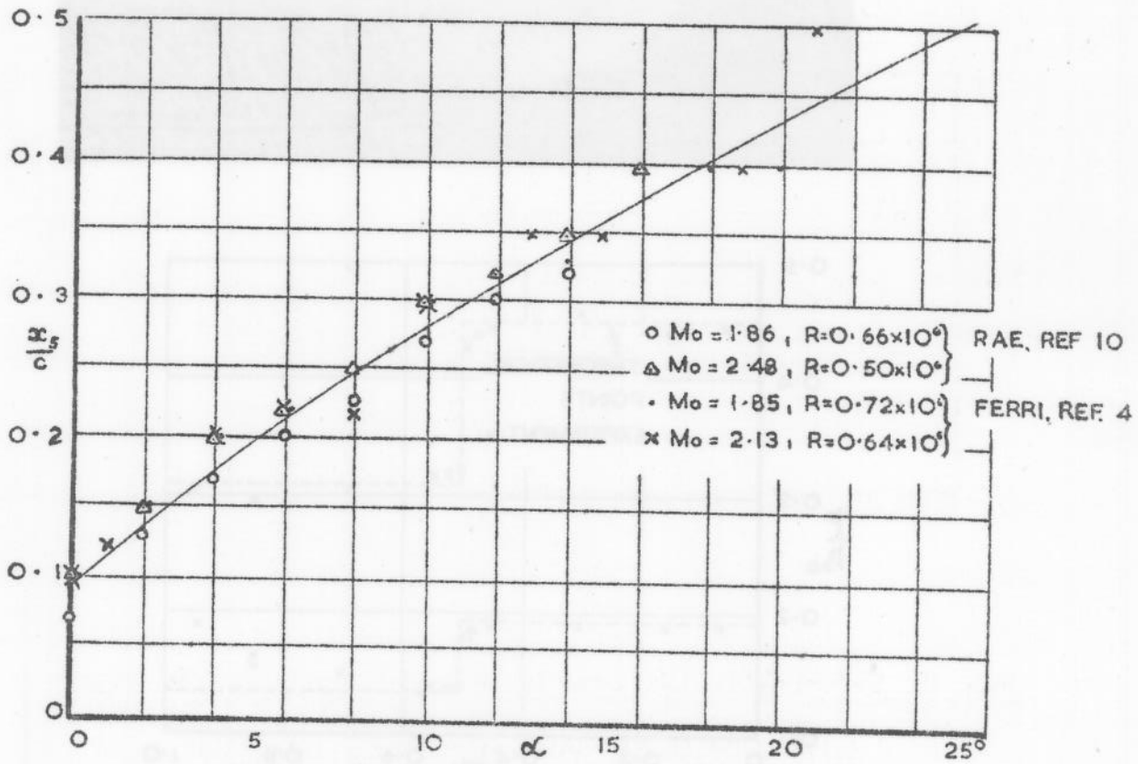

FIG. 16. VARIATION OF SIZE OF SEPARATED REGION
10% C.A. PROFILES; LAMINAR BOUNDARY LAYER

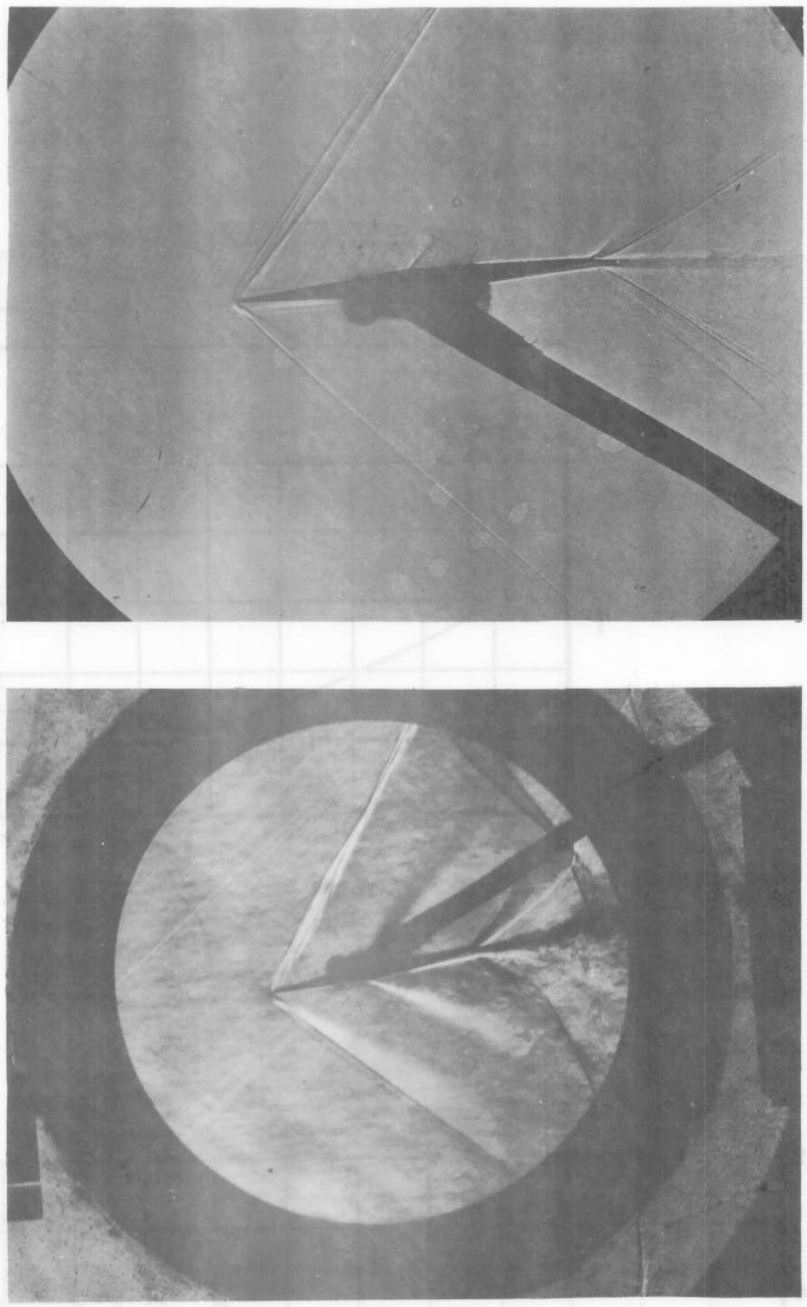

FIG. 17. 6% DOUBLE-WEDGE SECTION AT M=1·57, $\alpha = 8^\circ$ (N.P.L REF. 9)

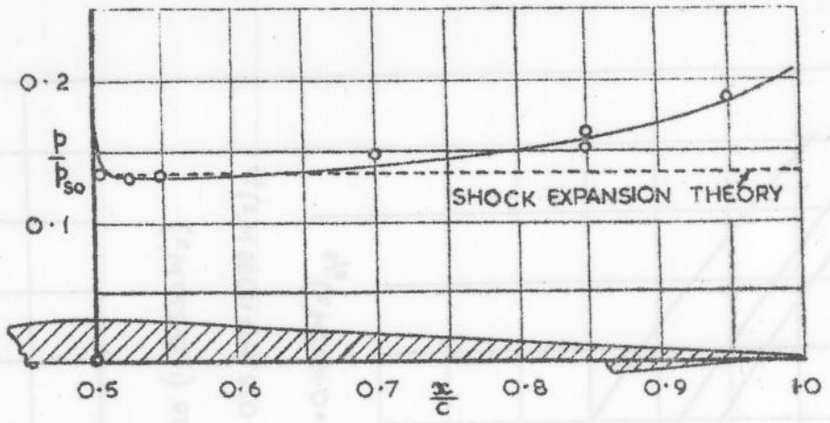

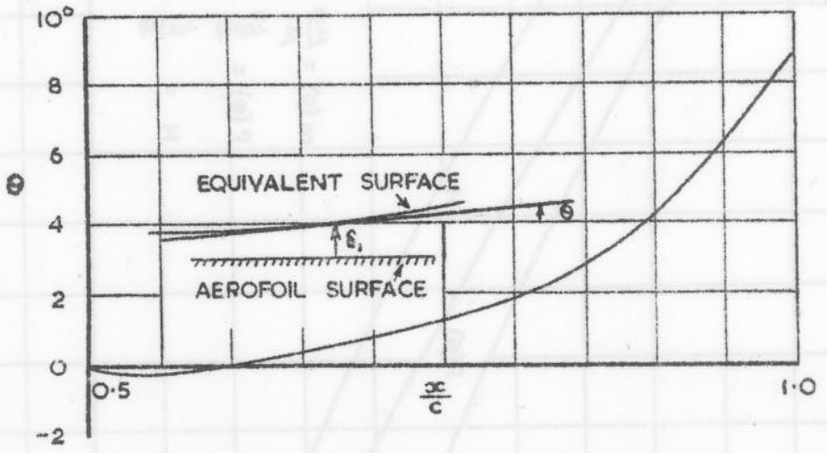

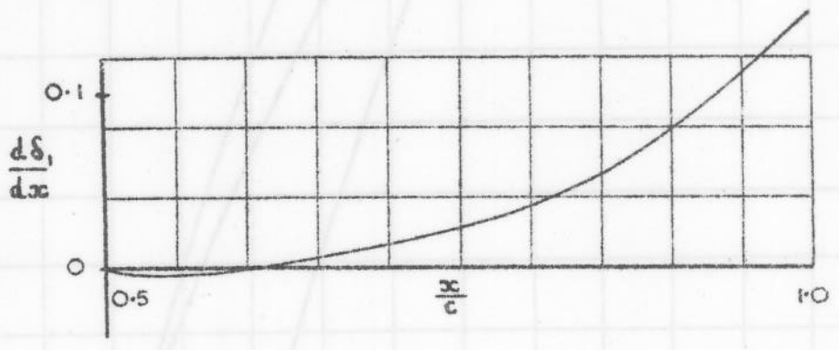

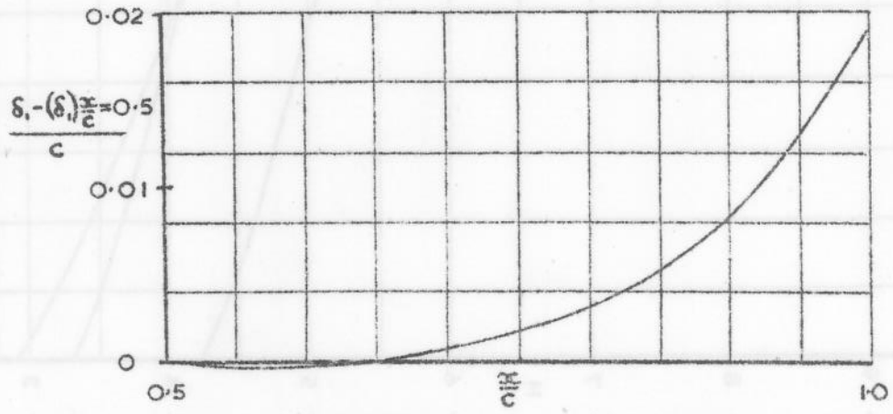

FIG. 17 (CONTINUED) DEDUCED SHAPE OF THE EQUIVALENT SURFACE TO GIVE EXPERIMENTAL PRESSURE DISTRIBUTION

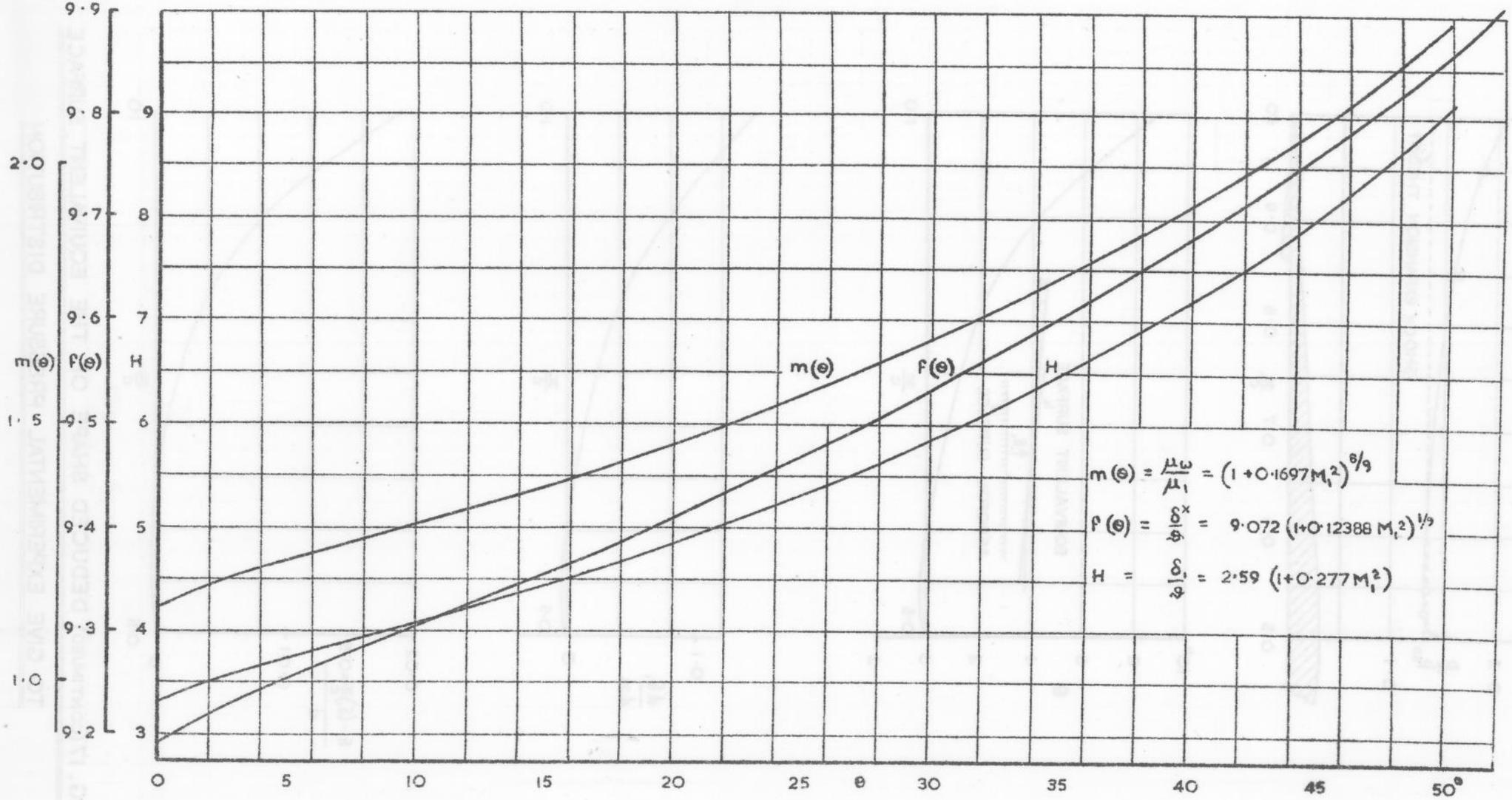

FIG. 18(a) THE LAMINAR BOUNDARY LAYER FUNCTIONS USED IN THE NEW INTEGRAL RELATIONS

(a) FUNCTIONS m(θ), f(θ) & H

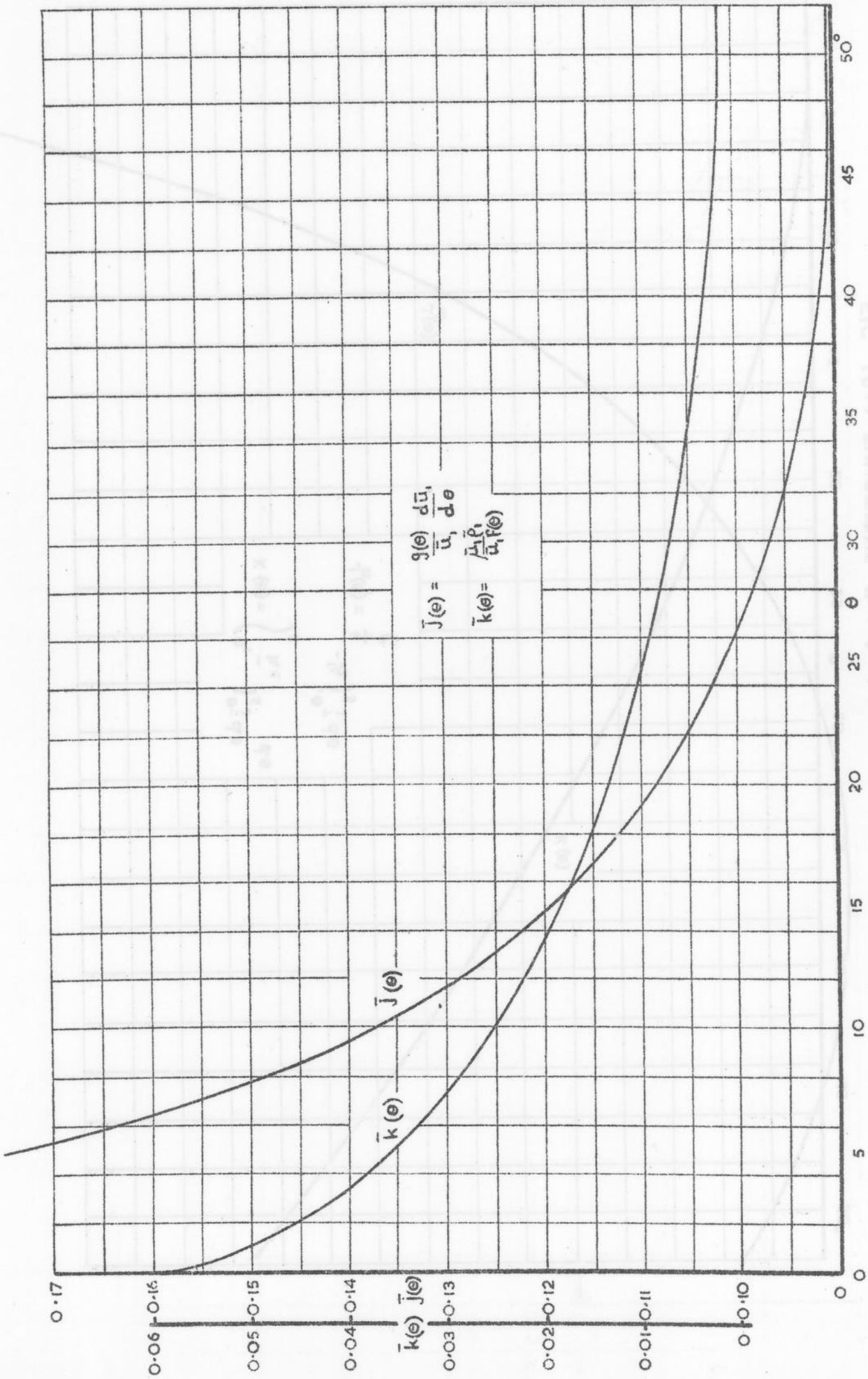

FIG. 18(b) FUNCTIONS $\bar{j}(\theta)$ & $\bar{k}(\theta)$

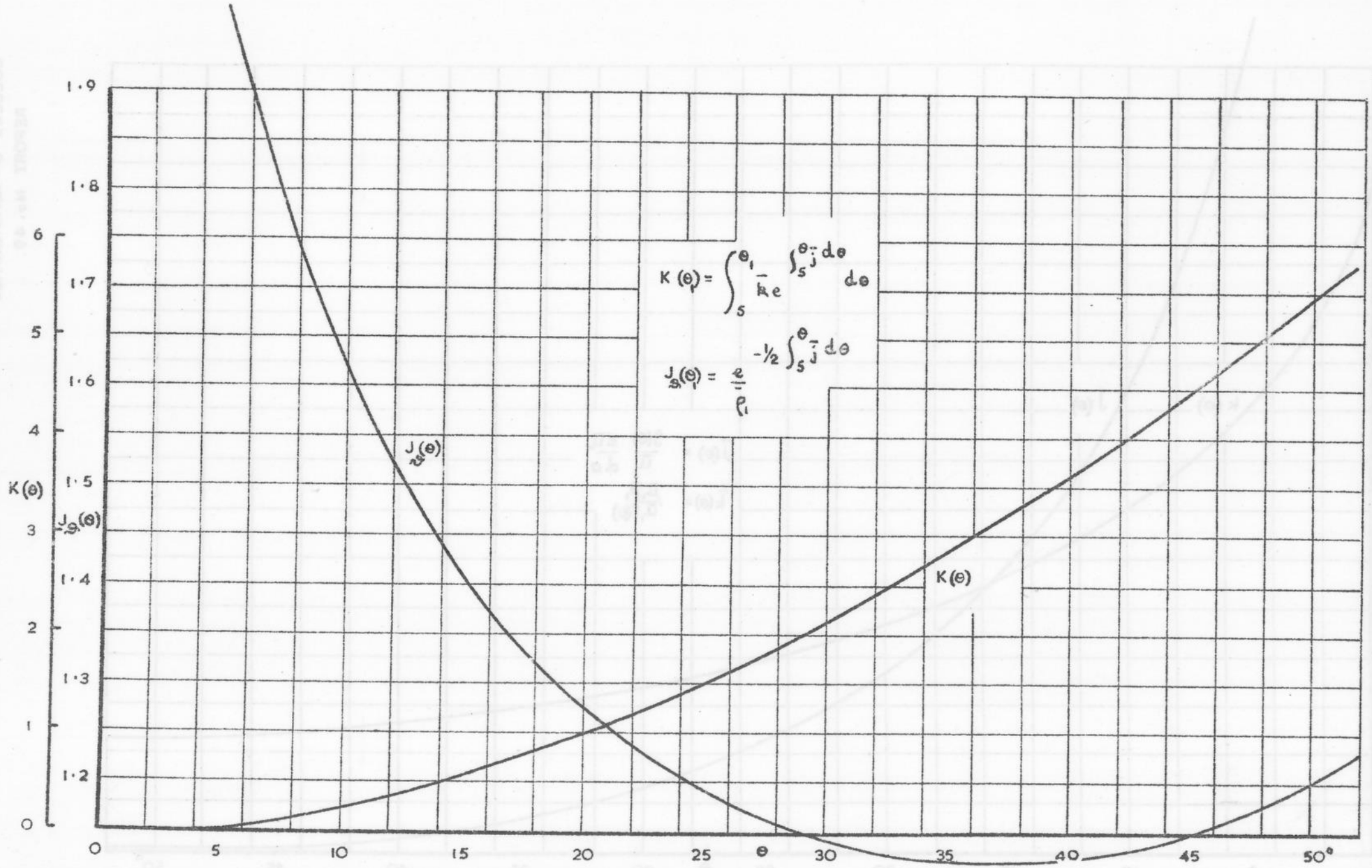

FIG. 18(c) FUNCTIONS $K(\theta)$ & $J_{2s}(\theta)$

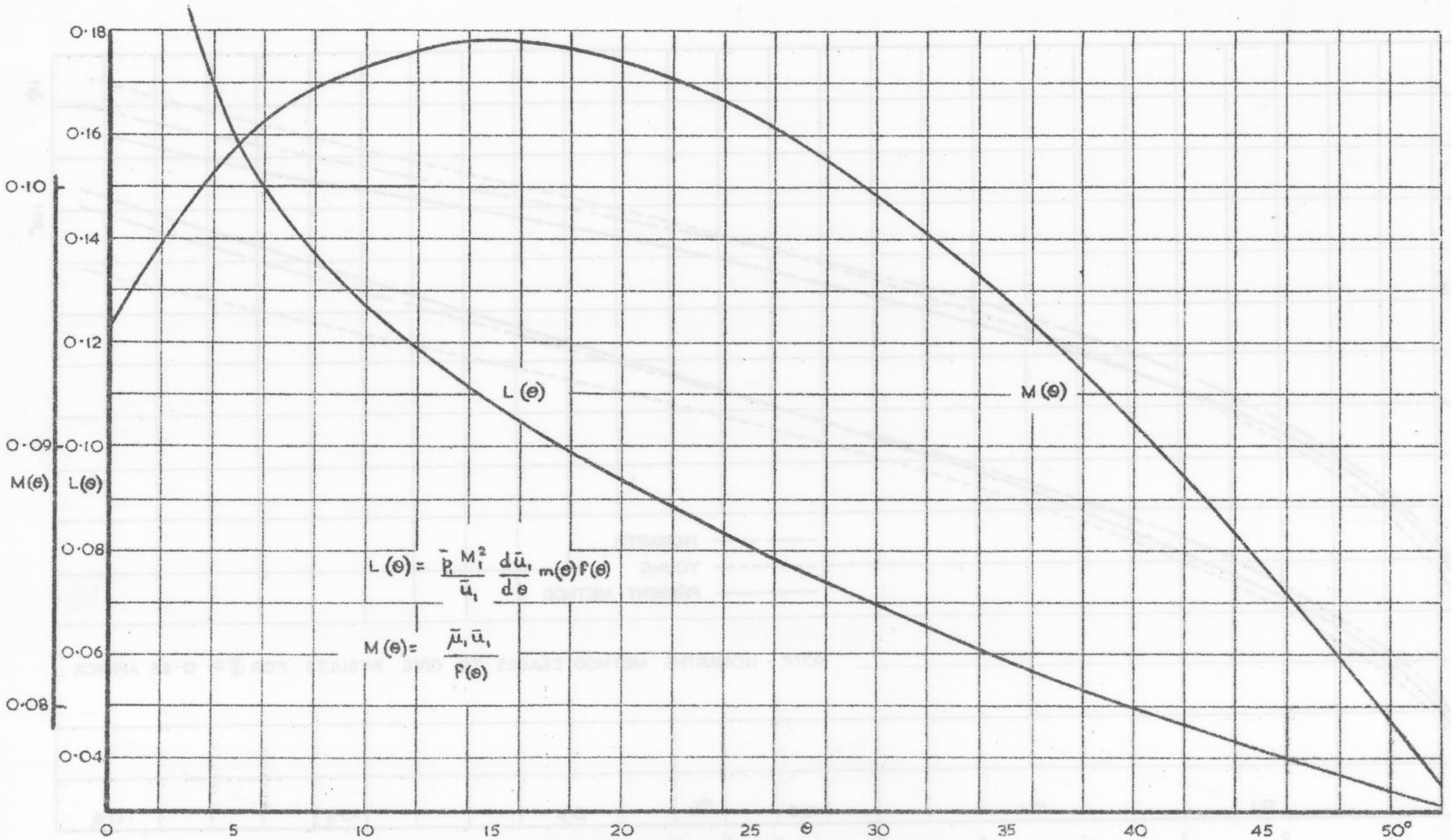

FIG 18 (d) FUNCTIONS L(θ) & M(θ)

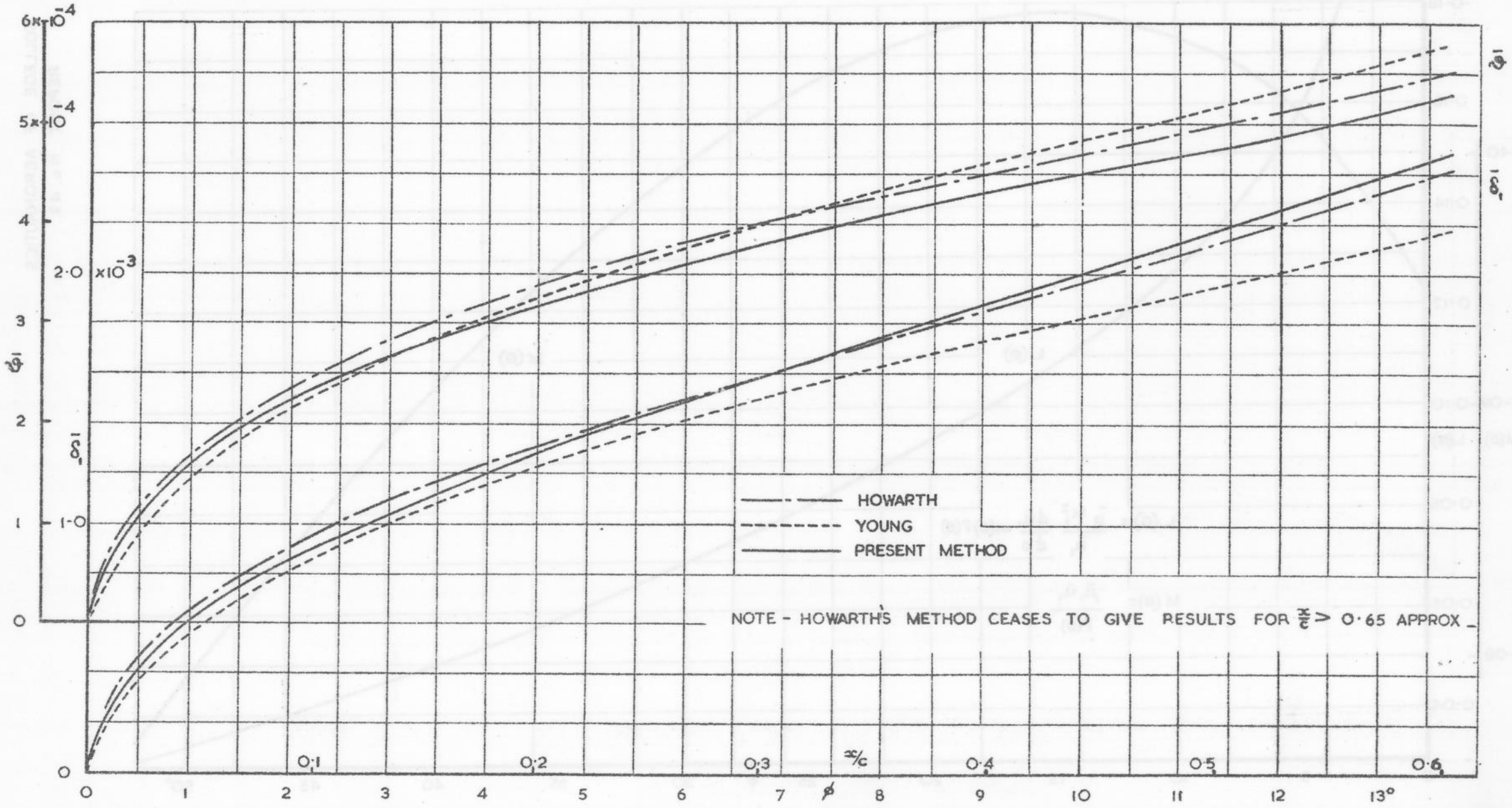

FIG. 19. LAMINAR BOUNDARY LAYER ON THE LOWER SURFACE OF 10% C.A. PROFILE AT $M_\infty = 2{\cdot}13$, $R_{\bar{\delta}} = 0{\cdot}64 \times 10^6$, $\alpha = 10°$

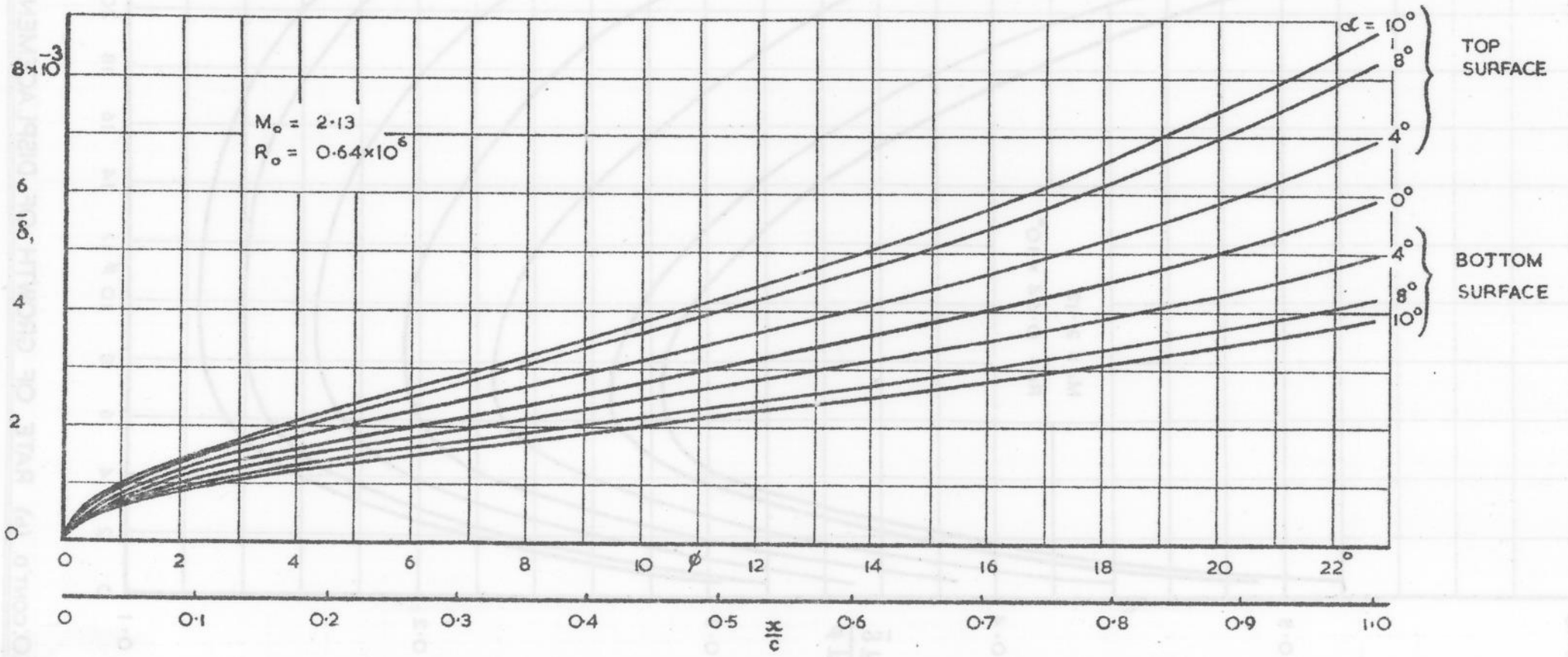

FIG. 20. BOUNDARY LAYER DEVELOPMENT ON 10% C.A PROFILE, IGNORING EFFECTS OF SHOCK WAVES

(a) DISPLACEMENT THICKNESS

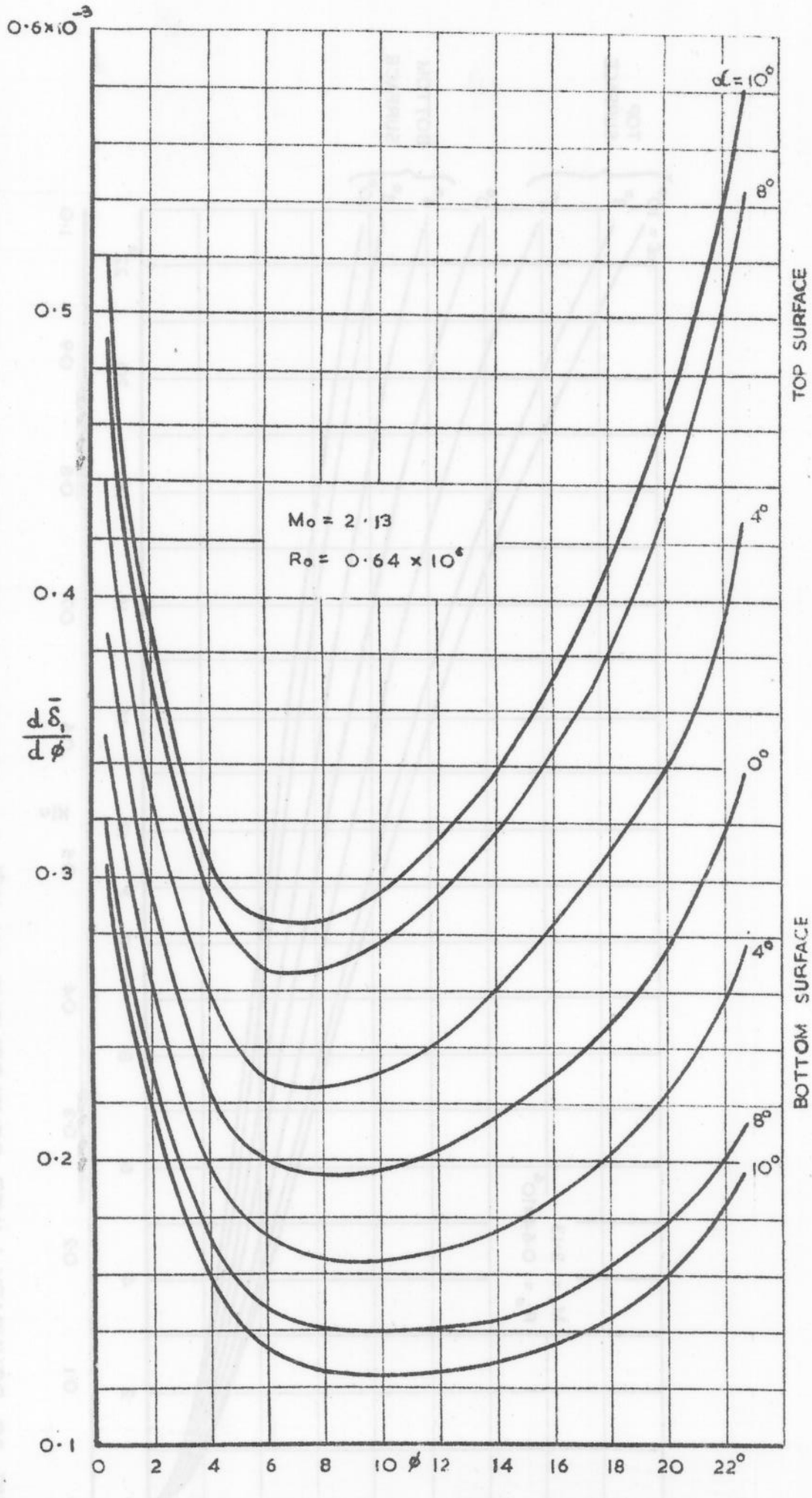

FIG. 20. CONT'D. (b) RATE OF GROWTH OF DISPLACEMENT THICKNESS

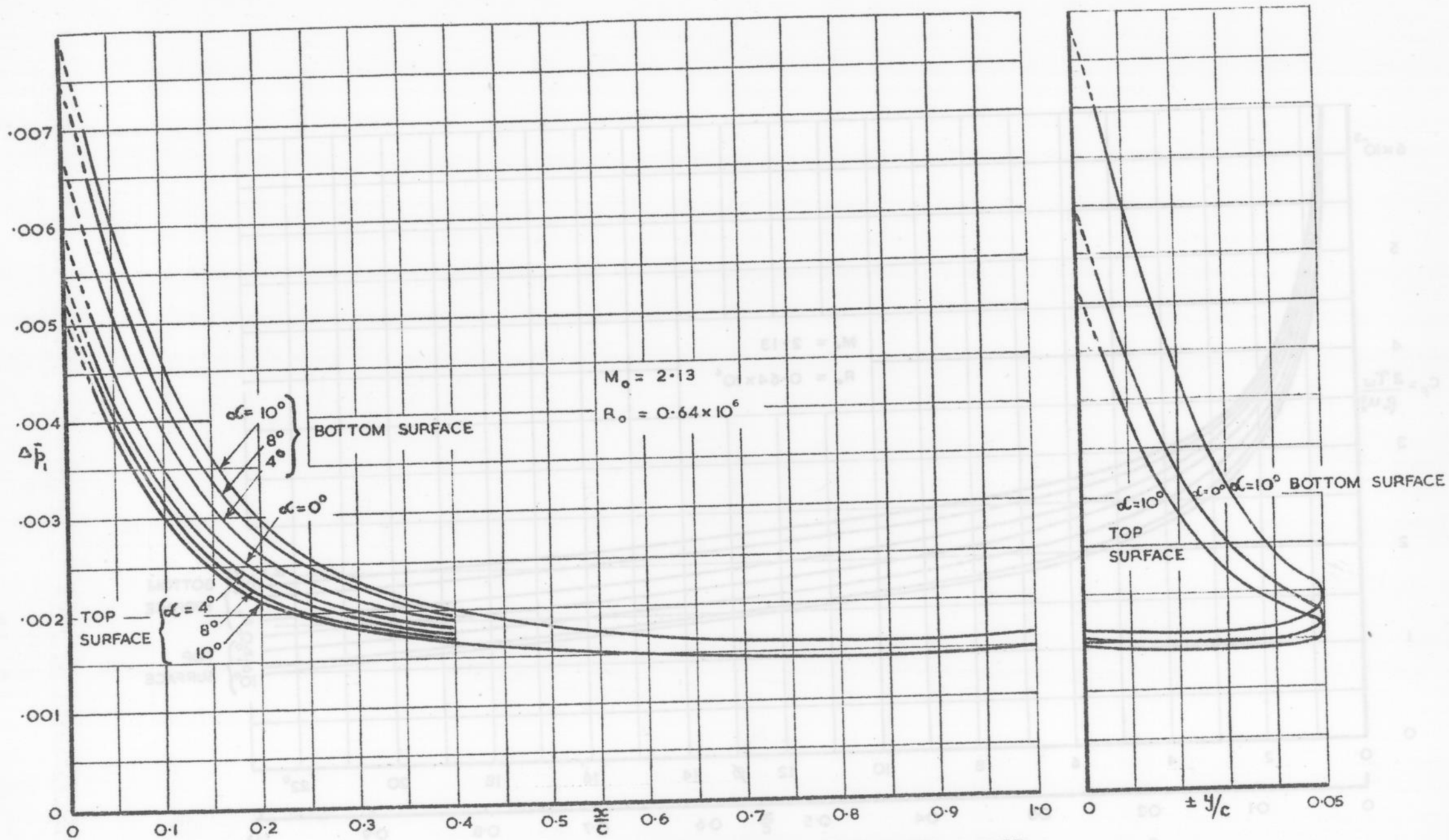

FIG 21. 10% C.A. PROFILE - PRESSURE INCREMENTS DUE TO BOUNDARY LAYER (IGNORING EFFECT OF SEPARATION)

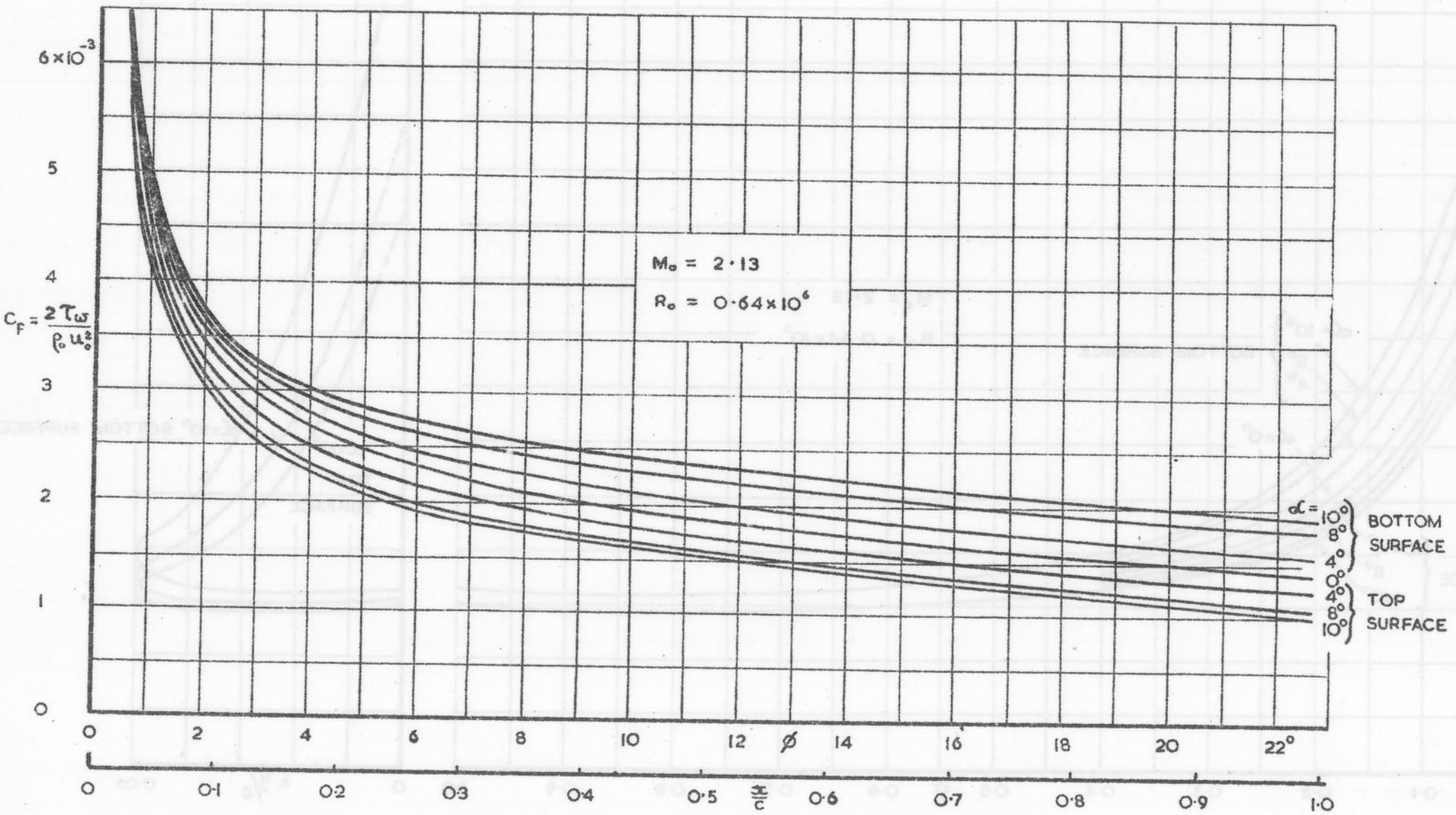

FIG 22 10% C.A. PROFILE - LOCAL SKIN FRICTION COEFFICIENT

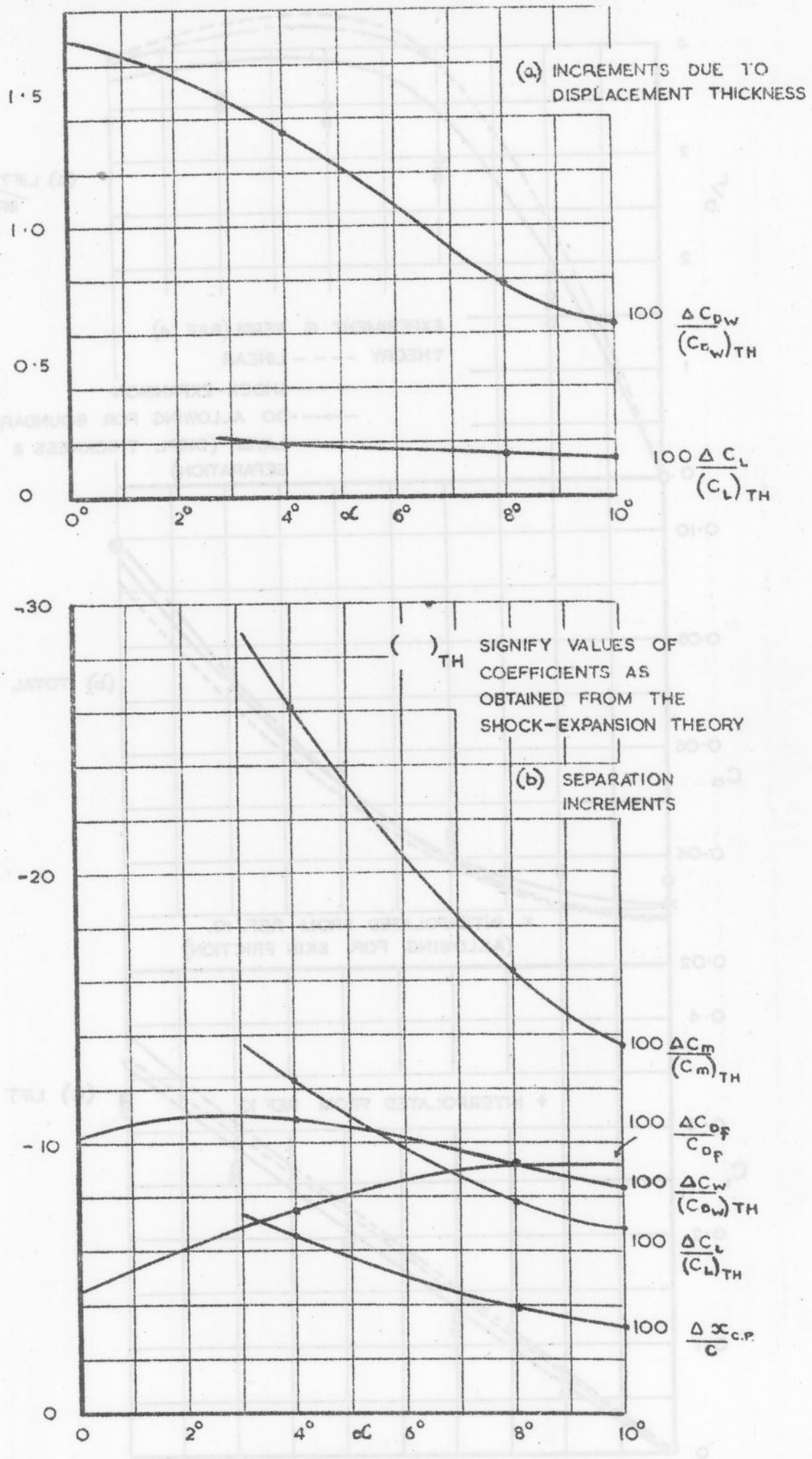

FIG. 23. 10% C.A. PROFILE - CHANGES IN AERODYNAMIC COEFFICIENTS DUE TO THE BOUNDARY LAYER

$M_o = 2{\cdot}13 \quad R_o = 0{\cdot}64 \times 10^6$

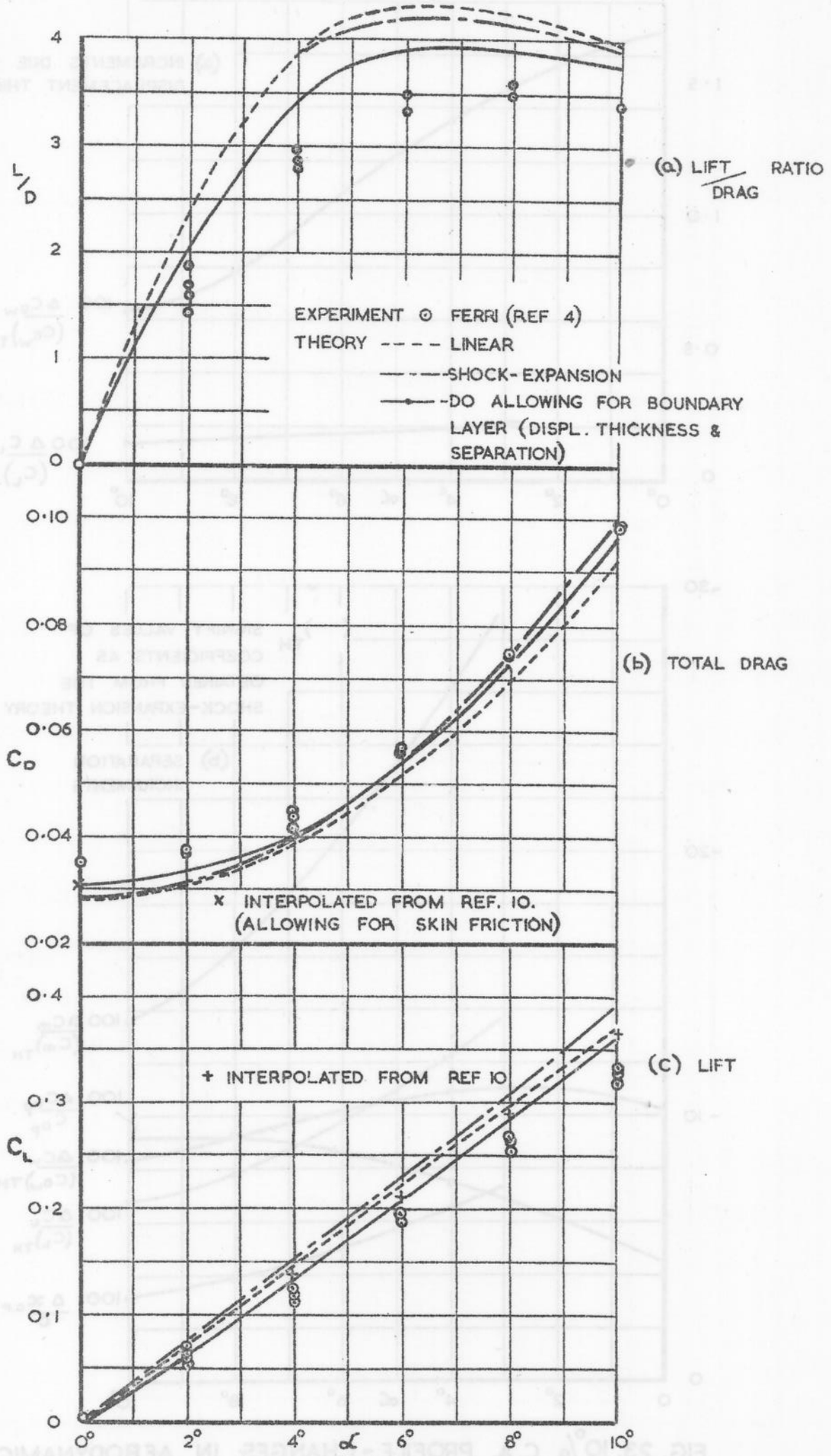

FIG. 24. 10% C.A. PROFILE- COMPARISON OF THEORY AND EXPERIMENT $M = 2{\cdot}13$ $R_c = 0{\cdot}64 \times 10^6$

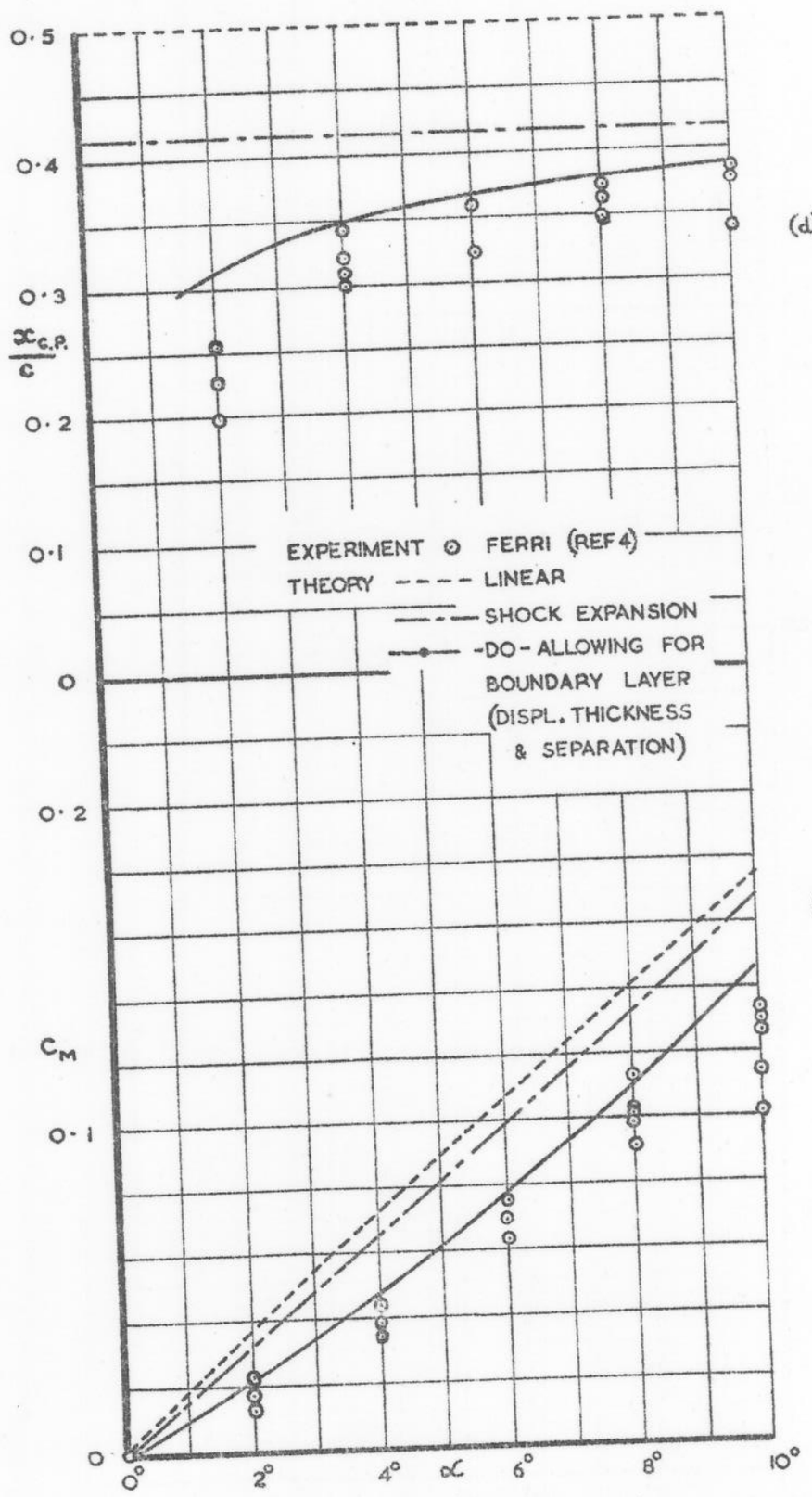

FIG. 24. CONTINUED

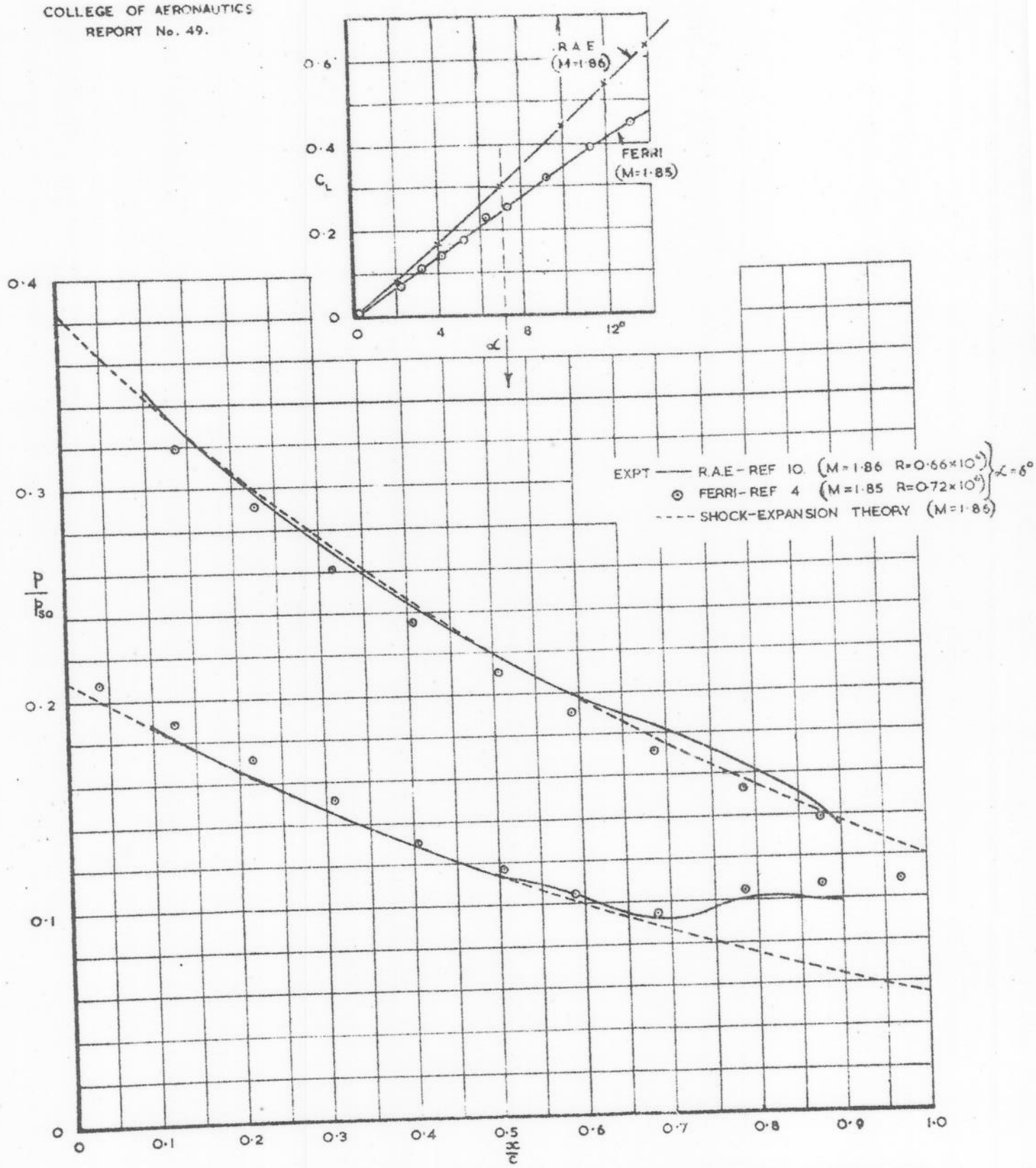

FIG. 25. 10% CIRCULAR ARC PROFILE - COMPARISON OF EXPERIMENTAL RESULTS.

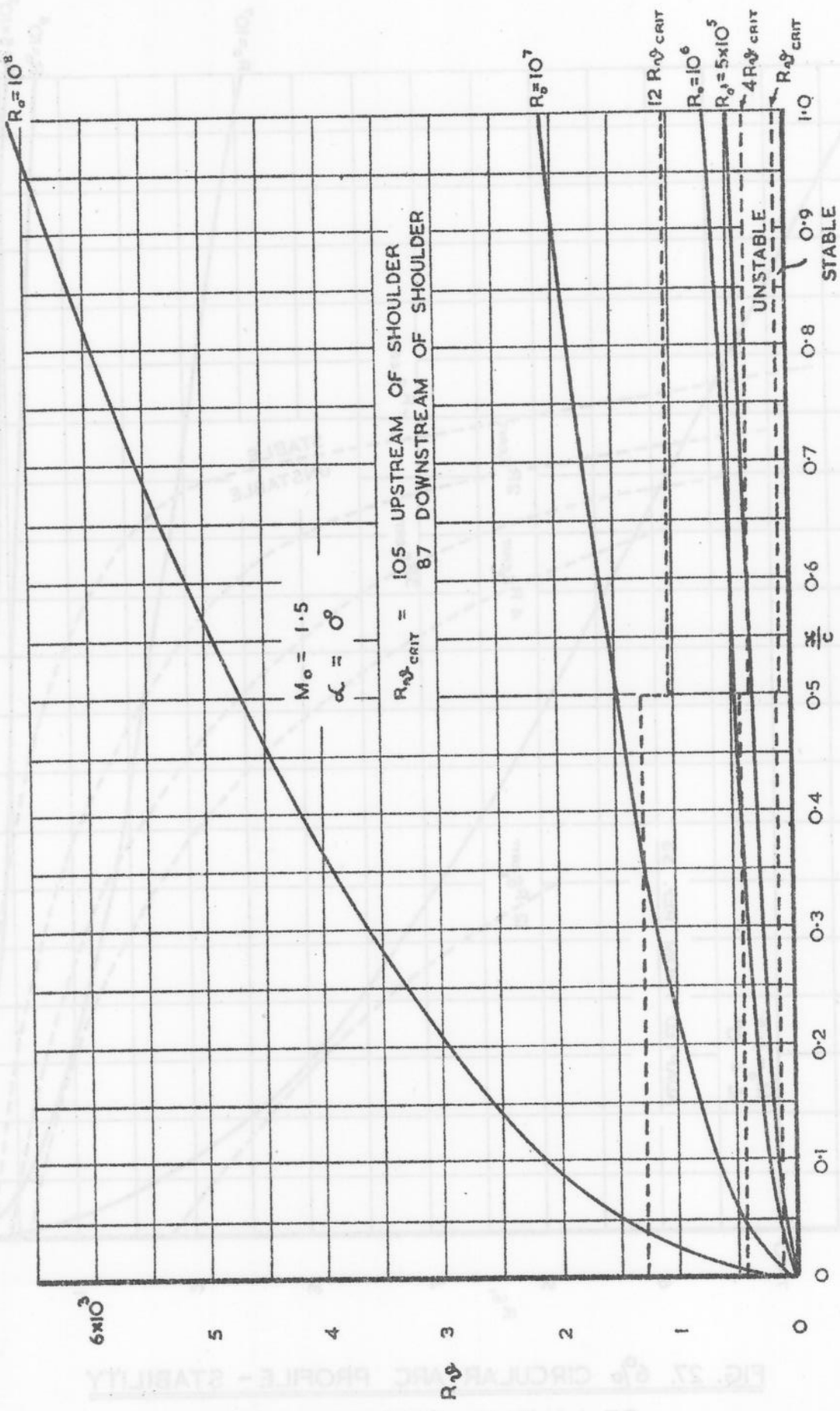

FIG. 26. 6% DOUBLE-WEDGE PROFILE - STABILITY OF LAMINAR BOUNDARY LAYER

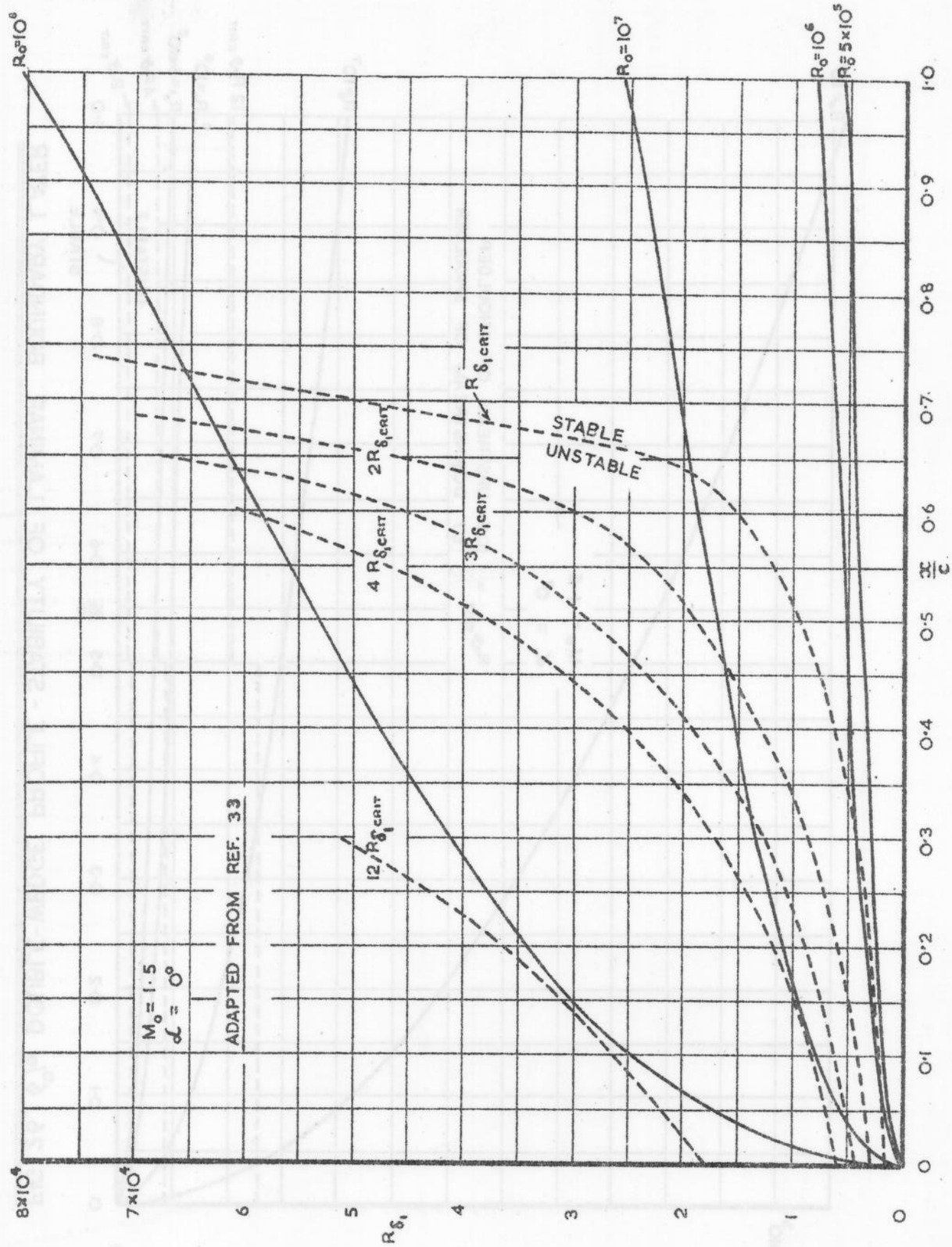

FIG. 27. 6% CIRCULAR ARC PROFILE – STABILITY OF LAMINAR BOUNDARY LAYER

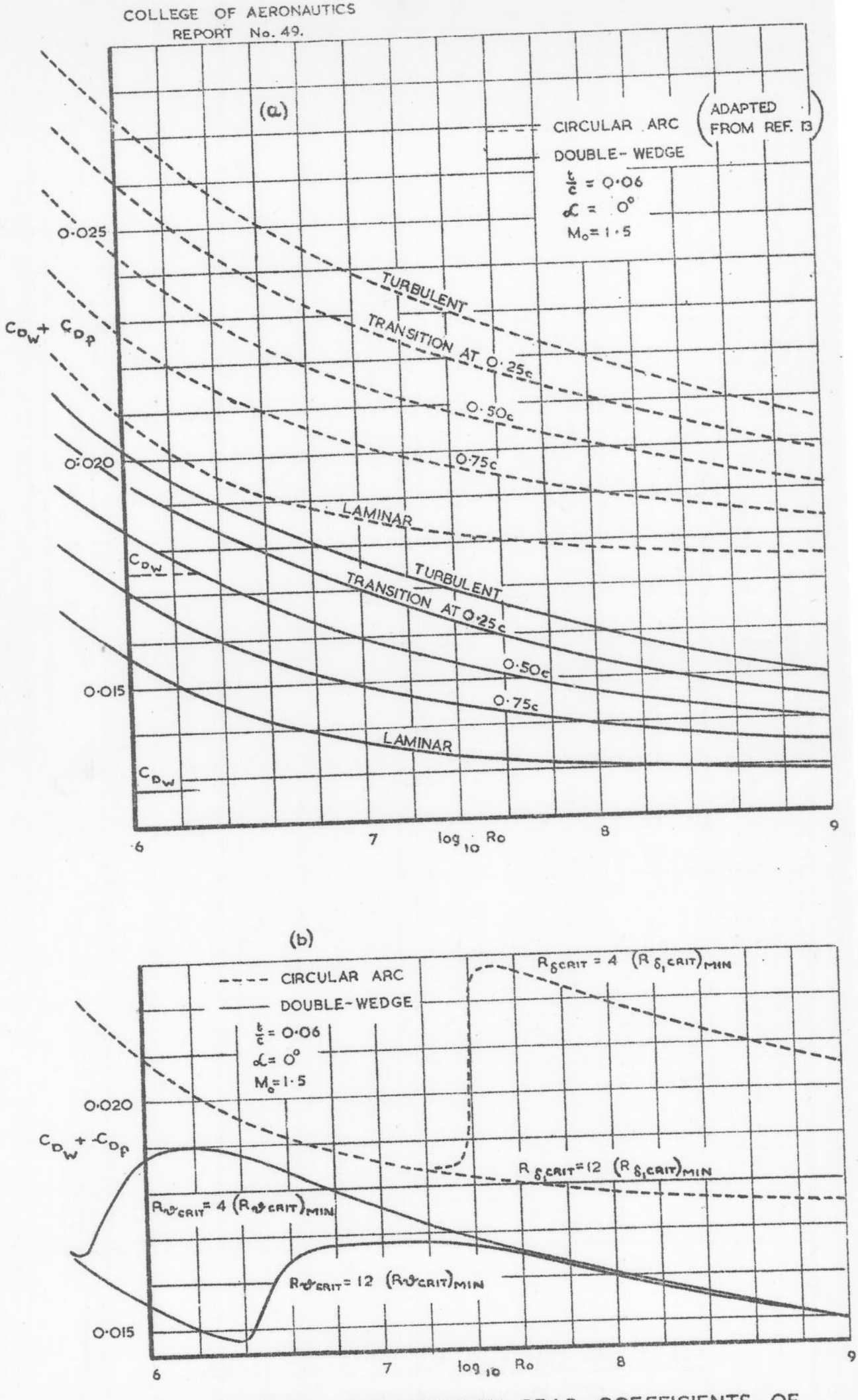

FIG. 28. WAVE & SKIN FRICTION DRAG COEFFICIENTS OF 6% C.A. & D.W. PROFILES